

Tuning the Electrochemical Properties of Manganese Dioxide Based Composites to Enhance Capacitive Properties



By

Muhammad Mahad Ahmed Siddiqui

(Registration No: 00000362323)

Department of Materials Engineering

School of Chemical and Materials Engineering

National University of Sciences & Technology (NUST)

Islamabad, Pakistan

(2024)

Tuning the Electrochemical Properties of Manganese Dioxide Based Composites to Enhance Capacitive Properties



By

Muhammad Mahad Ahmed Siddiqui

(Registration No: 00000362323)

A thesis submitted to the National University of Sciences and Technology, Islamabad,

in partial fulfillment of the requirements for the degree of

Master of Science in
Nanoscience and Engineering

Supervisor: Dr. Amna Safdar

School of Chemical and Materials Engineering

National University of Sciences & Technology (NUST)

Islamabad, Pakistan

(2024)

THESIS ACCEPTANCE CERTIFICATE



THESIS ACCEPTANCE CERTIFICATE

Certified that final copy of MS Thesis entitled "Turning the Electrochemical Properties of Manganese Dioxide Based Composites to Enhance Capacitive Properties" written by Mr Muhammad Mahad Ahmed Siddiqui (Registration No 00000362323), of School of Chemical & Materials Engineering (SCME) has been vetted by undersigned, found complete in all respects as per NUST Statues/Regulations, is free of plagiarism, errors, and mistakes and is accepted as partial fulfillment for award of MS degree. It is further certified that necessary amendments as pointed out by GEC members of the scholar have also been incorporated in the said Thesis.

Signature: AS

Name of Supervisor: Dr Amna Safdar

Date: 17-12-2024

Signature (HOD): [Signature]

Date: 17-12-24

Signature (Dean/Principal): [Signature]

Date: 17/12/24

TH - 1

Form TH-1

National University of Sciences & Technology (NUST) MASTER'S THESIS WORK


Formulation of Guidance and Examination Committee (GEC)

Name: Muhammad Mahad Ahmed Siddiqui NUST Reg No: 00000362323
Department: Department of Materials Engineering Specialization: Master of Science in Nanoscience & Engineering
Credit Hour Completed: 24.0 CGPA: 3.63

Course Work Completed

S/No:	Code:	Title:	Core/Elective:	CH:	Grade:
1.	MSE-854	Characterization Of Materials	Compulsory	3.0	B+
2.	MSE-856	Nano Material and Processing	Compulsory	3.0	A
3.	MSE-954A	Advanced Characterization Of Materials	Elective	3.0	B
4.	RM-898	Research Methodology	Additional	2.0	Q
5.	NSE-813	Essentials of Nanoscience and Engineering	Compulsory	3.0	A
6.	NSE-842	Nano Materials For Energy Applications	Elective	3.0	A
7.	NSE-845	Nanolithography And Device Fabrication	Elective	3.0	B
8.	NSE-847	Essentials of NEMS MEMS	Elective	3.0	A
9.	ESE-836	Li-ion and Next Generation Batteries	Elective	3.0	B+
10.	GMN-1	German Language- A1	Additional	2.0	Q

Date: 16-Mar-2023

Student's Signature: 

Thesis Committee

Name: Amna Safdar (Supervisor)
Department: Department of Materials Engineering

Signature: 

Name: Sofia Javed (Internal)
Department: Department of Materials Engineering

Signature: 


Name: Nasir Mahmood Ahmad (Internal)
Department: Department of Materials Engineering

Signature: 

Name: Amna Safdar (External)
Department: Department of Materials Engineering

Signature: 

Name: S-DR MASHKOOZ AHMED SORELI
Date: 16-Mar-2023

Signature of Head of Department: 

APPROVAL

Date: 16-Mar-2023

Signature of Dean/Principal: 

TH - 4



National University of Sciences & Technology (NUST)

FORM TH-4

MASTER'S THESIS WORK

We hereby recommend that the dissertation prepared under our supervision by

Regn No & Name: 00000362323 Muhammad Mahad Ahmed Siddiqui

Title: Turning the Electrochemical Properties of Manganese Dioxide Based Composites to Enhance Capacitive Properties.

Presented on: 04 Dec 2024 at: 1130 hrs in SCME

Be accepted in partial fulfillment of the requirements for the award of Masters of Science degree in Nanoscience & Engineering.

Guidance & Examination Committee Members

Name: Dr Nasir M. Ahmed

Signature: [Signature]

Name: Dr Sofia Javed

Signature: [Signature]

Name: Dr Mashkoor Ahmad (Co-Supervisor)

Signature: [Signature]

Supervisor's Name: Dr Amna Safdar

Signature: [Signature]

Dated: 06-12-2024

[Signature]
Head of Department

Head of Department

Date 6/12/24

COUNTERSIGNED

06-12-24

Date

[Signature]

Dean/Principal

School of Chemical & Materials Engineering (SCME)

AUTHOR'S DECLARATION

I Marghoob Ahmed hereby state that my MS thesis titled "Tuning the Electrochemical Properties of Manganese Dioxide Based Composites to Enhance Capacitive Properties" is my own work and has not been submitted previously by me for taking any degree from National University of Sciences and Technology, Islamabad or anywhere else in the country/ world.

At any time if my statement is found to be incorrect even after I graduate, the university has the right to withdraw my MS degree.

Name of Student: Muhammad Mahad Ahmed Siddiqui

Date: 21 December 2024

PLAGIARISM UNDERTAKING

I solemnly declare that research work presented in the thesis titled “Tuning the Electrochemical Properties of Manganese Dioxide Based Composites to Enhance Capacitive Properties” is solely my research work with no significant contribution from any other person. Small contribution/ help wherever taken has been duly acknowledged and that complete thesis has been written by me.

I understand the zero-tolerance policy of the HEC and National University of Sciences and Technology (NUST), Islamabad towards plagiarism. Therefore, I as an author of the above titled thesis declare that no portion of my thesis has been plagiarized and any material used as reference is properly referred/cited.

I undertake that if I am found guilty of any formal plagiarism in the above titled thesis even after award of MS degree, the University reserves the rights to withdraw/revoke my MS degree and that HEC and NUST, Islamabad has the right to publish my name on the HEC/University website on which names of students are placed who submitted plagiarized thesis.

Student Signature: 

Name: Muhammad Mahad Ahmed Siddiqui

DEDICATION

" This thesis is dedicated to my beloved parents, whose unwavering love, sacrifices, and encouragement have been the foundation of my success. Their endless support and belief in me have made this journey possible."

ACKNOWLEDGEMENTS

First and foremost, I thank Allah for His mercy and guidance throughout my academic journey. I am truly blessed for His constant support in my endeavors.

I am profoundly grateful to my father, Aamir Siddiqui; my mother, Ayesha Sultana; my aunt Prof. Zafar Sultana; and my brothers, Muhammad Maaz Ahmed Siddiqui, and Muhammad Mohsin Ahmed Siddiqui. Their love, encouragement, and unwavering belief in me have been my pillar of strength and the driving force behind my accomplishments. I dedicate my success to them, and I am eternally thankful for their presence in my life.

I would like to express my deepest gratitude to Dr. Amna Safdar and Dr. Mashkooor Ahmad for their invaluable guidance, support, and mentorship throughout this research. Their expertise has greatly shaped the course of this work, and I am truly thankful for the opportunities they have provided for my academic development.

I extend my sincere thanks to my committee members, Dr. Sofia Javed and Dr. Nasir M. Ahmed, for their insightful feedback, constructive criticism, and dedication to enhancing the quality of my research. Your valuable perspectives have significantly enriched this study.

Finally, I wish to acknowledge the support of Mr. Marghoob Ahmed, Ms. Aqsa Zaheen, Mr. Arslan, their moral support and contributions have been vital in completing this research. I truly appreciate all the help and encouragement I received from each one of them.

Muhammad Mahad Ahmed Siddiqui

TABLE OF CONTENTS

ACKNOWLEDGEMENTS	IX
TABLE OF CONTENTS	X
LIST OF TABLES	XIII
LIST OF FIGURES	XIV
LIST OF SYMBOLS, ABBREVIATIONS AND ACRONYMS	XVI
ABSTRACT	XVII
CHAPTER 1: INTRODUCTION	1
1.1 Background	1
1.2 Fundamentals of Capacitor	4
1.3 Supercapacitor Charge Storage Mechanisms	5
1.4 Material Criteria for Supercapacitors	7
1.4.1 Surface Area	7
1.4.2 Electronic and Ionic Conductivity	8
1.4.3 Mechanical & Chemical Stability	8
1.5 Nanomaterials for Supercapacitors	8
1.5.1 0-D Nanomaterials	8
1.5.2 1-D Nanomaterials	10
1.5.3 2-D Nanomaterials	11
1.5.4 3-D Nanomaterials	13
1.6 Problem Statement	14
1.7 Objective of the Study	19
CHAPTER 2: LITERATURE REVIEW	20
2.1 History of Conventional Capacitors	20
2.2 Origin and Development of Supercapacitors	23
2.3 Classification of Supercapacitors	25
2.4 Symmetric Supercapacitors	26
2.4.1 Electric Double Layer Capacitors (EDLC)	26
2.4.2 Pseudocapacitors	28
2.5 Asymmetric Supercapacitors	30
2.6 Hybrid Supercapacitor	31
2.7 Components of Supercapacitors	33
2.8 Electrode	33
2.9 Electrolyte	36
2.10 Separator	38
2.11 Current Collector	39
2.12 Electrode Materials for Supercapacitors	39

2.13	Carbon-based materials	40
2.13.1	Activated Carbon	41
2.13.2	Carbon Nanotubes	42
2.13.3	Graphene	43
2.14	Metal oxides-based materials	45
2.14.1	Ruthenium Oxide	45
2.14.2	Nickel Oxide	46
2.14.3	Manganese Oxide	48
2.15	Conducting polymer-based materials	49
2.15.1	Polyaniline (PANi)	50
2.15.2	Polypyrrole (Ppy)	51
2.15.3	Polythiophene (Pth)	51
2.16	MnO₂-based composite materials	52
2.16.1	MnO ₂ binary composites	52
2.16.2	MnO ₂ ternary composites	55
CHAPTER 3: MATERIALS AND METHODS		59
3.1	Reagents & Materials	59
3.2	Synthesis of MnO₂	59
3.3	Synthesis of MnO₂/CeO₂	60
3.4	Synthesis of MnO₂/CeO₂/MWCNT	61
3.5	Fabrication of Working Electrode	62
CHAPTER 4: CHARACTERIZATION		63
4.1	Instrumentation and Measurements	63
4.2	X-ray diffraction (XRD)	64
4.2.1	Working Principle	65
4.3	Raman Spectroscopy	67
4.3.1	Working Principle	68
4.4	Scanning Electron Microscopy	69
4.4.1	Working Principle	70
4.5	Transmission Electron Microscopy	73
4.5.1	Working Principle	73
4.6	X-ray Photoelectron Spectroscopy (XPS)	75
4.6.1	Working Principle	76
4.7	Brunauer, Emmett and Teller Analysis (BET)	78
4.7.1	Working Principle	78
4.8	Cyclic Voltammetry (CV)	80
4.8.1	Working Principle	81
4.8.2	Result Interpretation	82
4.9	Galvanic Charge Discharge (GCD)	83
4.9.1	Working Principle	84
4.9.2	Result Interpretation	85
4.10	-Electrochemical Impedance Spectroscopy (EIS)	86
4.10.1	Working Principle	86
CHAPTER 5: RESULTS AND DISCUSSION		88

5.1	Structural, Compositional, and Morphological Analysis	88
5.1.1	X-Ray Diffraction Analysis (XRD)	88
5.1.2	Raman Analysis	89
5.1.3	Morphological Analysis	91
5.1.4	Brunauer, Emmett and Teller Analysis (BET)	93
5.1.5	X-ray Photoelectron Spectroscopy Analysis	95
5.2	Electrochemical performance of MnO₂/CeO₂/MWCNT electrode	100
5.2.1	Cyclic Voltammetry (CV)	100
5.2.2	Galvanostatic Charge Discharge	104
5.2.3	Electrochemical Impedance Spectroscopy (EIS)	108
5.3	Electrochemical performance of MnO₂/CeO₂/MWCNT // AC Asymmetric Coin Cell	113
CHAPTER 6: CONCLUSIONS AND FUTURE RECOMMENDATION		118
6.1	Conclusion	118
6.2	Future Recommendations	118
REFERENCES		119

LIST OF TABLES

Table 2.1: Electrochemical performance of MnO ₂ -based binary composites	53
Table 2.2: Electrochemical performance of MnO ₂ based ternary composites.....	57
Table 5.1: Electrochemical performance of MnO ₂ /CeO ₂ /MWCNT electrode compared with other electrode materials reported in the literature.....	111

LIST OF FIGURES

Figure 1.1: Components of a supercapacitor.....	3
Figure 1.2: Schematic of a fundamental capacitor.....	4
Figure 1.3: Ragone plot among energy storage devices.....	15
Figure 2.1: Schematic of a dielectric capacitor.....	21
Figure 2.2: Historical development of supercapacitor.....	23
Figure 2.3: Schematic of pseudocapacitance mechanisms.....	29
Figure 4.1: Working principle of XRD.....	66
Figure 4.2: Working principle of Raman spectroscopy.....	69
Figure 4.3: Working principle of scanning electron microscopy.....	72
Figure 4.4: Working principle of transmission electron microscope.....	75
Figure 4.5: Working principle of x-ray photoelectron spectroscopy.....	78
Figure 4.6: Working principle of BET.....	80
Figure 4.7: Cyclic voltammogram for an electrochemically reversible redox process ...	83
Figure 4.8: Schematic illustration of a GCD plot.....	85
Figure 4.9: Schematic illustration of a Nyquist plot.....	87
Figure 5.1: XRD pattern of (a) MnO ₂ /CeO ₂ /CNT and (b)MnO ₂	89
Figure 5.2: Raman plot of MnO ₂ , MWCNTs, MnO ₂ /CeO ₂ , MnO ₂ /CeO ₂ /MWCNT.....	90
Figure 5.3: (a) SEM (b) TEM image of MnO ₂ /CeO ₂ /MWCNT nanocomposite (b) Corresponding EDS, and (d-f) HRTEM images taken from different parts of MnO ₂ /CeO ₂ /MWCNT composite.	91
Figure 5.4: (a-b) SEM images of CeO ₂ and MnO ₂ nanostructures respectively, and (c-e) TEM images of CeO ₂ , MnO ₂ and MnO ₂ /CeO ₂ nanostructures respectively.	92
Figure 5.5: (a) Nitrogen absorption-desorption isotherm, and (b) pore size distribution behavior of MnO ₂ , MnO ₂ /CeO ₂ , and MnO ₂ /CeO ₂ /MWCNT composite.	94
Figure 5.6: XPS Survey spectrum of MnO ₂ /CeO ₂ /CNT nanocomposite.	95
Figure 5.7: High-resolution XPS spectrums of Mn 2p.....	96
Figure 5.8: High-resolution XPS spectrums of O1s.....	97
Figure 5.9: High-resolution XPS spectrums of Ce 3d.....	98
Figure 5.10: High-resolution XPS spectrums of C1s.....	99
Figure 5.11: CV plots of MnO ₂ , MnO ₂ /CeO ₂ , and MnO ₂ /CeO ₂ /MWCNT at the scan rate of 20mVs ⁻¹	101
Figure 5.12: CV plots of MnO ₂ /CeO ₂ /MWCNT at different scan rates.....	102
Figure 28: CV plots at different scan rates of (a) pristine MnO ₂ and (b) MnO ₂ /CeO ₂ composite.	103
Figure 5.14: GCD curves of MnO ₂ , MnO ₂ /CeO ₂ , and MnO ₂ /CeO ₂ /MWCNT at the current density of 2.5 Ag ⁻¹	104
Figure 5.15: GCD curves of the MnO ₂ /CeO ₂ /MWCNT electrode at various current densities.....	105
Figure 5.16: GCD plots of (a) pristine MnO ₂ and (b) MnO ₂ /CeO ₂ composite.	106

Figure 5.17: <i>Specific capacitance vs current density for MnO₂/CeO₂/MWCNT, MnO₂/CeO₂, and MnO₂.....</i>	107
Figure 5.18: <i>Nyquist diagram for MnO₂/CeO₂/MWCNT, MnO₂/CeO₂, and MnO₂.....</i>	108
Figure 5.19: <i>(a) Comparison of specific capacitance obtained at different current densities of the present and the previously reported work (b) Comparative analysis of maximum specific capacitance achieved by MnO₂/CeO₂/MWCNT and the previously reported MnO₂-based binary and ternary composites.....</i>	110
Figure 5.20: <i>Coin cell assembly for asymmetric supercapacitor.</i>	113
Figure 5.21: <i>(a-b) CV curves of MnO₂/CeO₂/MWCNT//AC asymmetric supercapacitor at different scan rates and potential windows respectively.</i>	114
Figure 5.22: <i>GCD curves of asymmetric supercapacitor at different current densities and potential windows respectively.</i>	114
Figure 5.23: <i>Specific capacitance vs. current density plot.</i>	115
Figure 5.24: <i>Ragone plot of asymmetric supercapacitor.....</i>	116
Figure 5.25: <i>Nyquist diagram of the asymmetric supercapacitor.</i>	117
Figure 5.26: <i>Cycling performance of asymmetric supercapacitor.</i>	117

LIST OF SYMBOLS, ABBREVIATIONS AND ACRONYMS

Asymmetric supercapacitor	ASC
Cyclic voltammetry	CV
Energy Density	ED
Galvanostatic charge-discharge	GCD
Electrochemical impedance spectroscopy	EIS

ABSTRACT

The design of advanced nanomaterials has significantly transformed the development of innovative electrode materials for energy storage systems. In this study, a ternary composite of manganese dioxide (MnO_2) nanorods, cerium dioxide (CeO_2) nanoparticles, and multi-walled carbon nanotubes (MWCNTs) was synthesized and thoroughly examined for its potential in supercapacitor applications. The combination of these materials results in enhanced electrochemical performance through increased surface defects, higher specific surface area, and improved electron and ion transport. Extensive characterization techniques such as field emission scanning electron microscopy (FESEM), transmission electron microscopy (TEM), X-ray diffraction (XRD), and Raman spectroscopy confirmed the morphology, structure, and successful synthesis of the composite. The well-dispersed MnO_2 nanorods and CeO_2 nanoparticles on the MWCNT framework further supported the integrity of the composite structure.

Electrochemical evaluation using cyclic voltammetry (CV), galvanostatic charge-discharge (GCD), and electrochemical impedance spectroscopy (EIS) demonstrated the superior performance of the $\text{MnO}_2/\text{CeO}_2/\text{MWCNT}$ composite, showing a specific capacitance of 1204 F g^{-1} at 2.5 A g^{-1} . This enhanced capacitance, compared to binary $\text{MnO}_2/\text{CeO}_2$ and pristine MnO_2 , is attributed to the improved redox activity of MnO_2 , defect engineering via CeO_2 , and the excellent conductivity of MWCNTs. Additionally, the composite retained 82% of its capacitance at a higher current density of 10 A g^{-1} , indicating excellent rate capability.

To demonstrate its practical application, a coin cell asymmetric supercapacitor (ASC) was fabricated using $\text{MnO}_2/\text{CeO}_2/\text{MWCNT}$ as the positive electrode and activated carbon (AC) as the negative electrode. The device exhibited a specific capacitance of 102 F g^{-1} at 1 A g^{-1} and operated within a voltage window of 2 V. It achieved an energy density of 36 Wh kg^{-1} at a power density of 800 W kg^{-1} , making it suitable for high-energy applications. The ASC also showed excellent cycling stability, retaining 94% of its initial capacitance after 10,000 cycles at 10 A g^{-1} .

These findings underscore the potential of MnO₂/CeO₂/MWCNT composites in developing high-performance supercapacitors for real-world applications. This work also encourages further exploration into the synergistic effects of combining MnO₂ with other rare earth metal oxides and carbon-based materials to optimize energy storage devices.

Keywords: Nanomaterials, Ternary composite, Electrochemical performance, Characterization techniques, Electrode material, Specific capacitance, Asymmetric supercapacitor, Energy density.

CHAPTER 1: INTRODUCTION

1.1 Background

Global energy demand is projected to surge by as much as double within the next two decades. This dramatic rise is fueled by several key factors. Firstly, population growth is a significant driver. As the world's population continues to swell, there will be a corresponding increase in the number of people requiring energy for essential needs like heating, transportation, and powering appliances. Secondly, rapid industrialization and urbanization are major contributors. These processes lead to a significant rise in energy consumption for various purposes, including manufacturing, construction, transportation infrastructure, and powering buildings in densely populated areas [1].

Beyond these primary drivers, several other factors are influencing the energy landscape. Economic development plays a crucial role. As nations become wealthier, their citizens adopt more energy-intensive lifestyles, leading to a higher overall demand. Additionally, the electrification of industries that were previously reliant on fossil fuels is a growing trend. While this shift offers environmental benefits, it also contributes to increased demand for electricity generation. Finally, the ever-present threat of climate change cannot be ignored. Mitigating the effects of climate change will necessitate significant investments in renewable energy sources and energy efficiency measures, further impacting global energy demand [2].

Our continued reliance on non-renewable energy sources and the accelerating depletion of natural resources have heightened public awareness of global warming. This growing concern has prompted a paradigm shift in many countries, with a renewed focus on developing renewable energy solutions [3]. Solar and wind energy, for example, offer significant advantages – they are both clean and abundant. However, their inherent variability presents a challenge. The unpredictable nature of these sources makes it difficult to consistently generate optimal power output. This is where energy storage systems play a vital role. These systems are crucial for not only meeting peak energy demands but also for maintaining a clean and stable energy grid. Energy storage systems

can be broadly categorized into four main types based on their operating principles: electromechanical, electromagnetic, electrochemical, and electrostatic [4].

Electrochemical storage technologies, particularly those employing lithium-ion and alkali metal-ion batteries, have been extensively researched and successfully implemented in a wide range of applications across the globe. Lithium-ion battery technology has become a dominant force, especially within the electric vehicle (EV) and plug-in electric vehicle (PEV) sectors. These batteries typically feature a carbon-based anode and a cathode composed of a lithium-based compound. The electrolyte used in the cell is mostly a common lithium salt such as lithium hexafluorophosphate (LiPF_6). While significant research efforts over the past few decades have focused on making this technology economically viable, limitations persist in areas such as safety, stability, and, most importantly, power density [5].

Supercapacitors, also known as ultracapacitors, classified under electrostatic and electrochemical energy storage systems, can be utilized as a promising alternative to batteries in areas demanding high power delivery, rapid charge and discharge cycles, and low overall energy storage requirements [6].

These devices boast several additional advantages, including low internal resistance, a wide operational temperature range, and high efficiency in energy transfer. However, it's important to acknowledge their trade-off: supercapacitors offer a relatively low energy density compared to other storage solutions [7]. Despite this limitation, their advantageous characteristics make them well-suited for various applications. Supercapacitors can function independently or be strategically combined with high-energy storage devices to manage power fluctuations (sinking and sourcing) in real-world industrial settings.

The exploration of supercapacitor technology can be traced back to the pioneering work of Hermann von Helmholtz in 1853. Helmholtz's groundbreaking research revealed that electrical charges could be stored not only on the surface of conductive materials but also at the crucial "double-layer" interface between the electrode and electrolyte [8]. This discovery laid the foundation for a revolutionary technology capable of achieving high

capacitance. Initially, research focused on carbon-based materials for electrode construction. However, the advent of pseudocapacitors in the 1980s introduced a new storage mechanism distinct from the electric double-layer phenomenon [9].

As illustrated in Figure 1.1, a supercapacitor's core components include an electrolyte solution, two electrodes, and a separator membrane. This separator plays a critical role, acting as a selective barrier. It allows ions (charged particles) to freely move between the electrodes while simultaneously preventing direct electrical contact, which would cause a short circuit. Additionally, the process of electrolyte impregnation facilitates the typical electrostatic charge transfer mechanisms within the supercapacitor, contributing to its high reusability.

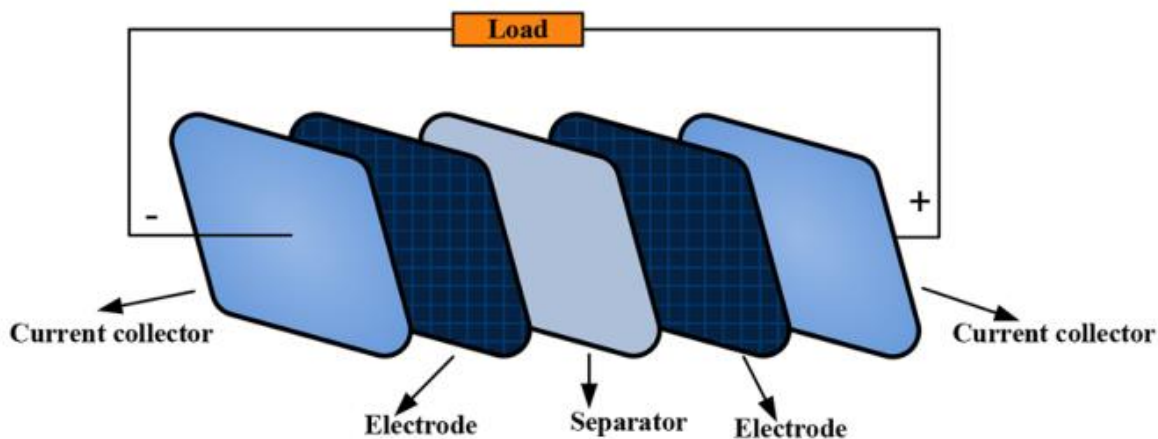


Figure 1.1: *Components of a supercapacitor*

To achieve even greater capacitance, modern research focuses on developing innovative electrode materials. These materials are ideally porous, highly conductive, and boast a large specific surface area. This characteristic – a large surface area – is particularly crucial, as it provides more real estate for storing electrical energy. Consequently, recent research efforts have been directed toward creating these advanced electrode materials to significantly enhance the capacity and energy density of supercapacitors.

1.2 Fundamentals of Capacitor

Within the field of electromagnetism, a capacitor is a passive electrical component characterized by its ability to store electrical potential energy. As depicted in Figure 1.2, a capacitor consists of two parallel conducting plates separated by a dielectric material. This dielectric serves the critical function of insulating the plates while permitting the establishment of an electric field between them.

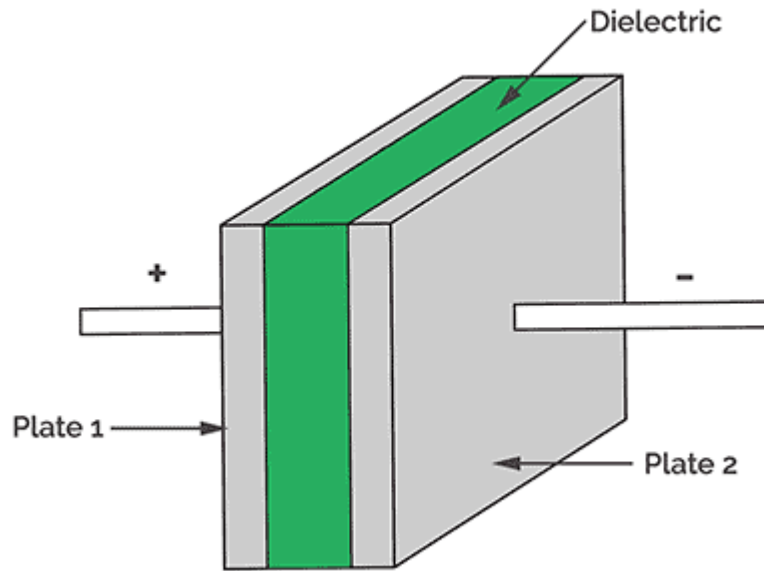


Figure 1.2: *Schematic of a fundamental capacitor*

When a voltage source is applied across the capacitor's terminals, a redistribution of electric charges occurs. These charges accumulate on the opposing surfaces of the plates, confined within the static electric field. This process results in a progressive increase in the stored energy within the capacitor. Notably, the relationship between the stored energy and the applied voltage is linear [8].

In an ideal capacitor, capacitance (C) is a fundamental property that quantifies the device's capacity for charge storage. This parameter is mathematically described by the following equation:

$$C = \frac{Q}{V} \quad (1)$$

Where C is the capacitance in farads (F), Q is the stored electric charge in coulombs (C), and V is the applied voltage across the two-conducting plate in volts (V). The above equation highlights the dependence of capacitance on both the charge stored and the voltage [8].

For a specific type of capacitor known as a parallel-plate capacitor, where the space between the plates is a vacuum, the capacitance can be calculated using a simplified form of the equation:

$$C = \epsilon \frac{A}{d} \quad (2)$$

Where ϵ is the permittivity of the vacuum and has a fixed value of 9×10^{-12} F/m, A is the area of each plate (square meter), and d is the distance between the plates (meters) [8].

The energy and power density of a capacitor have been derived from the equation 1.1 and 1.2 and are as follows:

$$E = \frac{1}{2} CV^2 \quad (3)$$

And,

$$P = \frac{1}{2} IV \quad (4)$$

Where E represents the energy density, P is the power density of the device, and I is the current across the capacitor [8].

1.3 Supercapacitor Charge Storage Mechanisms

Supercapacitors employ two primary mechanisms for charge storage: non-faradaic and faradaic. In the non-faradaic mechanism, also known as the electrostatic double-layer

capacitance (EDLC) mechanism, charge storage occurs through a purely physical process. There is no electron transfer between the electrode material and the electrolyte ions.

When a voltage is applied, ions within the electrolyte solution migrate across the separator and into the porous structure of the oppositely charged electrode. However, these electrodes are specifically designed to prevent the recombination of these ions with the electrode material. This selective adsorption process leads to the formation of an electrical double layer at the electrode-electrolyte interface. This double layer, comprised of separated positive and negative charges, is responsible for the electrostatic energy storage within the supercapacitor. Supercapacitors that rely solely on this non-faradaic mechanism are categorized as electric double-layer capacitors (EDLCs) and they generally utilize carbon-based materials as electrodes [10].

The faradaic mechanism, in contrast to the non-faradaic mechanism, relies on electron transfer processes occurring at the electrode-electrolyte interface. This electron transfer facilitates the storage of electrical energy through a combination of three primary mechanisms: electrosorption, redox reactions (reduction-oxidation), and intercalation. Supercapacitors employing this faradaic mechanism typically utilize pseudocapacitive electrodes comprised of conducting polymers or transition metal compounds [9].

Supercapacitor configurations can be broadly classified into two categories based on their electrode design: symmetric and asymmetric. Symmetric supercapacitors utilize identical electrode materials with the same mass for both the positive (anode) and negative (cathode) electrodes. This design offers advantages in terms of fabrication simplicity and balanced charge distribution. Notably, both electrochemical double-layer capacitors (EDLCs) and pseudocapacitors can fall under the umbrella of symmetric supercapacitors, depending on their primary charge storage mechanism.

In contrast, asymmetric supercapacitors, also known as hybrid supercapacitors, employ electrodes with distinct materials and potentially different masses. This configuration strategically leverages the complementary properties of the chosen electrode materials. One electrode, typically a pseudocapacitive electrode, can undergo faradaic reactions to achieve high energy density. The other electrode, often an EDLC

electrode, excels in rapid electrostatic charge storage, contributing to high power density. This combination allows asymmetric supercapacitors to potentially achieve both higher overall energy density and faster charge-discharge rates compared to their symmetric counterparts [11].

1.4 Material Criteria for Supercapacitors

The development of effective supercapacitor electrodes hinges on several critical factors, all inextricably linked to the employed materials. A high specific capacitance, which quantifies the energy stored per unit mass, volume, or area of the active material, is heavily influenced by the intrinsic properties and structure of the electrode material. Similarly, a large rate capability, reflected in the retention of capacitance at high scan rates or current densities, is strongly dependent on the material's conductivity, surface area, and the kinetics of ion diffusion. Furthermore, maintaining high cycle stability over extended use is directly linked to the material's structural integrity and its resistance to degradation mechanisms such as electrode dissolution or structural transformations. Additionally, the environmental and economic sustainability of the electrode design necessitates careful consideration of the toxicity and cost of the employed active materials. Therefore, the selection of electrode materials that effectively balance these diverse requirements is paramount for the realization of high-performance supercapacitor electrodes. To fabricate an exceptional electrode material for a supercapacitor following are the key parameters that need to be fulfilled.

1.4.1 Surface Area

In supercapacitors, the primary mechanism for charge storage is through electrostatic interactions at the electrode-electrolyte interface. Consequently, the specific capacitance, which represents the amount of electrical energy stored per unit mass of the electrode material, is directly influenced by the surface area available for these interactions. Therefore, employing electrode materials with a highly porous or nanostructured morphology offers a strategic approach to enhance the specific capacitance of a supercapacitor significantly [12].

1.4.2 Electronic and Ionic Conductivity

High electronic and ionic conductivity within the electrode material is crucial for maximizing a supercapacitor's performance. This translates to minimal energy loss during charge/discharge (rectangular CV curves, symmetrical GCD curves) and minimized capacitance loss at high scan rates/current densities. Strategies to achieve this include binder-free electrode design and nanostructured current collectors for improved electronic conductivity, and precise pore size control and hierarchical pore structures for enhanced ionic conductivity [12].

1.4.3 Mechanical & Chemical Stability

Cycle stability, crucial for supercapacitors, hinges on the mechanical and chemical resilience of electrode materials. Degradation during cycling occurs through phase changes, dissolution, and side reactions. Strategies to improve cycle life involve developing robust materials and employing surface protection techniques to mitigate these degradation mechanisms [12].

1.5 Nanomaterials for Supercapacitors

Nanomaterials, typically defined by dimensions ranging from 1-100 nanometers, offer significant advantages for supercapacitor performance due to their unique properties. Their high surface area provides a multitude of sites for charge storage, leading to enhanced specific capacitance. Additionally, the ability to tune the band gap of certain nanomaterials allows for optimized electronic properties within the electrode material. Furthermore, nanomaterials often exhibit exceptional mechanical and chemical resilience, contributing to improved cycle stability and durability of the supercapacitor device. The following sections will explore the specific characteristics and supercapacitor performance of various nanomaterials in greater detail.

1.5.1 0-D Nanomaterials

Zero-dimensional (0D) nanostructures, according to the conventional definition, are spherical particles with all three dimensions confined to the nanoscale, typically

ranging from 1 to 100 nanometers. However, in practice, the term "nanoparticle" can extend to particles with diameters up to 1 millimeter, as the benefits associated with their small size have been demonstrably observed within this broader size range. Zero-dimensional (0D) nanostructures, particularly solid nanoparticles, have emerged as a prominent class of electrode materials for supercapacitors. Carbon materials, including activated carbon, carbon nanospheres, and mesoporous carbon, are widely employed due to their inherent advantages [13]. Transition metal oxides, such as MnO_2 , NiO , and Fe_3O_4 , also represent another category of attractive 0D electrode materials [14].

Solid nanoparticles offer a high surface area within a compact volume, which is crucial for maximizing charge storage capacity. However, recent research has focused on exploring alternative 0D nanostructures with potentially even better performance. Hollow 0D structures, typically synthesized through template-based methods, offer several advantages. Their lower density translates to higher specific capacitance per unit weight. Additionally, the hollow interiors and porous nature create a high surface area-to-volume ratio, providing more sites for charge storage. Furthermore, these structures offer shorter diffusion pathways for both ions and electrons within the electrode, facilitating faster charge transport and potentially leading to improved rate capability [13].

Transition metal oxides (TMOs) hold immense promise as electrode materials for supercapacitors due to their unique properties when engineered at the nanoscale (0D). These 0D TMO nanostructures, encompassing quantum dots, nanocrystals, nanocages, and nanospheres, have attracted significant research interest for various applications beyond supercapacitors, including lithium metal batteries, metal-oxygen batteries, catalysis, and microwave absorption [14].

One of the key advantages of utilizing 0D TMOs in supercapacitors lies in their potential to achieve high energy densities due to their pseudocapacitive behavior. This behavior involves fast and reversible faradaic reactions at the electrode-electrolyte interface, enabling efficient energy storage. However, a significant challenge associated with 0D TMOs is their tendency to agglomerate during synthesis or electrochemical cycling. Agglomeration reduces the effective surface area available for charge storage, ultimately leading to a decrease in capacitance. Additionally, some TMOs inherently

possess low electronic conductivity, hindering efficient electron transport within the electrode and impacting device performance [15].

To address these limitations, researchers are actively exploring strategies to manipulate the morphology of 0D TMOs and create composite or alloyed electrode materials. Morphological control can involve techniques to prevent agglomeration and ensure the nanostructures remain well-dispersed. Composite and alloy formation strategies often involve combining TMOs with conductive materials (e.g., carbon nanotubes, graphene) to create synergistic effects. These composite electrodes can leverage the high energy density potential of TMOs while benefiting from the enhanced electronic conductivity provided by the conductive component. Optimizing the morphology and exploring composite materials are crucial approaches for unlocking the full potential of 0D TMOs in high-performance supercapacitors[15].

1.5.2 1-D Nanomaterials

One-dimensional (1D) nanostructures have garnered significant research interest due to their unique combination of chemical and physical properties. A defining characteristic of 1D nanostructures is their elongated geometry, often referred to as the longitudinal axis. This geometry offers distinct advantages for supercapacitor applications. It facilitates efficient transport pathways for both ions and electrons, enabling faster charge and discharge rates. Additionally, 1D nanostructures can provide similar benefits to zero-dimensional (0D) nanostructures in terms of increased surface area for charge storage, but due to their two nanoscale dimensions. These advantages arise from the high aspect ratio of 1D nanostructures, where two dimensions are confined at the nanoscale. Furthermore, 1D nanomaterials can be further classified into two categories: homostructures and heterostructures.

1D homostructures, such as nanorods, nanowires, and nanotubes, are categorized based on their aspect ratios and can be synthesized using template-assisted or template-free methods. Template-assisted methods involve using sacrificial templates, like AAO templates, followed by template removal. Template-free methods, such as hydrothermal synthesis, CVD, and electrodeposition, directly grow 1D homostructures. Vertical growth

of active material on conductive substrates, achieved through "bottom-up" or "top-down" methods, is emerging as a promising electrode design approach. This design facilitates efficient electron transport and rapid ion transfer due to the binder-free nature and void spaces between nanostructures [12].

In contrast to homostructures, which consist of a single material, 1D heterostructures are composite materials comprised of two or more integrated components. This integration offers a significant advantage: the synergistic enhancement of the intrinsic properties of each individual component. By strategically combining different materials, researchers can design 1D heterostructures that exhibit improved electrical conductivity, faster ionic transport, enhanced electrochemical reversibility and cycle stability, and even greater mechanical strength. These combined advantages position 1D heterostructures as promising candidates for next-generation supercapacitor electrode designs. One prominent category of 1D heterostructures is the core-shell structure, where a core material is encapsulated by a different material forming a shell. Additionally, 1D heterostructures can also be composites containing a combination of 0D and 1D nanomaterials.

1.5.3 2-D Nanomaterials

Two-dimensional (2D) nanomaterials have emerged as a promising class of electrode materials for supercapacitors due to their exceptional properties. The high surface area offered by 2D materials is particularly attractive, as it translates directly to enhanced capacitance through the provision of more sites for charge storage. Additionally, 2D materials often exhibit remarkable mechanical resilience, durability, flexibility, and even transparency. These combined characteristics make them highly desirable for supercapacitor applications.

However, a crucial challenge hindering the full exploration of 2D materials lies in the limited understanding of their behavior and properties within supercapacitors, particularly when employed in aqueous or organic electrolytes. Further research is necessary to elucidate the specific interactions between various 2D materials and different electrolyte environments. Despite this challenge, the inherent advantages of 2D materials,

particularly their exceptional surface area, suggest their potential to revolutionize the field of electrochemical capacitors [16].

Graphene, a prototypical 2D homostructure, has garnered significant attention for supercapacitor applications due to its exceptional mechanical strength and electrical conductivity. These properties contribute to improved electrode performance [17]. Similarly, transition metal oxides (TMOs) such as RuO_2 , IrO_2 , MnO_2 , NiO , Co_2O_3 , and V_2O_5 have been successfully synthesized in 2D structures, demonstrating their potential to alter supercapacitor performance. Various deposition methods, including spin coating, anodization, electrodeposition, atomic layer deposition, spray deposition, and sputtering, have been extensively explored for fabricating smooth and low-defect 2D TMO thin films for electrode applications[18].

Transition metal dichalcogenides (TMDCs) represent another promising class of 2D materials for supercapacitors. These materials are celebrated for their outstanding characteristics in nanoelectronics, optoelectronics, and sensor technologies. However, their high cost remains a significant barrier to widespread practical application in supercapacitors [19].

MXenes, a class of 2D transition metal carbides and nitrides (M = early transition metal, A = group 13 or 14 element, X = C and/or N), have emerged as promising electrode materials for supercapacitors due to their exceptional charge storage capabilities. This primarily stems from a phenomenon known as intercalation pseudocapacitance, where cations (Mg^{2+} , K^+ , Na^+ , Al^{3+} , NH_4^+ , Ba^{2+} , Ca^{2+} , Cs^+ , Li^+) can reversibly intercalate between the MXene layers. The hydrophilic nature and predominant hydroxyl-termination on their surfaces further enhance their electrochemical performance. MXenes are typically synthesized by selectively etching the A-group element from MAX phases, a precursor layered ternary compound [20].

The development of 2D heterostructures represents another promising strategy for enhancing supercapacitor performance. These composite materials combine the unique properties of two or more individual components. For example, integrating transition metal oxides, conducting polymers, or metal dichalcogenides with graphene-based

electrode materials has demonstrated remarkable results. This approach not only leverages the high electrochemical activity of these complementary materials but also addresses limitations associated with graphene, such as its inherently low conductivity and modest thermal and mechanical stability. Heterostructures incorporating graphene with metal oxides, hydroxides, or dichalcogenides are particularly promising avenues for further exploration [21].

1.5.4 3-D Nanomaterials

Three-dimensional (3D) porous architectures have become a cornerstone in the design of high-performance supercapacitor electrodes. These intricate structures offer a trifecta of advantages that significantly contribute to enhanced energy storage capabilities: high surface area, efficient electrolyte transport, and enhanced mechanical strength.

The interconnected network of pores within a 3D architecture maximizes the overall surface area available for charge storage. This expanded surface area directly translates to increased capacitance, as there are more sites for either ion adsorption (in electrical double-layer capacitors) or faradaic reactions (in pseudocapacitors) to occur [22].

Electrolyte transport plays another crucial role in supercapacitor performance. 3D porous architectures address this challenge by featuring well-defined pore networks. These networks allow for efficient infiltration of the electrolyte throughout the electrode, minimizing diffusion limitations. Minimized diffusion limitations ensure that electrolyte ions can readily access the entire active material, promoting faster charge and discharge kinetics. This ultimately leads to a more efficient and responsive supercapacitor device [22].

The mechanical stability of an electrode is paramount for maintaining long-term performance and durability within a supercapacitor. Compared to simpler electrode designs, 3D architectures often exhibit superior mechanical strength and structural integrity. This improved mechanical resilience helps the electrode material withstand the

repeated charge-discharge cycles experienced during supercapacitor operation without degradation [23].

Two primary approaches are employed for fabricating 3D supercapacitor electrodes:

Metal Foam Templates: This method leverages highly porous and conductive metal foams, such as nickel foam, as a current collector and scaffold. These foams serve as a substrate for the deposition of various active materials, including graphene, carbon nanotubes (CNTs), conjugated polymers, and metal oxides. The inherent conductivity of the metal foam promotes efficient electron transport throughout the entire electrode. However, metal foams often possess a higher density and lower specific surface area compared to some alternative 3D architectures [24].

3D Nanostructured Active Materials: This approach involves directly engineering the active materials themselves into 3D nanostructures. Mesoporous carbon (MC) serves as a prime example. MC offers a large specific surface area due to its intricate network of interconnected pores with tunable size. Studies have revealed that the pore size and symmetry of MC significantly impact supercapacitor performance by influencing the accessibility and transport of electrolyte ions. Researchers are actively exploring additional strategies to further enhance performance with this approach. These strategies include doping MC with conductive elements or depositing electrochemically active materials like metal oxides and polyaniline (PANI) onto the MC template, creating composite electrodes with synergistic properties [23, 24].

1.6 Problem Statement

Supercapacitors are rapidly emerging as contenders for energy storage, particularly complementing batteries in specific applications like uninterruptible power supplies, power electronics, hybrid energy storage systems, electric vehicles, and hybrid electric vehicles. Their appeal stems from several key advantages. Supercapacitors boast exceptional cycle life, enduring a vast number of charge-discharge cycles without significant degradation, translating to superior long-term performance compared to

batteries. Additionally, minimal internal resistance allows for rapid energy delivery and absorption, making them ideal for applications requiring high power density. Unlike some battery chemistries, supercapacitors can function effectively across a broad temperature range, from very low to relatively high temperatures, offering greater versatility in operating environments. They further excel at delivering and absorbing energy at exceptionally high rates, making them well-suited for applications requiring short bursts of power, such as regenerative braking systems in electric vehicles. While the practical energy density of supercapacitors remains an ongoing area of research, their theoretical energy density suggests significant potential for substantial improvements in energy storage capacity through advancements in materials science and device design. Finally, supercapacitors generally utilize environmentally benign materials and electrolytes, making them an attractive choice from a sustainability perspective compared to some battery technologies [25].

However, a critical challenge currently hindering the widespread adoption of supercapacitors is their limited practical energy density which can be seen by the Ragone plot in Figure 1.3.

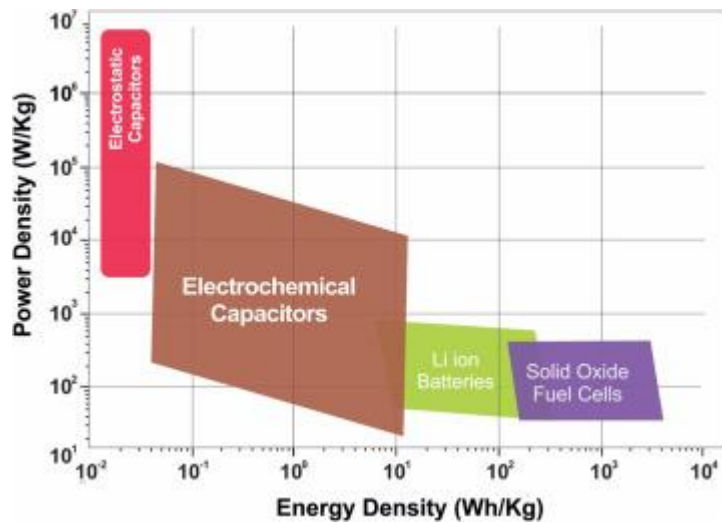


Figure 1.3: Ragone plot among energy storage devices

The plot depicts a comparison between energy and power density of various energy storage devices, and it can be observed that supercapacitors suffer from the lack of

energy density while they possess a substantial amount of power density. This limitation in energy storage capacity often restricts them from directly replacing batteries in all applications. The selection of electrode materials plays a pivotal role in determining the overall performance of supercapacitors. As these materials directly participate in the charge storage mechanisms, their properties significantly influence key parameters such as capacitance, energy density, and cycle life. Therefore, ongoing research efforts in the field of supercapacitors are heavily focused on developing novel electrode materials with optimized properties to address limitations and unlock the full potential of this promising energy storage technology.

Researchers are actively exploring various electrode materials that exhibit pseudocapacitive behavior. These materials hold significant promise for supercapacitors due to their ability to deliver enhanced capacitive performance, ultimately leading to higher energy density. Transition metals have emerged as frontrunners in this field due to their unique combination of desirable properties.

One key advantage of transition metals is their abundance in nature. This readily available source translates to cost-effective and sustainable electrode materials, making them an attractive proposition for large-scale production. Additionally, transition metals can be synthesized with precisely controlled morphologies. This allows researchers to engineer electrodes with high surface area, a critical factor for maximizing the amount of energy a supercapacitor can store. Furthermore, transition metals generally exhibit good chemical stability. This ensures that the electrode materials can withstand the repeated charge-discharge cycles experienced during supercapacitor operation without significant degradation, leading to improved long-term performance and durability[26].

Another significant advantage of transition metals for supercapacitor electrodes is their inherent electrical conductivity. This property allows for efficient electron transport throughout the electrode, minimizing internal resistance and facilitating rapid charge and discharge processes. Finally, the ability of transition metals to exist in multiple oxidation states unlocks additional faradaic charge storage mechanisms. These mechanisms go beyond the simple electrostatic interactions seen in traditional capacitors and contribute to further enhancing the overall capacitance of the electrode [26].

Examples of promising transition metal oxides identified in the literature for supercapacitor electrodes include RuO_2 [27], MnO_2 [28], NiO [29], V_2O_5 [30], Co_3O_4 [31], and CuO [32]. These materials not only boast exceptional theoretical capacities, indicating their potential for high energy storage, but also exhibit good reversibility. Good reversibility signifies that the charge storage processes are highly efficient, minimizing energy losses during the charging and discharging cycles. Among them, MnO_2 has been considered as a promising supercapacitor electrode material due to low cost as compared to its counterparts, environmental friendliness and a superior theoretical capacitance of 1370 Fg^{-1} [33]. In subsequent investigations, diverse morphologies, and polymorphs of MnO_2 were explored to gain deeper insights into its charge storage mechanism. Nonetheless, notable constraints emerged, including inadequate electronic conductivity [34], partial dissolution [28], and irreversible volume expansion during cycling [35]. These drawbacks pose obstacles to the real-world utilization of pure MnO_2 as an electrode material in supercapacitor applications.

Composite materials combining carbon-based substances with MnO_2 exhibit superior electrochemical performance due to several contributing factors, including their large specific surface area, excellent cyclic stability, efficient electron and ion transport capability, and high current conductivity. Carbon nanotubes (CNTs), among various carbon-based materials like graphene, activated carbon, and carbon powders previously discussed, represent a type of one-dimensional tubular carbon nanomaterial with a specific surface area ranging from approximately 200 to $800 \text{ m}^2\text{g}^{-1}$ and electrical conductivity in the range of 1000 to 2000 Scm^{-1} [34]. CNTs not only have good electronic and mechanical properties but also possess good chemical stability when combined in a composite. Combining CNTs with MnO_2 addresses MnO_2 's instability and low electrical conductivity, while MnO_2 enhances the composite's specific capacitance and surface area. Unfortunately, binary nanocomposites comprising MnO_2 face obstacles like inadequate electroactive mass loadings, processing difficulties, high production expenses, and limited capacitance, constraining their commercial feasibility [36]. As a result, approaches integrating three or more components have been implemented to foster synergistic effects within the device. This strategy seeks to improve capacitive performance, as well as charging and discharging kinetics, while extending cycle life.

In the quest for superior supercapacitor electrodes, researchers are exploring MnO₂-based ternary composites. These combine MnO₂, a promising pseudocapacitive material, with other functional components like graphene (conductivity) and conducting polymers (pseudocapacitance) to achieve synergistic effects. Examples from the literature include Graphene / MnO₂/PANI [37], CarbonFiber/MnO₂/PANI [38], α -Fe₂O₃/MnO₂/rGO [39], MnO₂/Graphene/CNT [40], and Carbonnanotube@MnO₂@Polypyrrole [41]. Each of these composites offers unique advantages, with the specific combination of materials influencing factors such as conductivity, surface area, and faradaic activity. For instance, graphene provides excellent electrical conductivity, while carbon fiber offers a robust structure. Meanwhile, conducting polymers like PANI can contribute additional pseudocapacitance. Continued investigation of these and other MnO₂-based ternary composites holds significant promise for the development of next-generation supercapacitors with improved energy storage capabilities.

However, researchers are also exploring alternative materials beyond MnO₂. Cerium oxide (CeO₂), a rare earth metal oxide, has attracted attention due to its exceptional chemical properties. Notably, CeO₂ exhibits reversible conversion between Ce³⁺ and Ce⁴⁺ during charge and discharge cycles [42]. This redox reaction contributes to high pseudocapacitance, long cyclic stability, and desirable electrochemical behavior in supercapacitor electrodes. Despite these advantages, CeO₂ suffers from limitations such as inadequate structural stability and low intrinsic conductivity. The reduction of Ce⁴⁺ to Ce³⁺ leads to lattice expansion, potentially causing structural degradation. Additionally, CeO₂ on its own lacks sufficient electrical conductivity for efficient electron transport [42]. Therefore, researchers are focusing on composite electrodes where CeO₂ is combined with metal oxides and carbon materials. These composites aim to address the limitations of CeO₂ by leveraging the synergistic effects of each material. Metal oxides can enhance faradaic activity and cyclability, while carbon materials improve electrical conductivity and structural stability. By optimizing these composite structures, researchers hope to unlock the full potential of MnO₂ for high-performance supercapacitors.

1.7 Objective of the Study

To address limitations in supercapacitor energy density, rate capability, cycle life, and cost, this research aims to develop advanced electrode materials and optimize their design for high-performance and sustainable energy storage through the following objectives:

1. Synthesis of MnO_2 , binary, and ternary composites for electrode materials for supercapacitors.
2. Characterization of material properties of the MnO_2 and its binary and ternary composite
3. Optimization of electrochemical properties of MnO_2 and its binary and ternary composite
4. Supercapacitor device fabrication of the optimized electrode for enhanced energy and power density

CHAPTER 2: LITERATURE REVIEW

2.1 History of Conventional Capacitors

Grasping the fundamental principles of conventional capacitors is crucial before exploring the intricate mechanisms and diverse types of supercapacitors. Conventional capacitors, categorized as passive electronic components, possess a straightforward design. They consist of two electrically conducting plates positioned in proximity, separated by an insulating dielectric material.

The history of electrical charge storage can be traced back to the Leyden jar experiment in 1745, conducted by Ewald Georg von Kleist and Pieter van Musschenbroek in Leiden. This pioneering device consisted of a glass jar lined with tin foil on the inner and outer surfaces, with a gap at the mouth to prevent accidental discharge. A metal rod electrode extended through the jar's lid and connected to the inner foil via a hanging chain, facilitating the charging process. Charge was transferred from a friction machine to the inner foil, while the outer foil remained grounded.

The presence of equal and opposite charges on the two separated surfaces enabled current flow when a connection was established [43]. This groundbreaking experiment paved the way for the development of various conventional capacitor technologies. In 1876, Desmond Fitzgerald introduced the paper capacitor, constructed by attaching metal foils to a waxed paper sheet and rolling it into a cylindrical shape [44]. The year 1896 witnessed the patenting of the first electrolytic capacitor, which utilized an etched aluminum foil with minimal impurities and alumina as the dielectric material [45]. The evolution of capacitors continued throughout the 20th century, with notable advancements including mica dielectric capacitors (1909), polyethylene terephthalate (PET)-based capacitors (1941), and plastic dielectric capacitors (1959) [46].

However, these historical capacitors have a serious limitation in practicability as they are not useful at a large scale. The two classifications of conventional capacitors are

dielectric capacitors and electrolytic capacitors. The basic structure of a dielectric capacitor has been shown in Figure 2.1.

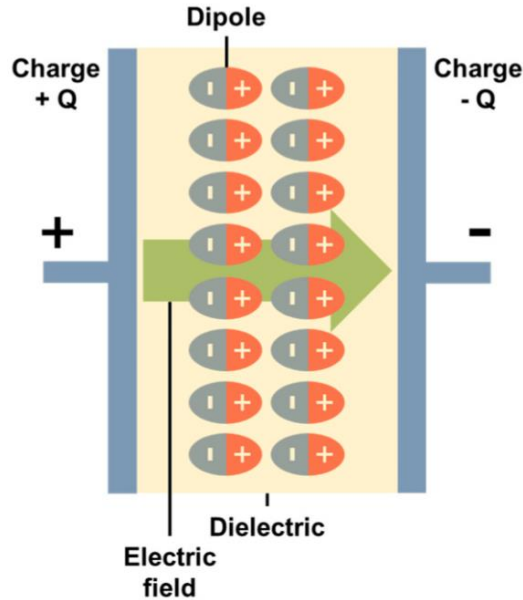


Figure 2.1: *Schematic of a dielectric capacitor*

It consists of dielectric materials and charge storage in it is due to the polarization of the dipole around the electrode and dielectric interface. An electrolytic capacitor consists of solid or liquid ionic conductor as an electrolyte, the charge storage mechanism proceeds when the cations are accumulated at interface between the electrolyte and negative electrode and same goes for the anions [47]. Compared to dielectric capacitors, electrolytic capacitors have an advantage in storing charges due to their greater mobility of electrons. Typically, the capacitance of an electrolytic capacitor is on the order of millifarads (mF), while dielectric capacitors store charge in microfarads (μF). Materials used for dielectric capacitors include polymers, ceramics, and their composites.

Although they offer various advantages, they also suffer from limitations. For example, polymers have the benefits of a strong breakdown field, low dielectric loss, convenient processing conditions, and flexibility. However, their major disadvantage is their inferior permittivity and weak thermal stability. Typical polymers utilized in dielectric capacitors include polyvinylidene fluoride and its copolymers, biaxially oriented

polypropylene (BOPP), polyethylene terephthalate, polycarbonate, and polyimide [48, 49]. The ceramic dielectrics exhibited elevated permittivity and satisfactory thermal stability; however, they experienced reduced breakdown strength [50, 51]. The lead-containing ceramics like $(1-x)[\text{Pb}(\text{Mg}_{1/3}\text{Nb}_{2/3})\text{O}_3]_x[\text{PbTiO}_3]$ (PMN–PT), $(\text{Pb}_{1-x}\text{La}_x)(\text{Zr}_y\text{Ti}_{1-y})_{1-x/4}\text{O}_3$ (PLZT), and $\text{PbZr}_x\text{Ti}_{1-x}\text{O}_3$ (PZT), as well as lead-free ceramics such as BaTiO_3 , AgNbO_3 , and NaNbO_3 , have been extensively investigated for capacitor applications [52].

To overcome the limitations of conventional capacitors, ceramic-based composites and polymer-based composites are a very interesting approach. In their research, Zhang et al. emphasized the importance of developing polymer nanocomposite dielectrics. They then analyzed the crucial material properties required for two specific types of these composites: those containing conductive nanoparticles and those containing ceramic nanoparticles [53]. Fan et al. provided a thorough analysis of recent developments in polymer-based film dielectrics. They focused on detailed methods for improving the performance of these films, exploring two main strategies: incorporating nanocomposites and using all-polymer dielectrics [54]. Recently, multilayer ceramic capacitors (MLCCs) are experiencing a boom in popularity across various sectors like smartphones, portable pseudocapacitors, and the automotive industry.

This surge in demand is driven by their ability to act as guardians of electronic devices. MLCCs control the flow of current within circuits, prevent unwanted electrical noise, and ultimately protect these devices from potential breakdowns [55]. Film capacitors have also attracted significant research attention due to their superior dielectric strength and volumetric energy density compared to bulk capacitors.

This advantage arises from the inverse relationship between dielectric strength and the thickness of the dielectric material [56]. A recent study by Pan et al. demonstrated a significant improvement in the energy storage capabilities of relaxor ferroelectric (FE) films. They achieved this by employing a super-period (super-PE) design in samarium-doped bismuth ferrite-barium titanate composites. This approach yielded an impressive energy density of 152 J/cm^3 while maintaining high efficiency (greater than 90%) at an electric field of 3.5 MV/cm [53].

2.2 Origin and Development of Supercapacitors

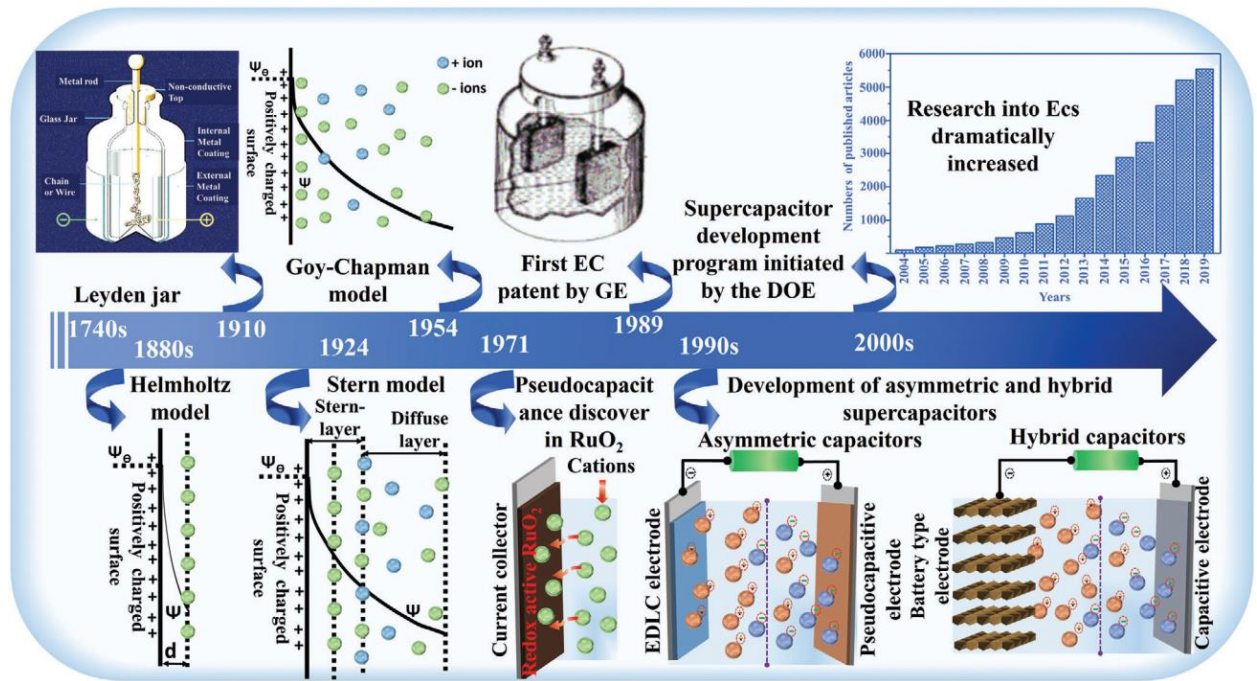


Figure 2.2: Historical development of supercapacitor

The development of the supercapacitor, an electrochemical energy storage device known for its exceptional power density and rapid charge/discharge capabilities, boasts a rich history with roots extending far beyond its recent commercialization. This review delves into the key milestones that shaped this technology, highlighting the contributions of pioneering researchers and the evolution of scientific understanding.

The narrative begins in the 18th century with the invention of the Leyden jar in 1745. While not a direct precursor to the supercapacitor, the pioneering work of German cleric Ewald Georg von Kleist and Dutch scientist Pieter van Musschenbroek marked the dawn of capacitor technology. This early device laid the foundation for comprehending electrical charge storage principles, paving the way for future advancements. The 19th century witnessed a significant contribution from Hermann von Helmholtz, a German physicist whose groundbreaking work shed light on the fundamental mechanisms governing charge storage in capacitors. His development of the first electrical double layer

model, utilizing a colloidal solution, provided a crucial explanation for the behavior of static electricity, a phenomenon previously shrouded in mystery [57].

The 20th century ushered in a period of rapid progress for supercapacitor development. The 1950s saw H. I. Becker of General Electric secure a patent for the first electrochemical capacitor. This invention, featuring porous carbon electrodes immersed in an aqueous electrolyte solution, offered a glimpse into the potential of high-performance energy storage. However, limitations in the operating voltage window hindered its immediate commercialization [58].

Undeterred by this setback, the quest for the supercapacitor continued. Robert Rightmire, a researcher at Standard Oil Co. of Ohio (SOHIO), achieved a significant breakthrough in the following years. His patent described an electrochemical capacitor that employed a nonaqueous electrolyte, leading to a substantially higher working voltage window (3.4-4 volts) and paving the way for enhanced performance [59].

Finally, in 1978, the tireless efforts of researchers culminated in a landmark achievement. Nippon Electric Corporation (NEC) successfully commercialized the first viable supercapacitor, leveraging the groundbreaking nonaqueous electrolyte technology developed by SOHIO. This marked a pivotal moment, demonstrating the practical applications of supercapacitors and opening the door for their widespread adoption [59].

Following the initial commercialization of supercapacitors in the late 1970s, the 1980s witnessed a period of significant advancement. A key development during this decade was the discovery of pseudocapacitance. This phenomenon, characterized by the involvement of Faradaic processes, offered a pathway towards achieving higher capacitance values in supercapacitors. Faradaic processes involve electron transfer across the electrode-electrolyte interface, leading to additional charge storage mechanisms beyond the pure electrostatic effects observed in conventional capacitors [60].

The discovery of pseudocapacitance opened doors for the development of high-performance supercapacitors. These devices boasted improved energy density, making them more attractive for a wider range of applications. However, a significant challenge

remained: the high cost of materials. This factor limited the commercial viability of these advanced supercapacitors, restricting their use primarily to military applications where cost considerations were less critical. Recognizing the potential of supercapacitors, the U.S. Department of Energy (DoE) initiated a crucial initiative in 1989. The DoE's focus on high-energy-density supercapacitors spurred research efforts and fostered collaborations between government agencies and private companies. Notably, this period saw the DoE partnering with companies like Maxwell Technologies, a leading player in the development and manufacturing of energy storage devices. These collaborations aimed to address the cost and performance limitations hindering the broader adoption of supercapacitors [61].

Since 2000, research in the field of supercapacitors has surged, driven by the escalating demand for energy storage solutions in modern society. Supercapacitors are capable of delivering high power density, excellent rate capability, and extended cycle life, establishing them as a critical area of investigation. Moreover, they offer a safety advantage over other electrochemical energy storage devices. The diverse charge storage mechanisms inherent in various supercapacitor devices underscore the need for continued and intensive research in this domain.

2.3 Classification of Supercapacitors

Supercapacitors, both those commercially available and those still under development, can be broadly classified into three main groups for easier understanding. These categories are:

1. Symmetric Supercapacitors
2. Asymmetric Supercapacitors
3. Hybrid Supercapacitors

This classification highlights the importance of cell designs, electrode materials and the fundamental operating principles such as physical or chemical processes, or a combination of the two. By recognizing these key categories and the underlying factors that influence them, researchers and engineers can develop supercapacitors tailored for

specific applications. This classification system serves as a valuable tool for navigating the diverse landscape of supercapacitor technology.

2.4 Symmetric Supercapacitors

Symmetric supercapacitors, the forerunners of modern Electric Double-Layer Capacitors (EDLCs), represent a straightforward and well-established design approach. The term "symmetric" aptly describes their defining characteristic: the use of identical electrode materials. Typically, both electrodes are constructed from a single material, such as activated carbon, with similar design features and, in practical terms, the same amount of material (mass loading) on each electrode.

This design philosophy ensures that the primary charge storage mechanism operates in the same way on both electrodes. This mechanism can be physical (electrostatic attraction), chemical (redox reactions), or a combination of both. Regardless of the specific process, its consistency across both electrodes defines the core functionality of symmetric supercapacitors.

The two major classes of symmetric supercapacitors that can be included in the symmetric category are:

- I. Electric double-layer capacitors (EDLC)
- II. Pseudocapacitors

2.4.1 Electric Double Layer Capacitors (EDLC)

Electric double-layer capacitors (EDLCs) exhibit a functionality that is shared with conventional capacitors – the capacity to store electrical energy. However, EDLCs employ a distinct mechanism to achieve this objective. Unlike their conventional counterparts, which rely on the dielectric layer within their structure, EDLCs leverage the interfacial region between their electrodes and the electrolyte solution.

This interfacial region plays a critical role in EDLC operation. When a voltage is applied, an "electric double layer" forms at this interface. This layer is characterized by a

separation of charges. Positive ions from the electrolyte accumulate on the surface of the electrode, attracted by the opposing charge applied. This accumulation creates a region of stored energy, readily available for release when required [62].

A key advantage of EDLCs lies in their remarkable reversibility. The charge storage and discharge processes within them are purely physical phenomena, involving the movement and separation of ions. In contrast to batteries, which undergo chemical reactions during charge and discharge cycles, EDLCs do not experience any material transformations. This characteristic translates to a demonstrably extended cycle life, as the electrodes are not subjected to degradation through chemical reactions [63].

While the capacitance (the ability to store charge) of a conventional capacitor is dictated by the thickness of the dielectric separator, as expressed in Equation 1.2, EDLCs operate on a different principle. Their capacitance is primarily determined by the thickness of the electric double layer formed at the electrode/electrolyte interface. This double layer is significantly thinner compared to the separator in a conventional capacitor. According to Equation 1.2, this implies that EDLCs possess the inherent capability to achieve considerably higher capacitance values compared to their conventional counterparts.

Carbon is abundant, lightweight, and an exceptional conductor, available in a variety of morphologies, ranging from 1D to 3D structures. The carbon utilized in supercapacitors boasts a specific surface area (SSA) of 1000 m²/g. In the fabrication of EDLC electrodes, three primary types of carbon-based materials are commonly employed. The first category comprises carbon aerogels, carbon foams, and carbide-derived carbon (CDC) materials. The second includes carbon nanotubes (CNTs) and graphene, while the third type encompasses activated carbon (AC) [64].

In essence, EDLCs exploit the power of interfaces to create a highly efficient and durable energy storage solution. Their unique charge storage mechanism and exceptional cycle life make them valuable assets in diverse applications demanding rapid charge/discharge cycles and extended operational lifespans.

2.4.2 Pseudocapacitors

The term "pseudocapacitor" originates from the Greek word "pseudés," translating to "false" or "erroneous." This nomenclature reflects the distinct charge storage mechanism employed by these devices, which diverges significantly from that of Electric Double-Layer Capacitors (EDLCs). As defined by B. E. Conway, pseudocapacitors, also referred to as Faradaic supercapacitors, rely on rapid and reversible Faradaic redox reactions occurring at the electrode-electrolyte interface for energy storage [65]. The pseudocapacitance, C_{PC} for the electrode material storing charge, Δq with an operating window of ΔV is given by Eq (1.5) [66]:

$$C_{pc} = \frac{d(\Delta q)}{d(\Delta V)} \quad (1.5)$$

In contrast to EDLCs, where charge accumulation primarily stems from the formation of an electric double layer, pseudocapacitors predominantly utilize Faradaic processes such as electrosorption, redox reactions, and intercalation. The reliance on Faradaic mechanisms in pseudocapacitors enables them to achieve substantially elevated energy densities compared to EDLCs, often exhibiting a doubling of capacity. However, this enhancement in energy storage comes at the expense of reduced cycle life.

The Faradaic reactions underpinning pseudocapacitive charge storage are characterized by relatively slow kinetics and can induce volume expansion of the electrode material during repeated charge-discharge cycles, consequently compromising the device's longevity.

Despite the fundamental differences in charge storage mechanisms, pseudocapacitive materials share certain electrochemical characteristics with EDLC materials. Both exhibit quasi-rectangular cyclic voltammetry (CV) curves and nearly linear galvanostatic charge-discharge (GCD) profiles. These similarities in electrochemical behavior have contributed to the classification of pseudocapacitors as a subset of supercapacitors [63, 66].

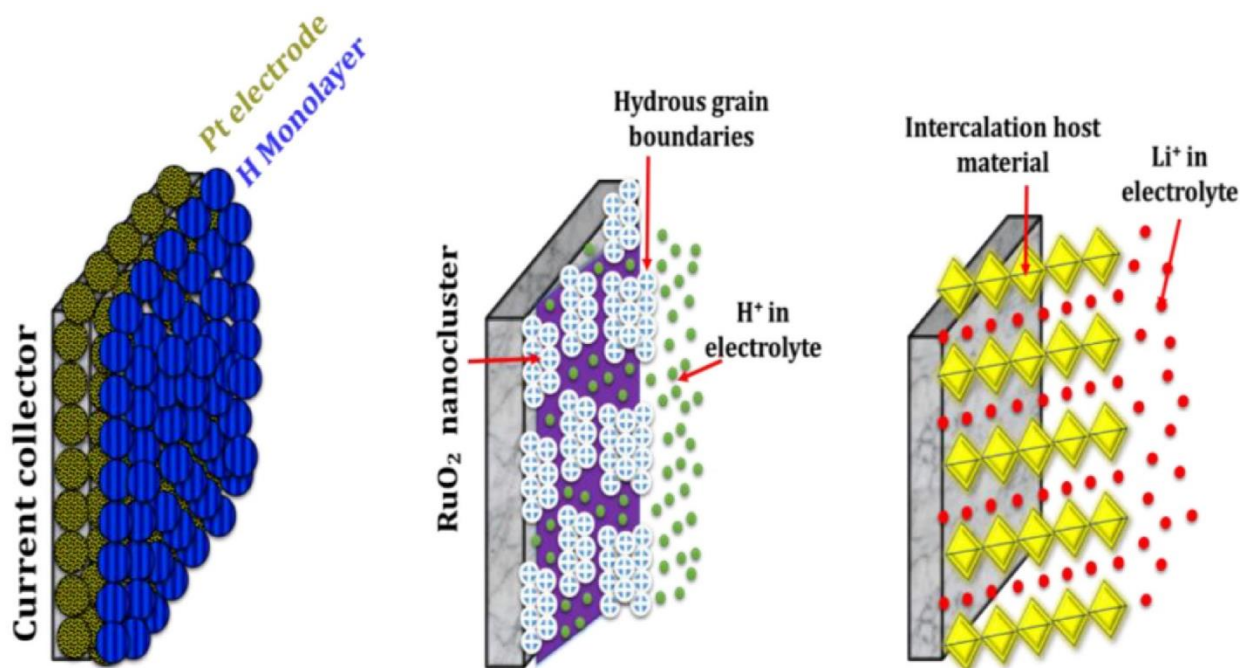


Figure 2.3: *Schematic of pseudocapacitance mechanisms*

Scientists and researchers have categorized pseudocapacitance mechanisms into three different kinds i.e., (1) Underpotential deposition (2) Redox reactions (3) Intercalation/de-intercalation [67]. Figure 2.3 shows the schematic representation of these mechanisms. Underpotential deposition involves the deposition of a monolayer of metal ions on the surface of another metal at a potential higher than their redox potential, a phenomenon that is rarely observed. Redox pseudocapacitance, also known as intrinsic pseudocapacitance or surface redox pseudocapacitance, is the most common type of pseudocapacitive charge storage mechanism. This mechanism involves ion adsorption on or near the material surface through faradaic redox reactions, predominantly occurring in aqueous electrolytes such as H_2SO_4 , KOH , Na_2SO_4 , NaOH , KCl , and NH_4Cl , which are used in supercapacitors. The electrochemical response of intrinsic pseudocapacitors closely resembles that of EDLC materials, exhibiting quasi-rectangular cyclic voltammetry (CV) curves and quasi-triangular galvanostatic charge-discharge (GCD) curves. However, this does not imply that charge storage occurs solely through the formation of the electric double layer (EDL). Instead, the material stores charge through both double layer formation and surface redox mechanisms. The rapid faradaic redox reactions in

pseudocapacitors lead to an electrochemical response similar to that of EDLCs. Typical materials exhibiting intrinsic pseudocapacitive behavior include conducting polymers (CPs) and transition metal oxides (TMOs) such as RuO_2 , MnO_2 , Mn_3O_4 , MnOOH , and iron oxide.

Intercalation pseudocapacitance arises from faradaic redox reactions due to the intercalation of electrolytic ions into the stacked layers of redox-active electrode materials. This type of charge storage predominantly occurs in non-aqueous electrolyte systems. Unlike surface-limited redox processes, intercalation pseudocapacitance involves the bulk material, utilizing it for faradaic redox reactions. Typical materials exhibiting intercalation pseudocapacitive charge storage include transition metal oxides (such as MoO_3 , Nb_2O_5 , TiO_2 , WO_3 , V_2O_5) and transition metal sulfides (such as MoS_2 , TiS_2 , VS_2) [68-70].

2.5 Asymmetric Supercapacitors

Asymmetric capacitors (ASCs) represent a unique class of energy storage devices that leverage the strategic design of their electrodes to achieve optimized performance. Unlike conventional or symmetric supercapacitors, which utilize electrodes with similar characteristics, ASCs employ electrodes with intentionally disparate capacitances. This disparity is achieved through the selection of electrode materials with inherently different specific capacitances.

Within an ASC, one electrode, known as the positive electrode, is specifically chosen for its superior specific capacitance. This translates to a significantly higher absolute capacitance value compared to the other, "negative" electrode. Interestingly, the physical size of the larger, positive electrode can be comparable to, or even smaller than, the smaller capacitance electrode. This seemingly counterintuitive design approach is crucial for optimizing the overall performance of the ASC [71]. Asymmetric supercapacitors (ASCs) enhance the charge and discharge processes by providing distinct potential windows for each electrode, thereby increasing the device's operational voltage. Unlike aqueous-based symmetric systems, which are typically limited to about 1.2 V, ASCs can achieve operating voltages exceeding 2.0 V, significantly boosting their energy density.

By strategically selecting materials with a significantly higher specific capacitance for the positive electrode, even when its physical size is smaller, the overall capacitance of the ASC can be maximized. This optimization allows for the achievement of a higher energy density compared to a symmetric supercapacitor with electrodes of equal capacitance.

The concept of asymmetric supercapacitors (ASCs) emerged with the pioneering work of Amatucci et al. in 2001. This innovative design approach has since attracted considerable research interest, with numerous groups striving to unlock its full potential. A compelling example of this progress is the work of Wu et al. (2010). They successfully assembled an ASC utilizing MnO₂ nanowires and graphene, achieving an impressive energy density of 30.4 Wh/kg. This value stands in stark contrast to the significantly lower energy densities observed in symmetric supercapacitors composed entirely of graphene (2.8 Wh/kg) or MnO₂ (5.2 Wh/kg). This stark difference highlights the remarkable potential of ASCs to significantly enhance energy storage capabilities [72].

Further advancements were made by Fan et al. (2011). They incorporated MnO₂ directly into graphene, creating a composite electrode. This electrode was then paired with an AC nanofiber-based electrode to form an ASC. This design yielded an outstanding energy density of 51.1 Wh/kg, further solidifying the promise of ASC technology [72].

Commercial applications are also emerging. Fuji Heavy Industry developed a commercially available ASC utilizing lithium-ion-doped activated carbon electrodes. This device boasts an energy density of up to 25 Wh/kg (Naoi and Simon, 2008) [72].

It is important to acknowledge a trade-off inherent in ASC design. While the inclusion of Faradaic materials like MnO₂ can significantly boost energy density, it may come at the expense of cycle stability – the ability of the device to maintain performance over repeated charge/discharge cycles [72].

2.6 Hybrid Supercapacitor

Hybrid supercapacitors represent a sophisticated advancement in energy storage technology, characterized by the strategic combination of distinct electrode materials and

chemistries to optimize overall performance. This approach aims to transcend the limitations of conventional supercapacitors by creating a synergistic system that capitalizes on the complementary attributes of its constituent components.

A primary objective of hybrid supercapacitor research is to bridge the performance gap between conventional supercapacitors and electrochemical batteries. By meticulously selecting and integrating electrode materials, researchers endeavor to enhance energy density, power capability, and cycle life while simultaneously mitigating costs. This involves exploring a wide array of configurations, including those that incorporate elements from conventional electrolytic capacitors.

The fundamental architecture of a hybrid supercapacitor comprises two electrodes composed of disparate materials that operate through distinct mechanisms. One electrode typically exhibits pseudocapacitive behavior, characterized by Faradaic reactions, while the other displays capacitive behavior, relying on the formation of an electric double layer. This heterogeneous composition enables hybrid supercapacitors to harness the advantages of both electrode types, resulting in a device that often surpasses the performance metrics of its individual components [63].

Three primary categories of hybrid supercapacitors have emerged:

- I. Hybrid electrolytic capacitors
- II. Composite supercapacitors
- III. Battery-like supercapacitors

By carefully selecting and combining different electrode materials and chemistries, hybrid supercapacitors offer the potential to create energy storage devices that excel in both energy density and power delivery. This combination is particularly advantageous for applications that demand high levels of both energy and power, such as electric vehicles, renewable energy integration, and portable electronics. Additionally, the ability to tailor the properties of hybrid supercapacitors through material selection and design provides opportunities for optimizing performance for specific applications. Ultimately, hybrid

supercapacitors represent a promising avenue for advancing energy storage technology and addressing the growing demand for high-performance energy storage solutions.

2.7 Components of Supercapacitors

A supercapacitor, a high-performance energy storage device, is composed of four primary components, each playing a crucial role in its overall functionality:

- I. Electrode
- II. Electrolyte
- III. Separator
- IV. Current collector

The synergistic interplay of electrodes, electrolyte, separator, and current collector within a supercapacitor enables the rapid storage and release of electrical energy. This unique combination of components empowers supercapacitors to excel in applications demanding high power density, rapid charge-discharge cycles, and extended lifespan. The careful selection and optimization of these components are paramount in determining the overall performance and suitability of a supercapacitor for specific applications. As technology advances, ongoing research and development efforts continue to explore novel materials and designs to push the boundaries of supercapacitor performance, unlocking their full potential for a wide range of energy storage challenges.

2.8 Electrode

The electrode constitutes a pivotal component within a supercapacitor, exerting a profound influence on the device's overall performance. At the core of its function lies the capacity to store electrical charge when subjected to an applied potential. This charge accumulation is essential for the energy storage capabilities of the supercapacitor [73].

To facilitate efficient energy transfer, the electrode material must exhibit high electrical conductivity. This property ensures unimpeded electron transport between the

electrode and the external circuit, optimizing the device's power delivery characteristics. The essential conditions for the standard electrode are as follows [74, 75]:

- A paramount attribute of an optimal electrode material is a substantial specific surface area. This characteristic is crucial for maximizing the interaction between the electrode and the electrolyte ions. An expansive surface area effectively exposes a greater proportion of the electrode material to the electrolyte, thereby facilitating an increased density of charge accumulation at the interface. Consequently, this augmented interaction leads to an enhancement in both specific capacitance and energy density of the electrode material. In essence, a high specific surface area provides a more extensive region for electrochemical reactions to occur, resulting in improved overall performance of the supercapacitor.
- The porosity of an electrode material, specifically the size and distribution of pores, exerts a substantial influence on its electrochemical performance, notably specific capacitance and rate capability. For optimal performance, pore dimensions must exceed the size of electrolyte ions to facilitate their adsorption onto the electrode surface. This adsorption process is fundamental to charge storage within the supercapacitor. A judicious control over pore size distribution is essential. Micropores, characterized by their diminutive dimensions, contribute significantly to specific capacitance by providing ample surface area for ion adsorption. Conversely, mesopores and macropores, with their larger dimensions, enhance ion transport within the electrode structure, thereby improving rate capability. A balanced pore size distribution is often desirable to achieve an optimal combination of energy and power density.
- High electronic conductivity is a paramount attribute of an electrode material, significantly influencing the supercapacitor's rate capability and power density. This property facilitates the efficient transfer of electrons between the electrode and the external circuit by minimizing electrical resistance. A material with superior electronic conductivity enables rapid charge and discharge processes,

thus enhancing the device's ability to deliver high power outputs. Conversely, low conductivity impedes electron transport, leading to energy losses and diminished performance.

- The presence of electroactive sites on the electrode surface is crucial for enhancing supercapacitor performance. These sites function as anchors for electrolyte ions, facilitating their adsorption and subsequently contributing to the pseudocapacitive behavior of the electrode material. Electroactive species, such as oxygen and nitrogen functional groups, are commonly incorporated to increase the density of these sites. Beyond their role in charge storage, these functional groups also contribute to the electrode's overall conductivity, further augmenting its performance.
- The longevity and performance of a supercapacitor are significantly influenced by the electrode's ability to withstand the rigors of repeated charge-discharge cycles. During these cycles, the movement of ions within the device can generate heat, necessitating electrodes with robust thermal stability to prevent degradation. Moreover, the electrode material must exhibit resistance to chemical degradation and corrosion to maintain structural integrity and optimal functionality over time. These attributes collectively contribute to the overall lifespan and reliability of the supercapacitor.
- Beyond the technical attributes, the economic viability and environmental impact of electrode materials are paramount. A low-cost electrode material significantly contributes to reducing the overall manufacturing cost of the supercapacitor, thereby enhancing its commercial competitiveness. Moreover, the utilization of environmentally benign materials aligns with sustainability goals and minimizes the device's ecological footprint. These factors, coupled with the technical performance metrics, are crucial in the development of commercially viable and sustainable supercapacitors.

2.9 Electrolyte

The electrolyte serves as a critical component in electrochemical energy storage systems, with its physical and chemical characteristics significantly influencing the overall efficiency and performance of the cell. It plays a pivotal role in determining the device's capacitance, energy density, power density, rate capability, cycle life, and safety, while also maintaining charge equilibrium between the two electrodes. The selection of electrolytes is a key consideration, as it profoundly impacts the electrode-electrolyte interface. However, an ideal electrolyte that fulfills all the criteria for supercapacitor applications has yet to be discovered. The fundamental requirements for electrolytes in electrochemical devices are as follows [76]:

- The dimensions of ions within the electrolyte exert a substantial influence on supercapacitor performance. A direct correlation exists between ionic size and capacitance, with smaller ions demonstrating superior mobility. These smaller ions exhibit enhanced capability to diffuse into the intricate pore structure of the electrode and subsequently adsorb onto its surface. This augmented interaction between electrolyte ions and the electrode material significantly contributes to improved overall supercapacitor performance, including increased capacitance and rate capability [77].
- The electrolyte's conductivity is a critical factor determining the overall performance of a supercapacitor. A highly conductive electrolyte facilitates the rapid transport of ions between the electrodes, thereby enhancing the device's power density and rate capability. The electrolyte's ionic conductivity is influenced by several factors, including the concentration of charge carriers, the mobility of ions, and their valency. Aqueous electrolytes, such as sulfuric acid (H_2SO_4) and potassium hydroxide (KOH), generally exhibit higher conductivity compared to their non-aqueous counterparts due to their lower viscosity. This lower viscosity enables ions to move more freely within the solution, leading to improved ionic conductivity. The specific conductivity of electrolytes follows a general trend: $\text{H}_2\text{SO}_4 > \text{KOH} > \text{KCl} > \text{Na}_2\text{SO}_4$. It is

essential to note that ionic size also plays a role in conductivity, as smaller ions tend to exhibit higher mobility in solution.

- An ideal electrolyte must readily dissociate into its constituent ions when dissolved in a solvent. This dissociation process is crucial as it minimizes internal resistance within the supercapacitor, thereby enhancing its overall performance. The specific conductance of an electrolyte, a measure of its ability to conduct electricity, is influenced by both the concentration of ions and the degree to which the electrolyte dissociates. Strong electrolytes, which fully dissociate in solution, exhibit higher specific conductance compared to weak electrolytes that only partially ionize.
- The electrochemical stability of an electrolyte is a crucial parameter influencing the overall safety and performance of a supercapacitor. This stability is determined by two primary factors: the interaction between the electrolyte and the electrode material, and the intrinsic properties of the electrolyte's constituent elements. A chemically compatible electrolyte minimizes side reactions with the electrode, preventing degradation and ensuring prolonged device life. Additionally, the electrolyte should exhibit resistance to electrochemical decomposition under operating conditions to maintain safety and prevent the formation of hazardous byproducts.
- The electrolyte's ability to withstand varying temperatures is crucial for optimal supercapacitor performance. Thermal stability becomes particularly important during rapid charge-discharge cycles, which can generate heat. The electrolyte's composition, including the specific salt, solvent, and any additives, significantly influences its thermal stability. An electrolyte that undergoes minimal degradation or phase changes under temperature fluctuations ensures the sustained performance and safety of the supercapacitor.

Electrolytes for electrochemical devices are generally classified into three categories:

- a. aqueous electrolytes,
- b. organic electrolytes,
- c. ionic electrolytes.

Among these, aqueous electrolytes exhibit high conductivity and capacitance at a relatively low cost. However, their limited operating voltage window results in a lower energy density, attributed to the electrolysis of water, which occurs at a potential difference of 1.23 V. In contrast, organic and ionic electrolytes can function within a higher potential window, but they are hindered by lower ionic conductivity. Organic electrolytes are also toxic and pose handling challenges, while ionic electrolytes are expensive and have limited access to the electrode surface due to the larger size of their ions [78].

2.10 Separator

A separator is a crucial component within a supercapacitor, serving as a protective barrier between the two electrodes. Its primary function is to prevent electrical short circuits while simultaneously facilitating ion transport. An ideal separator possesses the following key characteristics [79]:

- **Electrical insulation:** Prevents direct electrical contact between electrodes.
- **High porosity:** Allows for efficient ion movement between electrodes.
- **Chemical inertness:** Maintains stability in the electrolyte environment.
- **Mechanical strength:** Withstands internal pressures within the device.
- **Thermal stability:** Ensures consistent performance under varying temperatures.
- **Good wettability:** Facilitates electrolyte penetration for optimal ion transport.

- Uniform thickness: Provides consistent performance across the separator area.

By possessing these attributes, a separator significantly contributes to the overall performance, safety, and longevity of the supercapacitor.

2.11 Current Collector

The current collector plays a crucial role in supercapacitor operation by facilitating electron transport between the electrode and the external circuit. Key attributes include:

- High electrical conductivity: Ensures efficient electron flow, minimizing resistance.
- Corrosion resistance: Maintains integrity in the device's corrosive environment.
- Mechanical strength: Provides structural support to the overall cell.
- Compatibility: Compatible with various electrode and electrolyte materials.

To enhance performance, modern current collectors often employ:

- Nickel mesh: Offers increased surface area for better electrode distribution.
- Metal foams: Provide a three-dimensional structure for improved conductivity.
- Carbon cloth: Combines conductivity with flexibility.

These materials contribute to reduced contact resistance and improved overall supercapacitor efficiency [80].

2.12 Electrode Materials for Supercapacitors

The following section discusses the key electrode materials used in the application of supercapacitors.

2.13 Carbon-based materials

Carbon-based materials are the predominant choice for electrodes in commercially available supercapacitors. This preference is primarily due to their exceptional properties. Carbon electrodes are renowned for their cost-effectiveness, excellent corrosion resistance, superior cyclic stability, extended lifespan, and wide operating temperature range. These attributes, coupled with their high electronic conductivity, make them ideal candidates for energy storage applications [81].

To further enhance the specific capacitance of carbon electrodes, researchers focus on optimizing factors such as pore size distribution and surface functionalization. A well-defined pore structure, characterized by a balance of micropores, mesopores, and macropores, is essential for efficient ion transport and charge storage. Additionally, the introduction of functional groups on the carbon surface can create additional charge storage sites, contributing to improved capacitance [82]. In summary, carbon-based electrodes, with their combination of favorable properties and versatile structure, form the foundation of modern supercapacitor technology. Ongoing research aimed at optimizing pore structure and surface chemistry continues to drive advancements in this field [83].

The emergence of three-dimensional carbon nanostructures, such as activated carbon, carbide-derived carbon, and templated carbon, which possess large surface areas and porous architectures, is anticipated to hold significant promise for supercapacitor applications. However, on the flip side, their specific capacitance is constrained at high current densities, primarily due to their relatively low conductivity and the presence of micropores [84].

In conclusion, carbon nanostructures serve at least two key functions:

- They contribute to the high capacitance of composite materials.
- Due to their high conductivity, they provide efficient pathways for electron transport.

2.13.1 Activated Carbon

Activated carbons are the predominant choice for EDLC electrodes because of their cost-effectiveness. They possess an intricate porous network, featuring micropores (under 2 nm), mesopores (2 to 50 nm), and macropores (exceeding 50 nm), which collectively result in a substantial specific surface area (SSA) [85, 86]. Activated carbon can be produced using either physical or chemical activation methods from various carbon-rich sources such as wood, coal, and nutshells. Chemical activation typically involves using activating agents like sodium hydroxide, potassium hydroxide, or zinc chloride at relatively lower temperatures (400–700°C). In contrast, physical activation involves treating carbon precursors at higher temperatures (700–1200°C) in the presence of oxidizing gases like steam, CO₂, or air [87]. Varying activation processes result in distinct structures and pore sizes, which in turn influence the electrochemical properties that determine supercapacitor performance, yielding capacitance values ranging from 150 to 355 F/g [88].

Several researchers have explored the relationship between specific capacitance and the specific surface area (SSA) of activated carbon, revealing a discrepancy between the two. Despite achieving a high SSA of approximately 3000 m²/g, only a relatively low capacitance was observed, indicating that not all pores are effective in charge accumulation. This suggests that while SSA is crucial for performance in EDLCs, other factors, such as pore size distribution, also play a significant role in influencing the electrochemical performance of carbon materials. Moreover, excessive activation can lead to a large pore volume, which may result in drawbacks like reduced conductivity and material density, ultimately lowering energy density and diminishing power capability [89].

In summary, activated carbons are the most commonly used electrode material and have been widely adopted in commercial applications. However, their primary drawback is the limited energy density, stemming from the challenges in controlling the pore structure. As a result, their performance is constrained by limited energy storage capacity and rate capability.

2.13.2 Carbon Nanotubes

The advent of carbon nanotubes (CNTs) has ushered in a new era of exploration and innovation in the realm of carbon-based materials. A pivotal factor governing the power density of a supercapacitor is the overall internal resistance, encompassing contributions from various components. Owing to their exceptional attributes, CNTs have emerged as a prime candidate for supercapacitor electrode materials [90].

Characterized by a unique pore structure, coupled with robust mechanical and thermal stability, and unparalleled electrical conductivity, CNTs offer a compelling proposition for energy storage applications. These nanostructures are synthesized through the catalytic decomposition of hydrocarbons, where precise control over parameters facilitates the generation of diverse morphologies and crystalline structures [91].

A distinguishing feature of CNTs is their interconnected mesoporous architecture, in stark contrast to other carbon-based electrodes. This unique structure enables a uniform distribution of charge across the accessible surface area, leading to enhanced electrochemical performance. Moreover, the lower equivalent series resistance (ESR) exhibited by CNTs, compared to activated carbon, is attributed to the efficient diffusion of electrolyte ions within the mesoporous network.

Carbon nanotubes (CNTs) can be broadly categorized into two primary types: single-walled carbon nanotubes (SWCNTs) and multi-walled carbon nanotubes (MWCNTs). Both varieties have garnered significant attention as promising electrode materials for supercapacitors. Chunming et al. (2005) successfully prepared carbon nanotube sheet electrodes from catalytically grown CNTs, characterized by a narrow diameter distribution of approximately 80 Å. These electrodes exhibited impressive specific capacitances of 102 F/g and 49 F/g at current densities of 1 Hz and 100 Hz, respectively [92].

Beyond sheet electrodes, thin films of CNTs have also emerged as viable options for energy storage devices. Supercapacitors constructed with CNT thin film electrodes have demonstrated exceptional specific power densities exceeding 20 kW/kg. Furthermore,

the application of CNT coatings over conventional current collectors has been shown to enhance electrode performance, solidifying CNTs as a prime candidate for energy storage applications [93]. Furthermore, Liu et al. [92] conducted a comprehensive study on the influence of electrochemical oxidation on the performance of single-walled carbon nanotube (SWCNT) supercapacitors. Their findings revealed that the introduction of nanosized mesopores and oxygen-containing functional groups through electrochemical oxidation significantly enhanced the specific capacitance of SWCNT electrodes. Notably, the electrochemically oxidized SWCNT supercapacitor demonstrated a remarkable specific capacitance of 113 F/g.

Furthermore, the study highlighted the superior frequency response of the electrochemically oxidized SWCNTs compared to conventional activated carbon supercapacitors. While the knee frequency (the point at which the specific capacitance starts to decline with increasing frequency) of activated carbon supercapacitors was around 316 Hz, the electrochemically oxidized SWCNTs exhibited a much higher knee frequency of approximately 631 Hz, indicating their ability to maintain high performance at higher frequencies.

These results underscore the potential of electrochemical oxidation as a promising strategy for tailoring the properties of SWCNT electrodes and optimizing the performance of supercapacitors.

CNTs can be utilized as electrode materials alongside emerging MXene materials, TMOs, and their composites, which are among the most commonly used electrode materials for supercapacitors.

2.13.3 Graphene

Graphene, a two-dimensional allotrope of carbon, has garnered significant attention as a potential electrode material for supercapacitors due to its exceptional properties. Its structure, consisting of sp^2 hybridized carbon atoms densely packed in a honeycomb lattice, imparts remarkable characteristics.

The most common method for obtaining graphene involves the oxidation of graphite-to-graphite oxide, followed by reduction using a suitable reducing agent like hydrazine solution. This process, often referred to as the Hummers or modified Hummers method, yields graphene with a high specific surface area, excellent thermal and chemical stability, a wide potential window, and good carrier mobility. These properties make graphene an ideal candidate for supercapacitor electrodes [94].

The high specific surface area of graphene ($2630 \text{ m}^2/\text{g}$) is particularly advantageous, as it provides ample surface area for electrolyte ion interaction, leading to enhanced charge storage capacity. Additionally, its excellent thermal conductivity ($5000 \text{ W/m}\cdot\text{K}$) and wide potential window contribute to the overall performance and stability of graphene-based supercapacitors [95].

Graphene-based supercapacitors have demonstrated impressive performance metrics. Studies have reported specific capacitances as high as 205 F/g , energy densities of 28.5 Wh/kg , and power densities of 10 W/g . These figures highlight the potential of graphene-based electrodes for high-performance energy storage devices [96]. Furthermore, flexible thin films fabricated from graphene have showcased exceptional properties. Such films have exhibited electrical conductivities of up to 5880 S/m and high specific surface areas of $2400 \text{ m}^2/\text{g}$. These characteristics translate to promising supercapacitor performance, with reported specific capacitances of 120 F/g and energy densities of 26 Wh/kg [97].

Ruoff and colleagues (2009) pioneered the use of chemically modified graphene (CMG) as an electrode material for EDLCs. Their research demonstrated that controlled agglomeration of individual graphene nanosheets into nanoparticles could lead to a significant enhancement in specific surface area, reaching values as high as $705 \text{ m}^2/\text{g}$. This, in turn, translated to a specific capacitance of 135 F/g [98].

Kannappan et al. (2012) further refined the synthesis of graphene, employing a modified Hummers method in conjunction with tip sonication. This approach yielded supercapacitors with exceptional stability, improved capacitance, and enhanced energy density. Notably, they achieved a discharge capacitance of 195 F/g and an energy density

of 83.4 Wh/kg at a current density of 2.5 A/g. Moreover, the device exhibited a discharge time of 25 seconds at an energy density of 64.18 Wh/kg when operated at 5 A/g [99].

These findings underscore the potential of graphene as a leading material for supercapacitor electrodes, offering a pathway to high-performance energy storage solutions.

2.14 Metal oxides-based materials

Metal oxides are regarded as promising candidates for electrochemical capacitors, with extensive research highlighting their advantageous properties, including low resistance and high specific capacitance. Transition metal oxides, in particular, offer superior specific capacitance, greater chemical stability compared to conductive polymers, and higher energy density relative to carbon-based materials. Commonly used metal oxides for electrochemical capacitors include nickel oxide (NiO), manganese oxide (MnO₂), ruthenium dioxide (RuO₂), iridium oxide (IrO₂), cobalt oxide (Co₃O₄), manganese dioxide (MnO₂), and zinc oxide (ZnO). While ruthenium dioxide is recognized as an optimal material for electrode fabrication due to its excellent performance, its high cost and environmental toxicity pose significant challenges. On the other hand, MnO₂ and ZnO, being abundant and capable of providing good capacitance, are considered suitable alternatives for supercapacitor applications [100].

2.14.1 Ruthenium Oxide

Ruthenium dioxide (RuO₂) has emerged as a leading candidate for energy storage applications due to its exceptional properties. Its unique combination of characteristics, including high electrical conductivity, a wide electrochemical potential window, and excellent redox behavior, makes it an ideal material for electrodes in devices such as supercapacitors.

The ability of RuO₂ to store and release energy rapidly and efficiently is attributed to its high conductivity, which facilitates the rapid transfer of electrons. Additionally, its wide potential window allows for the storage of a large amount of energy per unit mass.

Moreover, RuO₂'s reversible redox reactions ensure its long-term durability and performance.

Kim et al. [101] successfully fabricated a thin film ruthenium oxide electrode using the electrostatic spray deposition technique. This method allowed for the controlled deposition of RuO₂ particles onto a substrate. The resulting electrode exhibited an average specific capacitance of 650 F/g, indicating its potential for energy storage applications.

Park et al. [102] also prepared thin film ruthenium oxide electrodes and investigated the relationship between film thickness and specific capacitance. Their findings revealed that the highest specific capacitance of 788 F/g was achieved with a RuO₂ film thickness of 0.0014 g cm⁻². However, they observed an interesting phenomenon: as the film thickness increased, the specific capacitance decreased despite an overall increase in capacitance. This suggests that there is an optimal film thickness for maximizing the specific capacitance of RuO₂ electrodes.

While RuO₂ offers significant advantages, its high cost remains a challenge. Ongoing research is focused on developing more cost-effective synthesis methods and exploring alternative materials that can leverage the benefits of RuO₂ without the associated expense. As scientists continue to advance in this field, Ruthenium dioxide is poised to play a crucial role in shaping the future of energy storage technologies.

2.14.2 Nickel Oxide

Nickel oxide (NiO) is a promising material for electrodes due to its favorable properties such as chemical and thermal stability, availability, environmental friendliness, and affordability. Researchers have focused on improving NiO's performance by modifying its structure and morphology.

Zheng et al. [103] utilized a hydrothermal method to synthesize NiO and subsequently treated it at low temperatures to obtain nanostructured nickel oxide nanoflakes with a unique sandwich and cauliflower-like arrangement. This modified morphology enhanced the electrode's performance, resulting in excellent cyclic stability.

The NiO sample retained 91.6% of its initial capacitance after 1000 charge-discharge cycles, demonstrating its potential for long-term energy storage applications.

Patil et al. [104] employed a chemical synthesis technique to fabricate nickel oxide thin films on a glass substrate. The initial nickel hydroxide thin films were subjected to annealing at 623 K, resulting in the conversion of the β -phase hydroxide to the cubic phase of nickel oxide. This transformation also led to the formation of a unique honeycomb-like morphology. The resulting NiO electrodes exhibited a specific capacitance of up to 167 F/g, demonstrating their potential as promising candidates for energy storage applications.

The hydrothermal method is a versatile technique for synthesizing nickel oxide (NiO) materials with a wide range of morphologies. By carefully controlling the reaction conditions, researchers can produce nanocrystals, flower-shaped structures, nanowires, nanospheres, microspheres, and mesoporous nanowires [105].

Temperature, pressure, reactant concentration, pH, and surfactants are key factors that influence the morphology of NiO materials during hydrothermal synthesis. Higher temperatures generally lead to larger crystal sizes and more complex morphologies. Increasing pressure can accelerate the reaction rate and influence the nucleation and growth of NiO particles. The concentration of nickel precursors and hydroxide sources affects the rate of crystal growth and the final morphology. The pH of the reaction mixture can influence the solubility of nickel species and the formation of specific crystal facets. The addition of surfactants can modify the surface energy of NiO particles and control their growth direction [106].

By carefully adjusting these parameters, researchers can fine-tune the morphology of NiO materials to meet the specific requirements of different applications. For instance, nanocrystals with uniform size and shape are desirable for fundamental studies, while flower-shaped structures can enhance the surface area of electrodes for energy storage applications.

In conclusion, the hydrothermal method offers a powerful tool for tailoring the morphology of NiO materials. By understanding the key factors influencing morphology

and carefully controlling the synthesis conditions, researchers can produce NiO materials with desired properties for a wide range of applications.

2.14.3 Manganese Oxide

Manganese oxide, a transition metal oxide with multiple stable forms, has emerged as a promising candidate for electrode fabrication. The diverse crystal structures, morphologies, defects, and textures exhibited by manganese oxides contribute to their wide range of electrochemical properties. Despite its limitations, including poor conductivity and unsatisfactory cycle life, manganese oxide's high theoretical capacitance, ease of synthesis, non-toxicity, and low cost have attracted significant research interest. Efforts to address these challenges and improve the performance of manganese oxide electrodes are ongoing.

Modifications to manganese oxide electrodes can be achieved through two primary approaches:

1. **Mixed oxide formation:** Combining manganese oxide with other transition metals (TM), such as copper, iron, vanadium, cobalt, nickel, and ruthenium, can create mixed oxide electrodes with enhanced properties [107].
2. **Doping with foreign elements:** Introducing foreign metallic elements like tin, aluminum, or lead into the manganese oxide lattice can alter its electronic structure and improve its performance [107].

Godbane et al. [108] conducted a comprehensive study to investigate the influence of different structural morphologies on the charge storage performance of manganese dioxide (MnO_2). They prepared MnO_2 in various allotropic phases, including 1D channels, 2D layers, and 3D interconnected tunnels.

Their findings revealed a significant correlation between MnO_2 structure and its electrochemical properties. 3D interconnected tunnels exhibited the highest specific capacitance of $241 \text{ F}\cdot\text{g}^{-1}$, while 1D channels demonstrated the lowest specific capacitance

of 28 F·g⁻¹. This suggests that the 3D interconnected tunnel structure is particularly advantageous for charge storage applications.

Interestingly, Godbane et al. also observed that the electrochemical performance of MnO₂ was not significantly affected by its specific surface area (SSA). This implies that factors other than SSA, such as the structural arrangement of MnO₂, play a more dominant role in determining its charge storage capabilities.

Sun et al. [109] elucidated that the energy storage mechanism in manganese dioxide (MnO₂) is primarily dependent on the abundance of active manganese (Mn) sites. They discovered that reducing crystal size leads to an increase in the percentage of active Mn centers, resulting in higher specific capacitance. Contrary to previous assumptions, this study demonstrated that the morphological surface-to-volume ratio (SSA) also plays a significant role in influencing the electrochemical performance of MnO₂-based supercapacitors (SCs).

While significant progress has been made in the development of manganese oxide electrodes, there remains ample room for improvement to fully realize their potential. Combining MnO electrodes with other nanomaterials presents a promising avenue for enhancing their performance and addressing existing limitations.

2.15 Conducting polymer-based materials

Conductive polymers have emerged as promising materials for pseudocapacitors, offering advantages over traditional electric double-layer capacitors in terms of higher charge density, easier production, and lower cost [110]. Among the most used conductive polymers for energy storage electrodes are:

1. Polyaniline (PANi)
2. Polypyrrole (Ppy)
3. Polythiophene (PTh)

These polymers possess unique electrochemical properties that enable them to store and release energy through redox reactions, leading to enhanced energy density and power capability compared to traditional capacitors.

2.15.1 Polyaniline (PANi)

Polyaniline (PANi) stands out among conductive polymers due to its desirable properties, including flexibility, high specific capacitance, ease of synthesis, low cost, and controllable conductivity. However, PANi suffers from rapid degradation during repeated charge/discharge cycles and requires protic solvents or ionic liquids for optimal performance [111].

To address these limitations, researchers have explored strategies to enhance PANi's properties. One approach involves combining PANi with carbon materials or metal oxides. Sivakumar and co-workers successfully synthesized PANi nanofibers using interfacial polymerization, achieving a specific capacitance of 554 F/g at a current density of 1.0 A/g.

However, they observed a decline in specific capacitance and poor cyclic stability. To improve performance, they incorporated multi-walled carbon nanotubes (MWCNTs) into the PANi composite, resulting in a specific capacitance of 606 F/g [112].

Li et al. [113] conducted theoretical and experimental studies on polyaniline in sulfuric acid, revealing a significant discrepancy between calculated and experimental specific capacitance values. The maximum theoretical specific capacitance was estimated to be 2000 F/g, while experimental values fell far short.

While PANi has demonstrated potential as a conductive polymer for energy storage applications, its full potential remains untapped due to challenges such as poor cyclic stability and rapid degradation. Addressing these issues through strategies like composite formation with carbon materials or metal oxides is essential for realizing the practical application of PANi-based electrodes.

2.15.2 Polypyrrole (PPy)

Polypyrrole (PPy) is another conductive polymer with promising properties for energy storage applications. It offers high flexibility, ease of fabrication, excellent cyclic stability, and relatively high capacitance. Despite its high density, PPy exhibits a substantial capacitance per unit volume. However, challenges such as doping difficulty and relatively low specific capacitance per unit mass limit its performance.

To address these limitations, researchers have explored various strategies. Yang and co-workers proposed a synthesis method for freestanding PPy films for supercapacitors, incorporating surfactants to enhance the film properties. The films synthesized with surfactants exhibited smaller pore sizes and improved performance, achieving a maximum specific capacitance of 261 F/g and 75% capacitive retention [114].

Rajesh et al. [115] studied electropolymerized polypyrrole thin films doped with phytic acid and obtained a maximum specific capacitance of 343 F/g and a capacitance retention of 91% at 10 A/g after 4000 cycles. These results demonstrate the potential of PPy-based electrodes for energy storage applications, particularly when combined with appropriate doping strategies.

2.15.3 Polythiophene (PTh)

Polythiophene (PTh) has emerged as another promising conductive polymer for energy storage applications. It offers advantages such as good flexibility, ease of synthesis, excellent cyclic stability, and environmental friendliness. However, PTh is limited by its relatively low conductivity and specific capacitance compared to other materials [116].

Laforgue et al. [117] chemically synthesized PTh and its fluorinated derivative, PFPT, achieving specific capacitances of 7 mAh/g and 40 mAh/g, respectively. Patil and co-workers fabricated PTh thin films using the successive ionic layer adsorption and reaction (SILAR) method, employing FeCl₃ as an oxidizing agent. Their work reported a maximum specific capacitance of 252 F/g. In another study, PTh films were prepared using the chemical bath deposition method, resulting in a maximum specific capacitance of 300 F/g [118].

These results demonstrate the potential of PTh-based electrodes for energy storage applications. However, further research is needed to address its limitations and improve its overall performance.

2.16 MnO₂-based composite materials

Manganese dioxide (MnO₂) is a promising material for supercapacitor (SC) electrodes due to its environmental friendliness, abundance, high theoretical capacitance, and diverse oxidation states. However, its limitations, including low porosity, agglomeration tendency, low electrical conductivity, and electrolyte-mediated dissolution, have hindered its electrochemical performance.

To address these challenges, researchers have focused on modifying MnO₂ by combining it with highly conductive materials. These materials include carbonaceous materials such as carbon [119], carbon nanotubes (CNTs) [120], graphene and its derivatives [121], carbon nanofibers (CNFs) [122], conducting polymers [123], transition metal oxides/hydroxides, and layered double hydroxides [124].

The primary objective of forming hybrid composite structures is to harness the synergistic benefits of each individual component. By combining MnO₂ with these conductive materials, researchers aim to enhance its electrochemical performance, improve its conductivity, and mitigate its limitations.

2.16.1 MnO₂ binary composites

To overcome the limitations of pristine MnO₂, researchers have developed various synthetic methods for fabricating binary nanocomposites. These composites combine MnO₂ with a wide range of materials, including large surface area-based porous carbons, carbon nanotubes, functionalized graphenes, carbon fibers, activated carbons, conducting polymers, and non-carbonaceous materials like other metal oxides, hydroxides, sulfides, and nitrides. By creating these hybrid structures, researchers aim to leverage the synergistic benefits of the individual components, resulting in electrode materials with superior electrochemical performance compared to pure MnO₂ phases.

Table 2.1 presents a compilation of significant electrochemical achievements realized through the development of MnO₂ binary nanocomposites with carefully engineered nanostructures. These nanocomposites showcase remarkable advancements in electrochemical performance, surpassing the capabilities of pristine MnO₂ electrodes.

Table 2.1: Electrochemical performance of MnO₂-based binary composites

Sr. No.	Electrode Material	Synthesis Method	Electrolyte	Specific Capacitance (F/g)	Capacity Retention (%) (Cycles)	Ref.
1	MnO ₂ /Mn	Thermal Oxidation	1M Na ₂ SO ₄	937 (1.5 A/g)	98.5 (3000)	[125]
2	MnO ₂ /TiN	Electrodeposition	1M Na ₂ SO ₄	681 (2 A/g)	97 (1000)	[126]
3	Co ₃ O ₄ @MnO ₂	Redox Deposition	1 M LiOH	480 (2.6A/g)	97.3 (5000)	[127]
4	MnO ₂ @Ni(OH) ₂	Redox Deposition	1M Na ₂ SO ₄	355 (0.5 A/g)	97.1 (3000)	[128]
5	MnO ₂ @α-Fe ₂ O ₃	Redox Deposition	1M KOH	838 (2 mV/s)	98.5 (1000)	[129]
6	MnO ₂ /NiCo ₂ O ₄	Electrodeposition	2M KOH	1186 (1 A/g)	65 (3000)	[130]
7	MnO ₂ /SnO ₂	Template Method	6M KOH	542 (1 A/g)	-	[121]

8	$\text{Co}_3\text{O}_4/\text{MnO}_2$	Chemical Deposition	1M Na_2SO_4	616 (2 A/g)	83 (10000)	[131]
9	$\text{Mn}_3\text{O}_4/\text{MnO}_2$	Hydrothermal	1M Na_2SO_4	181 (2 A/g)	78 (4000)	[132]
10	$\text{CeO}_2/\text{MnO}_2$	Facile Synthesis	0.5 M Na_2SO_4	580 (0.5 A/g)	96(10,000)	[133]
11	MnO_2/CNT	Electrodeposition	0.5 M Na_2SO_4	579 (10 mV/s)	87.6 (500)	[134]
12	MnO_2/PPy	Electrodeposition	0.5 M Na_2SO_4	620 (5 mV/s)	90 (4000)	[135]
13	MnO_2/G	Layer by Layer	0.1 M Na_2SO_4	263 (0.2 A/g)	90 (1000)	[136]
14	$\text{MnO}_2/\text{PEDOT}$	Electrodeposition	0.5 M Na_2SO_4	420 (1 mV/s)	99.5 (4000)	[137]
15	MnO_2/PANI	Chemical Precipitation	0.1 M Na_2SO_4	500 (50 mV/s)	60 (5000)	[138]
16	MnO_2/CNF	Redox Deposition	1 M Na_2SO_4	311 (2 mV/s)	96 (1000)	[139]
17	MnO_2/RGO	Sonochemical	0.5 M Na_2SO_4	375 (1 A/g)	93 (500)	[140]

Investigations into the supercapacitive properties of MnO₂-based binary composites have consistently demonstrated significant enhancements in electrochemical performance compared to pristine MnO₂. These improvements are particularly evident in terms of capacitance, electrochemical stability, and conductivity. Moreover, the mechanical flexibility and environmental stability of these MnO₂-containing electrodes can be tailored through judicious selection of composite components [141].

While widely studied binary MnO₂/CNTs, MnO₂/graphenes, and other nanocarbon-based MnO₂ nanocomposites exhibit superior charge transfer kinetics and cyclic stability compared to their pure counterparts, they remain hindered by several limitations. These include inadequate electroactive mass loadings, challenges in material processing, and elevated manufacturing costs, which collectively impede their commercial viability [142].

MnO₂/conducting polymer nanocomposites, although readily accessible, offer relatively higher mass loadings and cumulative capacitive performance. However, they frequently succumb to rapid degradation, exhibit poor electrochemical stability, and possess a narrow operational voltage window. On the other hand, 'all-inorganic '-based MnO₂ binary nanocomposites demonstrate enhanced collective pseudocapacitance contributions and cyclic stability. Yet, they are often plagued by elevated interfacial and inter-/intra-grain contact resistances, which significantly curtail charge transport kinetics within the resulting nanocomposites [141, 143].

Crucially, the capacitance values attained from these binary nanocomposites to date fall far short of the levels required for practical commercial applications, necessitating further advancements.

2.16.2 MnO₂ ternary composites

Intensive research has revealed that the simultaneous optimization and fulfillment of all the essential criteria for electrochemical efficiency within simple binary nanocomposites often present significant challenges.

To overcome these limitations, strategies have been devised to meticulously integrate three or more components in appropriate proportions, fostering synergistic

interactions through the harmonious combination of their individual strengths while mitigating their respective weaknesses. This approach aims to achieve optimal device performance.

Ternary nanocomposites fabricated with other systems have demonstrated promising results in enhancing capacitive contributions, increasing the concentration of redox reaction sites, establishing desirable morphologies for accelerated electron/ion transfer kinetics, promoting smoother interfacial interactions, and improving mechanical flexibility, thereby enabling the development of advanced device architectures.

Consequently, numerous MnO_2 ternary hybrids have been designed with the pressing objective of effectively addressing the shortcomings in electrochemical performance [144].

MnO_2 has been meticulously combined with two additional components, which may be exclusively carbon-based, such as conducting polymers, carbon nanotubes (CNTs), graphene, or purely inorganic materials like oxides, sulfides, hydroxides, metal nanostructures, or a combination of organic and inorganic matter.

These components are carefully blended in optimal proportions to achieve the pinnacle of device efficiency [145].

A masterful composition would undoubtedly introduce maximal synergy among its constituent materials, facilitating interfacial electrochemical reactions for enhanced pseudocapacitance, establishing the desired morphology for accelerated ion transfer kinetics, and ensuring high conductivity. Moreover, such a composition would impart exceptional mechanical flexibility.

Table 2.2 provides a comprehensive overview of the substantial electrochemical advancements attained through the innovative design and fabrication of MnO_2 binary nanocomposites with meticulously engineered nanostructures.

These nanocomposites exhibit exceptional enhancements in electrochemical performance, significantly outperforming the capabilities of pristine MnO_2 electrodes.

Table 2.2: Electrochemical performance of MnO₂ based ternary composites.

Sr. No.	Electrode Material	Synthesis Method	Electrolyte	Specific Capacitance (F/g)	Capacity Retention (%) (Cycles)	Ref.
1	α -Fe ₂ O ₃ /MnO ₂ /rGO	Solvothermal	6M KOH	447 (1 A/g)	92 (5000)	[39]
2	MnO ₂ /CuO/rGO	Hydrothermal	2M KOH	658.9 (1 A/g)	83.7 (5000)	[146]
3	NiO/MnO ₂ /rGO	Ultrasonication	1M Na ₂ SO ₄	402 (1 A/g)	93 (14000)	[147]
4	CF/ MnO ₂ /PANI	Hydrothermal	1M H ₂ SO ₄	373 (1 A/g)	73 (1000)	[38]
5	CF@ γ -MnO ₂ /PANI	Hydrothermal	1M Na ₂ SO ₄	654.3(1 A/g)	75.94 (4000)	[148]
6	CeO ₂ - α -MnO ₂ -rGO	Hydrothermal	1M Na ₂ SO ₄	466 (1 A/g)	100 (10000)	[42]
7	Co ₃ O ₄ /NiO/MnO ₂	Hydrothermal	6M KOH	549 (0.5 A/g)	76 (600)	[149]
8	MnO ₂ @SnO ₂ /T-NC	Ultrasonication	1M H ₂ SO ₄	676 (1 A/g)	93 (6000)	[150]
9	MnO ₂ /T.rGO/A.P ANI	Ultrasonic assistance	6M KOH	1140 (1 A/g)	64 (5000)	[151]

10	MnO ₂ @PANI/graphene	Hydrothermal	6 M KOH	1369 (3 A/g)	83 (5000)	[152]
11	MnO ₂ /GNS/CNTs	Facile Chemical Method	1 M Na ₂ SO ₄	133 (0.5 A/g)	95 (1000)	[40]

CHAPTER 3: MATERIALS AND METHODS

3.1 Reagents & Materials

The experimental investigations employed a suite of high-quality reagents. Cerium nitrate hexahydrate ($\text{Ce}(\text{NO}_3)_3 \cdot 6\text{H}_2\text{O}$), a crystalline compound with a characteristic pale yellow hue, was obtained from Sigma Aldrich. Multiwalled carbon nanotubes (MWCNTs), a cylindrical arrangement of carbon atoms with exceptional mechanical properties, were also sourced from Sigma Aldrich. Additionally, potassium permanganate (KMnO_4), a deep purple crystalline solid with potent oxidizing capabilities, was acquired from the same supplier. Hydrogen peroxide (H_2O_2) and sodium sulfate (Na_2SO_4), a white crystalline powder with excellent solubility in water, were obtained from Merck. These reagents were employed in their pristine state without the need for additional purification, ensuring the reliability of the experimental outcomes. To maintain the purity and integrity of the experimental environment, deionized water was exclusively utilized as a solvent throughout the study.

3.2 Synthesis of MnO_2

Manganese dioxide (MnO_2) samples were synthesized through a controlled chemical reaction. Potassium permanganate (KMnO_4), a potent oxidizing agent with a deep purple hue, was employed as the starting material. Citric acid ($\text{C}_6\text{H}_8\text{O}_7$), a naturally occurring organic compound, acted as the reducing agent. In the initial step, a solution of potassium permanganate was prepared by dissolving 0.6 grams of KMnO_4 in 15 milliliters of deionized water, resulting in a vibrant purple liquid. Subsequently, a separate solution of citric acid was created by dissolving 0.77 grams of $\text{C}_6\text{H}_8\text{O}_7$ in 15 milliliters of deionized water. The citric acid solution, a colorless liquid, was then carefully added to the potassium permanganate solution while stirring vigorously. As the citric acid interacted with the potassium permanganate, a chemical reaction occurred, leading to the formation of manganese dioxide precipitates. These precipitates, a dark brown solid, were washed thoroughly with deionized water and ethanol to remove any impurities. The purified MnO_2 was then dried in a controlled environment at a temperature of 60 degrees Celsius, ensuring

complete removal of moisture. Finally, the dried MnO₂ was subjected to annealing in a muffle furnace at 400 degrees Celsius for a period of four hours. This high-temperature treatment further refined the structure and properties of the manganese dioxide, preparing it for subsequent experimental use.

3.3 Synthesis of MnO₂/CeO₂

The preparation of the MnO₂/CeO₂ nanocomposite commenced with the thorough combination of potassium permanganate (KMnO₄) and cerium nitrate hexahydrate (Ce(NO₃)₃·6H₂O) in a deionized water solution. The molar ratio of KMnO₄ to Ce(NO₃)₃·6H₂O was carefully maintained at 3.5:1, ensuring the desired stoichiometric balance for the subsequent reaction. The resulting solution was subjected to vigorous stirring for approximately 45 minutes, facilitating the complete dissolution of the reactants and promoting their interaction. To initiate the formation of the nanocomposite, 2 milliliters of hydrogen peroxide (H₂O₂) were added to the solution. Hydrogen peroxide, a potent oxidizing agent, played a crucial role in the redox reactions that led to the nucleation and growth of the MnO₂/CeO₂ nanoparticles.

The reaction mixture was then transferred into a Teflon-coated autoclave, a specialized pressure vessel designed to withstand high temperatures and pressures. The autoclave was heated to a temperature of 150 degrees Celsius for a duration of four hours, creating a controlled environment that facilitated the formation of the nanocomposite. The elevated temperature accelerated the chemical reactions and promoted the crystallization of the MnO₂/CeO₂ particles.

After the heating process, the autoclave was allowed to cool to ambient temperature, allowing the reaction products to stabilize. The synthesized MnO₂/CeO₂ nanocomposite was subsequently washed thoroughly with deionized water and ethanol to remove any residual impurities, ensuring the purity and integrity of the final product. The washed precipitates were then dried overnight in a muffle furnace at 60 degrees Celsius, removing any remaining moisture and preparing the sample for further processing. Finally, the dried MnO₂/CeO₂ nanocomposite was calcined at 400 degrees Celsius for four hours. This high-temperature treatment enhanced the crystallinity and stability of the

nanoparticles, optimizing their structural and functional properties for subsequent applications.

3.4 Synthesis of MnO₂/CeO₂/MWCNT

The preparation of the ternary composite MnO₂/CeO₂/MWCNT involved the meticulous combination of potassium permanganate (KMnO₄), cerium nitrate hexahydrate (Ce(NO₃)₃·6H₂O), and multiwalled carbon nanotubes (MWCNTs) in a deionized water solution. The molar ratios of KMnO₄ to Ce(NO₃)₃·6H₂O and MWCNTs were carefully maintained at 3.5:1 and 0.2:1, respectively, ensuring the desired stoichiometric balance for the subsequent reaction. The mixture was subjected to vigorous stirring and the addition of 2 milliliters of hydrogen peroxide (H₂O₂) for a duration of 45 minutes, facilitating the complete dissolution of the reactants and promoting their interaction.

The resulting solution was then transferred into a Teflon-coated autoclave, a specialized pressure vessel designed to withstand high temperatures and pressures. The autoclave was heated to a temperature of 150 degrees Celsius for a duration of four hours, creating a controlled environment that facilitated the formation of the ternary composite. The elevated temperature accelerated the chemical reactions and promoted the nucleation and growth of the MnO₂/CeO₂/MWCNT nanoparticles.

After the heating process, the autoclave was allowed to cool to ambient temperature, allowing the reaction products to stabilize. The synthesized MnO₂/CeO₂/MWCNT ternary composite, a dark brown precipitate, was washed thoroughly with deionized water and ethanol to remove any impurities, ensuring the purity and integrity of the final product. The washed precipitate was dried overnight in a muffle furnace at 60 degrees Celsius, removing any remaining moisture and preparing the sample for further processing. Finally, the dried MnO₂/CeO₂/MWCNT nanocomposite was calcined at 400 degrees Celsius for four hours. This high-temperature treatment enhanced the crystallinity and stability of the nanoparticles, optimizing their structural and functional properties for subsequent applications.

3.5 Fabrication of Working Electrode

The fabrication of the supercapacitor electrodes commenced with the preparation of a slurry containing acetylene black, polyvinylidene fluoride (PVDF), and the synthesized products as the active components. Acetylene black, a highly conductive carbon material, provided excellent electrical conductivity. Polyvinylidene fluoride (PVDF), a polymer with exceptional mechanical properties, served as a binder, ensuring the adhesion of the active materials to the electrode substrate. The synthesized products, namely MnO_2 , CeO_2 , and $\text{MnO}_2/\text{CeO}_2/\text{MWCNT}$, were incorporated into the slurry to enhance the electrochemical performance of the supercapacitor. These components were dispersed in N-methyl-2-pyrrolidone (NMP), a solvent with excellent solvating properties, to form a homogeneous mixture.

The resulting slurry was then applied to a 1 cm^2 graphite sheet electrode using a spin coater. This specialized instrument rotated the electrode at high speeds while simultaneously dispensing the slurry, ensuring a uniform and controlled coating. The solvent within the slurry evaporated during the coating process, leaving behind a thin, adherent layer of the active materials on the electrode surface. The fabricated electrodes were subsequently dried overnight at a temperature of 60 degrees Celsius to remove any residual solvent and ensure the complete solidification of the active material.

For the fabrication of the activated carbon (AC) electrode, a similar procedure was employed, with activated carbon replacing the synthesized products as the active material. Activated carbon is a porous carbon material with a high surface area, which is ideal for energy storage applications. The use of activated carbon in the AC electrode provided an alternative reference electrode for comparison with the synthesized materials.

CHAPTER 4: CHARACTERIZATION

4.1 Instrumentation and Measurements

A comprehensive characterization of the synthesized products was conducted to elucidate their structural, compositional, and electrochemical properties. A field-emission scanning electron microscope equipped with energy dispersive spectroscopy (FESEM-EDS) was employed to examine the surface morphology and elemental composition of the samples. The FESEM-EDS analysis provided valuable insights into the particle size, shape, and distribution of the elements within the synthesized materials. For detailed structural analysis, high-resolution transmission electron microscopy (HRTEM) was utilized. HRTEM allowed for the visualization of the crystallographic structure and lattice fringes of the nanoparticles, providing crucial information about the arrangement of atoms and the presence of defects. Raman spectroscopy, a technique that measures the vibrational properties of molecules, was employed to investigate the bonding and structural characteristics of the synthesized materials. The Raman spectra revealed information about the functional groups, crystal structure, and the presence of impurities. X-ray powder diffraction (XRD) was employed to determine the crystallographic structure and phase composition of the synthesized products. XRD analysis provided valuable information about the crystal lattice parameters, unit cell dimensions, and the presence of crystalline phases. X-ray photoelectron spectroscopy (XPS) was conducted to analyze the surface chemistry and electronic states of the elements within the synthesized materials. XPS provided insights into the oxidation states, chemical bonding, and the presence of surface contaminants. Electrochemical measurements were performed using a three-electrode setup to evaluate the electrochemical performance of the synthesized materials. A reference electrode (Ag/AgCl) was used to establish a stable potential, a counter electrode (platinum wire) was used to facilitate electron transfer, and a working electrode comprised of the synthesized MnO₂, MnO₂/CeO₂, or MnO₂/CeO₂/MWCNT composites was used as the active material. All experiments were conducted in a 1M Na₂SO₄ solution, a commonly used electrolyte for electrochemical studies. Cyclic voltammetry (CV) was performed at various scan rates to evaluate the electrochemical reversibility, specific capacitance, and

the rate capability of the synthesized materials. The CV curves provided information about the redox processes occurring at the electrode surface and the charge storage mechanism. Galvanostatic charge-discharge (GCD) measurements were conducted at different current densities to assess the specific capacitance, rate capability, and energy density of the synthesized materials. The GCD curves provided information about the charge and discharge characteristics and the self-discharge behavior. Electrochemical impedance spectroscopy (EIS) was employed to investigate the charge transfer kinetics, interfacial resistance, and diffusion limitations within the synthesized materials. The EIS spectra provided insights into the factors affecting the electrochemical performance and the suitability of the materials for supercapacitor applications.

An asymmetric coin cell supercapacitor device was fabricated using Na_2SO_4 as the electrolyte, with $\text{MnO}_2/\text{CeO}_2/\text{MWCNT}$ serving as the positive electrode and activated carbon as the negative electrode. The electrochemical performance of the asymmetric coin cell supercapacitor was evaluated using a two-electrode system. The asymmetric configuration allowed for a wider operating voltage window and enhanced energy density compared to symmetric supercapacitors.

4.2 X-ray diffraction (XRD)

X-ray diffraction spectroscopy is a powerful analytical technique that offers a profound understanding of the atomic and molecular structure of materials. Building upon the pioneering work of Max von Laue, William Henry Bragg, and William Lawrence Bragg, this technique leverages the principles of X-ray diffraction to illuminate the intricate details of crystallographic arrangements. By examining the diffraction patterns produced by X-rays interacting with a material, X-ray diffraction spectroscopy provides valuable insights into strains, defects within the crystal structure, and the average particle size of crystalline materials.

The technique involves the interaction of X-rays with a sample, resulting in the diffraction of the X-ray waves. When two X-ray waves with identical frequency and amplitude encounter each other, their crests and troughs can align, leading to constructive

interference and a reinforcement of the wave amplitude. Conversely, if the crest of one wave aligns with the trough of another, destructive interference occurs, resulting in the cancellation of the wave amplitudes.

There are three primary methods for analyzing crystal structures using X-ray diffraction: the Laue method, powder X-ray diffraction, and the rotating crystal method. Among these, powder X-ray diffraction is the most advanced and widely used technique, particularly for the characterization of nanomaterials. This technique involves the analysis of the diffraction patterns produced by a powdered sample, providing information about the crystal structure, phase composition, and crystallite size.

The crystallite size of nanoparticles in powder X-ray diffraction analysis can be determined using two methods: the Debye-Scherrer method and the diffractometer method. The Debye-Scherrer method involves analyzing the broadening of the diffraction peaks, while the diffractometer method utilizes the position and intensity of the diffraction peaks.

In powder XRD analysis, the sample is typically ground to a fine powder and mixed with a reference material, such as molybdenum or copper. The reference material serves as a calibration standard, allowing for accurate measurements and interpretation of the diffraction patterns.

4.2.1 Working Principle

X-ray diffraction (XRD) is a sophisticated analytical technique that provides a comprehensive understanding of the atomic arrangement within crystalline materials. Governed by Bragg's Law, XRD elucidates the conditions under which constructive interference occurs when X-rays interact with a regular array of atoms in a crystalline lattice. Bragg's Law, expressed as

$$2d \sin\theta = n\lambda,$$

establishes a relationship between the lattice spacing (d), incident angle (θ), X-ray wavelength (λ), and the order of diffraction (n). When the incident angle satisfies the Bragg condition, the X-rays are diffracted, revealing valuable information about the crystal structure.

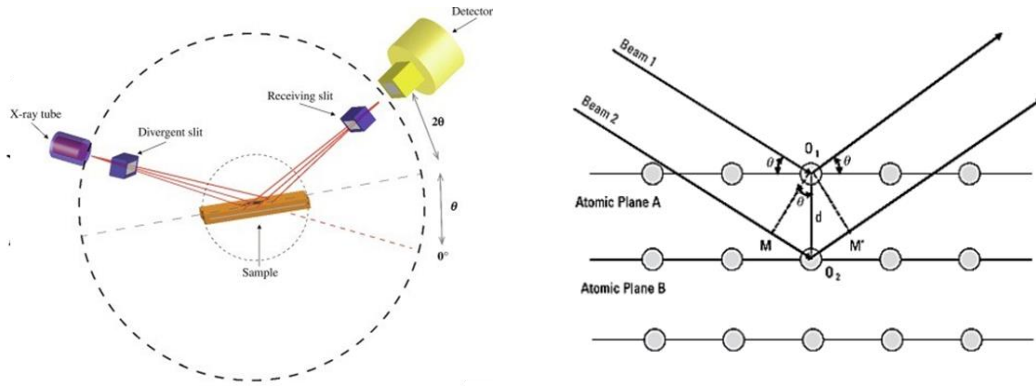


Figure 4.1: Working principle of XRD

An XRD instrument comprises three essential components: an X-ray source, a sample holder, and a detector. The X-ray source generates X-rays through the process of electron bombardment. A heated filament within a cathode ray tube produces electrons, which are then accelerated towards a target material, such as copper or molybdenum. The high-energy electrons penetrate the crystal structure of the target material, exciting inner shell electrons. As these electrons undergo transitions, they emit X-rays with characteristic wavelengths.

The generated X-rays are then directed towards the sample, which is placed in a sample holder. When the incident angle of the X-rays matches the reflected angle between the planes of atoms in the crystal, constructive interference occurs, resulting in a reinforced X-ray signal. This diffracted signal is detected by the detector, which records the intensity of the X-rays at various angles.

The data obtained from XRD analysis offers a wealth of information about the crystal structure and properties of the material. By analyzing the diffraction patterns, researchers can determine the lattice constant of the unit cell, which defines the size and shape of the crystal lattice. Additionally, XRD can be used to calculate the crystallite size,

which represents the average size of the crystalline domains within the material. Furthermore, XRD can provide insights into the material's density and pore fraction.

The lattice constant can be calculated using the formula

$$a = \lambda / (2 \sin \theta) * hkl,$$

where a is the lattice constant, λ is the X-ray wavelength, hkl are the Miller indices, and θ is the diffraction angle. The crystallite size can be determined using the Debye-Scherrer formula:

$$D = K\lambda / (\beta \cos \theta),$$

where D is the crystallite size, K is the Scherrer constant, λ is the X-ray wavelength, β is the full width at half maximum of the diffraction peak, and θ is the diffraction angle.

In summary, X-ray diffraction is a powerful analytical technique that provides invaluable insights into the atomic arrangement and structural properties of crystalline materials. By understanding the principles of X-ray diffraction and the intricacies of XRD analysis, researchers can extract valuable information about the crystal structure, lattice parameters, crystallite size, and other material properties.

4.3 Raman Spectroscopy

Raman spectroscopy is a versatile analytical technique capable of characterizing and identifying a wide range of materials, including solids, liquids, and gases. This non-destructive method provides valuable information about the molecular vibrational modes of a material without the need for physical contact or alteration. The Raman technique is based on the inelastic scattering of light by molecules. When a photon of light interacts with a molecule, it can excite the molecule to a higher vibrational energy state. Subsequently, the molecule relaxes back to its ground state by emitting a photon with a different energy, a process known as the Raman shift.

When a molecule scatters light, the oscillating electromagnetic field of the photon induces polarization in the molecular electron cloud, elevating the molecule's energy and

transferring the photon's energy to it. This transient interaction forms a short-lived complex between the photon and the molecule, often referred to as the virtual state. Due to the instability of the virtual state, the photon is quickly reemitted as scattered light.

In Raman spectroscopy, a laser beam of a specific wavelength is directed onto the sample, and the scattered light is collected and analyzed using a spectrometer. To enhance the signal of the generally weak Raman scattered light, techniques such as surface-enhanced Raman scattering (SERS) and resonance Raman scattering (RRS) can be employed.

4.3.1 Working Principle

The Raman effect arises from the interaction of light with matter, specifically when a monochromatic light beam, such as a laser, is directed onto a sample. This interaction results in two primary types of light scattering:

- Rayleigh Scattering: The majority of scattered light remains at the same wavelength (frequency) as the incident light. This type of scattering, known as Rayleigh scattering, does not provide significant information for Raman spectroscopy.
- Raman Scattering: A small portion of the incident light undergoes a change in frequency due to interactions with the molecules within the sample. This process is called Raman scattering and results in the scattered light having either a lower or higher frequency compared to the incident light. The shift in frequency corresponds to the vibrational energy levels of the molecules in the sample.

The energy difference between the incident and scattered light is directly related to the vibrational and rotational energy levels of the molecules. By analyzing the frequency shifts in the Raman-scattered light, researchers can determine the vibrational modes and rotational states of the molecules, providing valuable insights into the sample's molecular structure and composition.

There are two main types of Raman scattering:

- Stokes Raman Scattering: In this type, the scattered light has a lower frequency (longer wavelength) than the incident light. This occurs when the incident photons transfer energy to the molecules, exciting them to higher vibrational states.
- Anti-Stokes Raman Scattering: In this type, the scattered light has a higher frequency (shorter wavelength) than the incident light. This occurs when the molecules in the sample lose energy by emitting a photon during the scattering process, leading to a transition to lower vibrational states.

The Raman scattered light is collected and analyzed using a spectrometer, which separates the different frequencies of light, allowing researchers to obtain a Raman spectrum. The Raman spectrum serves as a unique fingerprint of the sample's molecular composition, facilitating the identification of chemical compounds and the study of molecular interactions. In summary, the working principle of Raman spectroscopy involves illuminating a sample with a laser, measuring the frequency shifts in the scattered light, and analyzing the resulting Raman spectrum to gain valuable information about the molecular structure and composition of the sample.

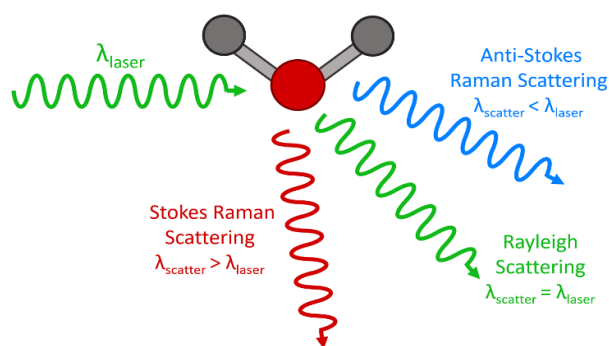


Figure 4.2: Working principle of Raman spectroscopy

4.4 Scanning Electron Microscopy

Scanning electron microscopy (SEM) is a sophisticated analytical technique that delves into the intricate interactions between high-energy electrons and matter, offering

valuable insights into the topography, composition, particle size, and phase mapping of materials at both the nanoscale and bulk levels. When a high-energy electron beam strikes a material, a myriad of interactions can occur, each providing unique information about the sample's properties.

As electrons in the electron beam collide with atoms on the sample's surface, they emit a variety of signals, including characteristic X-rays, backscattered electrons, secondary electrons, cathodoluminescence, transmitted electrons, and absorbed current. These signals collectively offer a comprehensive understanding of the sample's composition and topography. Secondary and backscattered electrons are the most commonly utilized signals for imaging samples. Secondary electrons, emitted from the surface of the sample, provide detailed information about the sample's topography, revealing the surface features, roughness, and three-dimensional structure. Backscattered electrons, which are high-energy electrons that have been elastically scattered back from the sample, provide information about the sample's composition. The intensity of backscattered electrons varies with the atomic number of the elements present in the sample, allowing for the visualization of compositional variations within multiphase materials.

4.4.1 Working Principle

Scanning electron microscopy (SEM) is a sophisticated analytical technique that employs a focused electron beam to probe the surface of a sample, generating high-resolution images with detailed information about the sample's morphology, composition, and structure. The working principle of SEM involves several key steps:

- **Electron Source:** SEM utilizes a high-energy electron source, typically a tungsten filament or a field emission gun (FEG), to generate a beam of electrons.
- **Electron Beam Focusing:** The electron beam is accelerated and focused using electromagnetic lenses, creating a fine probe that can be scanned across the sample surface.

- **Sample Preparation:** Prior to imaging in the SEM, the sample must undergo appropriate preparation. This typically involves dehydration, drying, and coating with a thin layer of conductive material (e.g., gold or carbon) to prevent charging effects during imaging.
- **Sample Interaction:** When the focused electron beam strikes the sample surface, various interactions occur between the electrons and the atoms in the sample. These interactions result in the generation of different signals that are used to create the SEM image.
- **Secondary Electron Emission:** One of the primary interactions is the emission of secondary electrons from the sample's surface due to the impact of the incident electrons. These secondary electrons carry information about the surface topography and are used to create the SEM image.
- **Backscattered Electrons:** Some of the incident electrons experience elastic scattering and are backscattered from the sample's atomic nuclei. The energy of backscattered electrons is related to the average atomic number of the sample material, providing compositional contrast in the SEM image.
- **X-ray Emission:** Inelastic scattering of electrons can lead to the emission of characteristic X-rays from the sample. The energy and intensity of these X-rays can be used for elemental analysis (EDS or Energy Dispersive X-ray Spectroscopy) to determine the chemical composition of the sample.
- **Scanning and Image Formation:** The focused electron beam is scanned across the sample surface in a raster pattern. As the beam scans, signals from secondary electrons, backscattered electrons, and X-rays are detected and processed to form the SEM image. The brightness and contrast in the SEM image correspond to variations in the sample's surface properties, such as roughness, composition, and topography.

- 3D Imaging: Advanced SEM systems can also use specialized techniques like electron beam lithography or focused ion beam (FIB) milling to create cross-sectional or 3D images of the sample, providing additional insights into the material's internal structure.

SEM is commonly equipped with an EDX device, which allows for the determination of the sample's chemical composition. EDX is an analytical technique that examines X-rays emitted by a sample. When a high-energy electron beam strikes a sample, it may energize an electron in an inner shell, ejecting it from the level and creating an electron-hole. A higher energy electron from an outer shell fills the electron hole, releasing the energy difference as an X-ray. An energy dispersive spectrometer can detect the energy emitted by a sample, and the elemental composition can be identified based on the relationship between the X-ray energy and the atomic structure of the element from which they were emitted.

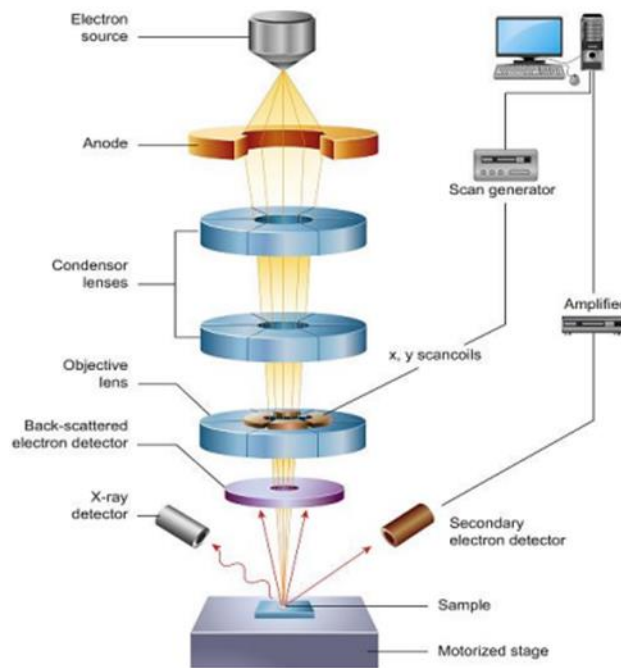


Figure 4.3: Working principle of scanning electron microscopy

In summary, SEM is a versatile and powerful analytical tool that offers detailed information about the surface morphology, composition, and structure of various materials. By understanding the underlying principles and techniques involved in SEM, researchers can gain valuable insights into the micro- and nanoscale properties of a wide range of samples.

4.5 Transmission Electron Microscopy

Transmission electron microscopy (TEM) is a sophisticated microscopy technique capable of visualizing and studying the internal structure of materials at exceptionally high magnifications and resolutions. Unlike scanning electron microscopy (SEM), which focuses on imaging the surface of samples, TEM allows researchers to penetrate thin specimens and observe the arrangement of atoms and nanoscale structures within the material.

In TEM, a focused electron beam is directed onto a thin sample, and the electrons that pass through the sample are collected and recombined by objective lenses to form an image. The high-energy electron beam operates at accelerating voltages ranging from 100 kV to 400 kV. The interaction between the electron beam and the sample results in the formation of a diffraction pattern, which provides valuable information about the crystal structure and orientation of the material.

To capture and magnify the image formed, a photographic film or a digital detector is utilized. TEM offers significantly higher resolution compared to conventional microscopes and scanning electron microscopes, enabling the visualization of fine details and nanoscale structures.

4.5.1 Working Principle

Transmission Electron Microscopy (TEM) is a powerful imaging technique used to observe the fine details of a specimen at the atomic or molecular level. The working principle of TEM is based on the interaction of electrons with matter. Here's how it works:

- **Electron Source:** TEM begins with an electron gun that emits a beam of electrons. These electrons are accelerated to high velocities using an electric field, typically reaching energies in the range of 100-300 keV. The high energy of the electrons allows them to pass through thin samples.
- **Electron Beam and Lenses:** The electron beam is focused and directed onto the sample using a series of electromagnetic lenses. These lenses are analogous to optical lenses in a light microscope but use magnetic fields to control the path and focus of the electrons.
- **Interaction with the Sample:** The sample, which must be extremely thin (typically less than 100 nm), is placed in the path of the electron beam. As the electrons pass through the sample, they interact with the atoms in the material, causing various scattering phenomena:
 - **Elastic Scattering:** Electrons are scattered without losing energy, often providing information about the structure of the sample.
 - **Inelastic Scattering:** Electrons lose energy as they interact with the sample, providing information about the composition and electronic properties of the material.
- **Formation of the Image:** The electrons that pass through the sample are collected by an imaging system. Electrons that are scattered in different directions and with different energies create contrast in the image. The electromagnetic lenses beneath the sample help form a magnified image of the sample on a fluorescent screen, a photographic film, or a digital camera.
- **Image Interpretation:** The resulting image is a two-dimensional projection of the sample, where contrast is derived from the density and thickness variations of the material. Heavier atoms scatter electrons more strongly, appearing darker in the image, while lighter atoms appear brighter.

- Additional Analytical Techniques: TEM can be coupled with other techniques, such as Energy-Dispersive X-ray Spectroscopy (EDS) or Electron Energy Loss Spectroscopy (EELS), to provide elemental composition or chemical bonding information.
- Resolution: TEM offers extremely high resolution, often down to the atomic level (around 0.1 nm), making it a vital tool for studying the microstructure, crystallography, and defects within materials.

The working principle of TEM allows researchers to visualize the internal structure of materials with exceptional detail, making it invaluable in fields such as materials science, biology, and nanotechnology.

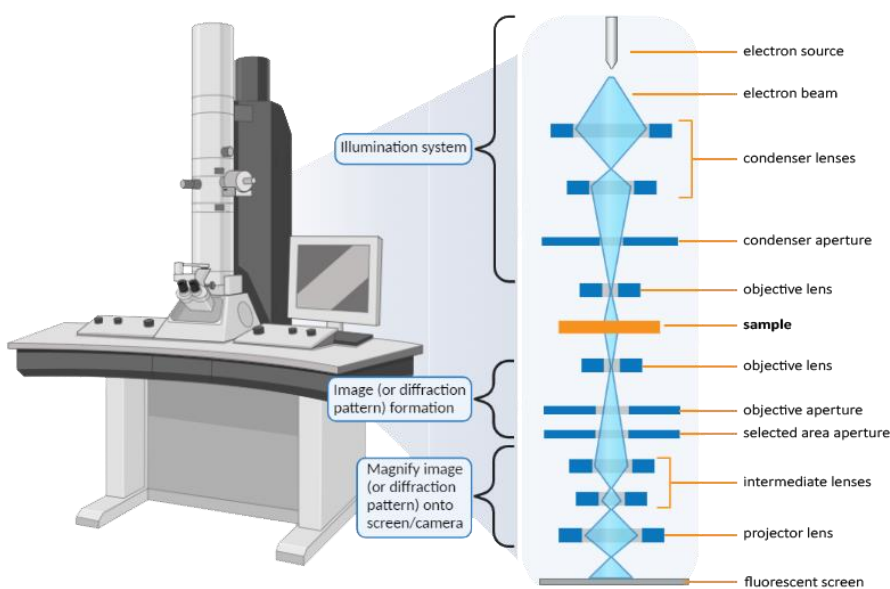


Figure 4.4: Working principle of transmission electron microscope

4.6 X-ray Photoelectron Spectroscopy (XPS)

X-ray photoelectron spectroscopy (XPS) is a sophisticated analytical technique that provides valuable insights into the elemental composition and chemical state of materials at the surface level. Operating on the principle of the photoelectric effect, XPS involves the interaction of X-rays with the surface of a sample, leading to the emission of

photoelectrons. By measuring the energy of these photoelectrons, XPS can accurately determine the elemental composition of the material.

X-ray photons with energies ranging from 200 to 2000 electron volts (eV) are employed in XPS to induce the emission of photoelectrons from the material's surface. The energy of the X-ray photons is sufficient to eject electrons from the inner shells of the atoms, creating a vacancy. To fill this vacancy, an electron from a higher energy level can transition to the lower energy level, releasing the energy difference in the form of a photoelectron. The kinetic energy of the emitted photoelectron is directly related to the binding energy of the electron in the atom, which is characteristic of each element. By analyzing the kinetic energies of the photoelectrons, XPS can accurately identify the elements present in the sample and determine their relative concentrations.

XPS is a highly sensitive technique that can detect elements with even trace concentrations. It is also capable of providing information about the chemical state of the elements in the sample. The binding energy of an electron can be influenced by its chemical environment, such as the presence of bonds or ligands. By analyzing the shifts in the binding energy of the photoelectrons, XPS can reveal the oxidation state, bonding configuration, and other chemical properties of the elements within the material.

4.6.1 Working Principle

X-ray photoelectron spectroscopy (XPS) is a surface-sensitive analytical technique that provides valuable insights into the elemental composition and chemical state of materials. The principle behind XPS lies in the photoelectric effect, which occurs when X-rays interact with the surface of a material, ejecting electrons known as photoelectrons.

- **X-ray Source:** XPS utilizes a monochromatic X-ray source, typically an Al K α X-ray source, to generate X-rays with a specific energy. The choice of X-ray energy is crucial for effectively ionizing the core-level electrons of the material being studied.
- **Photoelectric Effect:** When X-rays with sufficient energy strike the surface of the sample, they interact with the electrons in the innermost atomic shells (core levels)

of the atoms in the sample. The X-rays can cause these electrons to be ejected from the atom, a process known as the photoelectric effect.

- **Emission of Photoelectrons:** As a result of the photoelectric effect, core-level electrons are emitted from the sample, forming a photoelectron signal.
- **Kinetic Energy Measurement:** The emitted photoelectrons possess a kinetic energy that is characteristic of the element from which they originated and their specific chemical state. The kinetic energy is directly related to the energy of the X-rays used and the binding energy of the core-level electron.
- **Energy Analyzer:** The emitted photoelectrons are then directed towards an energy analyzer, such as a hemispherical electron energy analyzer or a cylindrical mirror analyzer. This analyzer separates the photoelectrons based on their kinetic energy and measures their intensity as a function of kinetic energy.
- **Spectrum Acquisition:** By scanning the kinetic energy of the photoelectrons emitted from the sample, an XPS spectrum is obtained. The spectrum displays the number of photoelectrons detected at different kinetic energies, providing information about the core-level binding energies and chemical composition of the material.
- **Data Analysis:** The XPS spectrum is analyzed to identify the elements present in the sample and to determine their chemical states. Each element has characteristic binding energies, and the fine structure of the peaks in the spectrum provides information about the chemical environment of the element.

X-ray photoelectron spectroscopy is widely used in materials science, surface chemistry, catalysis, nanotechnology, and various other fields to analyze the surface composition and chemical bonding of solid materials.

It provides valuable information about the elemental composition, oxidation states, and surface chemistry of materials, making it a powerful tool for materials characterization and surface analysis.

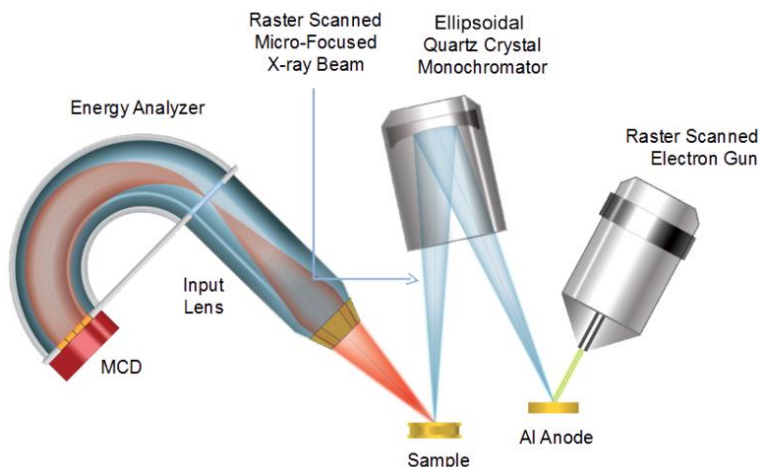


Figure 4.5: Working principle of x-ray photoelectron spectroscopy

4.7 Brunauer, Emmett and Teller Analysis (BET)

The Brunauer-Emmett-Teller (BET) analysis is a sophisticated technique designed to quantify the specific surface area of porous materials, including powders, catalysts, and adsorbents. Developed by Stephen Brunauer, Paul Emmett, and Edward Teller in the late 1930s, the BET method has become an indispensable tool in fields such as materials science, chemistry, and engineering. The specific surface area, a measure of the total accessible surface area per unit mass or volume, is a critical parameter that significantly influences the adsorption and reaction capabilities of porous materials.

The BET analysis is rooted in the principle that gases, typically nitrogen, can be physically adsorbed onto the surface of a solid material due to the presence of pores and crevices. By carefully measuring the amount of gas adsorbed at varying pressures, the BET method can accurately determine the surface area of the material. The analysis is based on the assumption that the gas molecules form a monolayer on the material's surface, followed by the formation of additional layers in a sequential manner. This multilayer adsorption model allows for the calculation of the specific surface area using a well-defined mathematical equation.

4.7.1 Working Principle

The Brunauer-Emmett-Teller (BET) analysis involves several key steps:

- **Degassing:** The sample material is initially degassed under elevated temperatures to remove any adsorbed impurities or gases that might interfere with the analysis. This ensures that the gas adsorption measured is solely attributed to the material's own surface.
- **Adsorption Isotherms:** The degassed sample is exposed to a gas, typically nitrogen, at a range of increasing pressures. The amount of gas adsorbed is recorded at each pressure point. The relationship between the amount of gas adsorbed and the pressure is known as an adsorption isotherm.
- **Langmuir Monolayer:** At low pressures, gas molecules begin to adsorb onto the material's surface, forming a monolayer. The Langmuir adsorption model assumes that each adsorption site can accommodate only one gas molecule. However, this model is limited to low pressures and does not accurately represent adsorption behavior at higher pressures.
- **Multilayer Adsorption:** As pressure increases, additional gas molecules begin to adsorb onto the surface, forming multilayers. The BET theory assumes that these multilayers are physically indistinguishable, and the relative pressure at which multilayer adsorption begins is termed the "BET C value."
- **BET Equation:** The BET equation correlates the amount of adsorbed gas with the relative pressure. It is given by:

$$\frac{V_m}{V} = \frac{C \cdot P}{(P_0 - P) \cdot (1 - C \cdot P)}$$

Where:

V_m is the volume of gas adsorbed at monolayer coverage.

V is the volume of gas adsorbed at the given pressure.

C is the BET constant related to the energy of adsorption.

P is the relative pressure.

P₀ is the saturation pressure.

- **Surface Area Calculation:** The specific surface area of the material can be calculated from the slope of the BET plot, which is obtained by plotting V against $P / (P_0 - P)$. The slope of the linear portion of the plot gives the BET constant C, and from this constant, the specific surface area can be calculated using the Avogadro number and the cross-sectional area occupied by a nitrogen molecule.

The BET analysis provides valuable information about the porosity and surface characteristics of materials, making it an essential tool in various scientific and industrial applications.

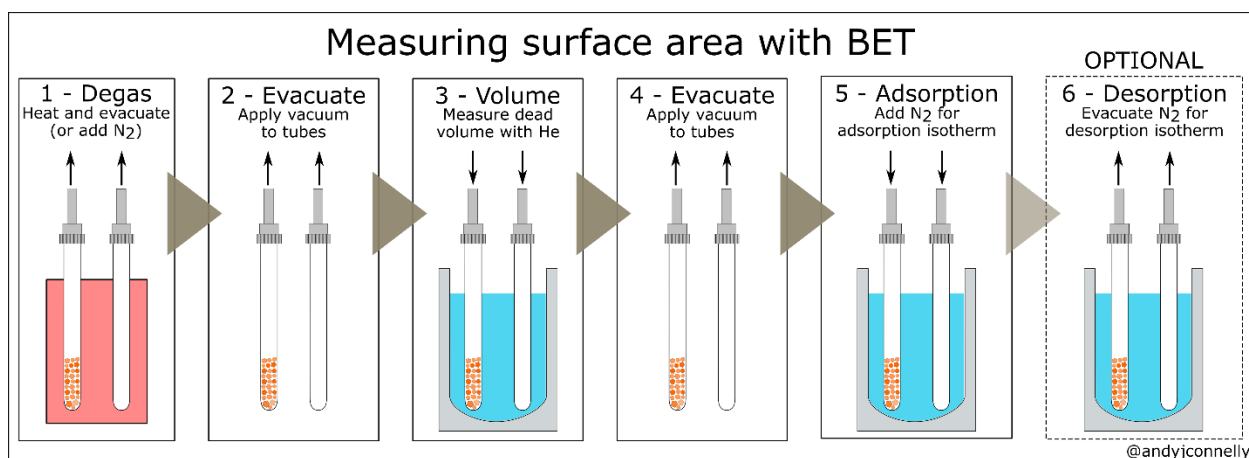


Figure 4.6: Working principle of BET

4.8 Cyclic Voltammetry (CV)

Cyclic voltammetry (CV) is a sophisticated electrochemical technique designed to elucidate the redox behavior and capacitive properties of materials within a three-electrode system. This fundamental method is extensively employed for characterizing supercapacitors and other electrochemical devices. The three-electrode system comprises a working electrode, a reference electrode, and a counter electrode. In the context of supercapacitor characterization, the working electrode represents the supercapacitor

electrode material, the reference electrode maintains a stable potential, and the counter electrode facilitates the flow of current between the working and reference electrodes.

During a CV experiment, the potential of the working electrode is systematically scanned between two predetermined limits, while the current flowing between the working and counter electrodes is measured. This cyclic potential sweep allows for the investigation of reversible redox reactions, the identification of electroactive species, and the evaluation of the electrochemical reversibility of the system. The shape and characteristics of the CV curves provide valuable information about the kinetics, thermodynamics, and mechanisms of the electrochemical processes occurring at the electrode surface.

4.8.1 Working Principle

- **Setup:** A three-electrode system for supercapacitors consists of a working electrode immersed in an electrolyte solution, connected to an external circuit. A reference electrode and a counter electrode are also submerged in the electrolyte. The reference electrode maintains a stable potential against which the working electrode's potential is measured, while the counter electrode facilitates current flow between the working electrode and the reference electrode.
- **Potential Cycling:** In cyclic voltammetry (CV), the potential of the working electrode is systematically altered between two predetermined limits, typically from a negative to a positive potential and then back again. This potential range is known as the "potential window." As the potential changes, electrochemical reactions occur at the interface between the electrode and the electrolyte.
- **Electrochemical Reactions:** During the forward scan (from negative to positive potential), the potential applied to the working electrode increases. Depending on the electrode material, various electrochemical processes can occur, such as redox reactions, ion adsorption/desorption, or double-layer capacitance formation. These processes involve the movement of electrons and ions at the electrode-electrolyte interface.

- **Current Measurement:** As electrochemical reactions occur, a current flows between the working electrode and the auxiliary electrode. This current is measured and recorded at various potentials as the potential is swept within the specified range. The resulting current-potential curve is known as a "voltammogram."
- **Reverse Scan:** After completing the forward scan, the potential is reversed and cycled back to the starting potential in the negative direction. This allows for the observation of reverse electrochemical reactions, and the corresponding current is recorded.
- **Data Analysis:** By analyzing the voltammogram, valuable information about the electrochemical properties of the working electrode can be obtained. The shape and characteristics of the voltammogram, such as the peak currents, peak potentials, and reversibility, provide insights into the redox reactions, charge storage mechanisms, and kinetic parameters of the electrode material.

4.8.2 *Result Interpretation*

The cyclic voltammogram obtained from the CV experiment offers valuable insights into the electrochemical behavior of the supercapacitor electrode material. The peaks and features observed in the voltammogram are directly linked to specific electrochemical processes:

- **Anodic Peak:** An increase in current during the forward scan indicates an oxidative reaction, which may involve ion desorption from the electrode surface.
- **Cathodic Peak:** A decrease in current during the forward scan suggests a reductive reaction, which could involve ion adsorption onto the electrode surface.
- **Double-Layer Capacitance:** The region near the reversible potential is associated with the formation of an electric double layer (EDL) at the electrode-

electrolyte interface. The slope of this region provides information about the specific capacitance of the material.

- Faradaic Processes: Peaks observed away from the reversible potential can indicate faradaic reactions involving redox chemistry.

By analyzing the shape, position, and magnitude of peaks in the cyclic voltammogram, researchers can infer important electrochemical parameters such as specific capacitance, reversibility of reactions, and the overall performance of supercapacitor electrode materials.

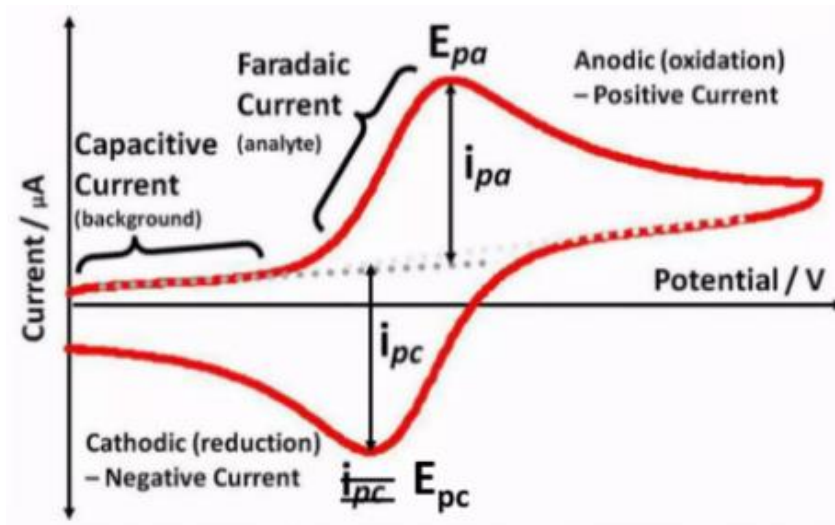


Figure 4.7: *Cyclic voltammogram for an electrochemically reversible redox process*

4.9 Galvanic Charge Discharge (GCD)

Galvanostatic charge-discharge (GCD) is a sophisticated electrochemical technique designed to elucidate the energy storage and discharge behavior of supercapacitors within a three-electrode system. This method provides valuable insights into the capacitance, energy density, power density, and internal resistance of the supercapacitor electrode material. The three-electrode system comprises a working electrode, a reference electrode, and a counter electrode.

In a GCD experiment, a constant current is applied to the working electrode, and the resulting potential change over time is monitored. During the charging process, the applied current forces ions to intercalate into the electrode material, storing energy. During the discharging process, the stored ions are released, resulting in the generation of electrical energy. By analyzing the charge-discharge curves obtained from GCD measurements, researchers can evaluate the electrochemical performance of supercapacitors and optimize their design for various applications.

4.9.1 Working Principle

- **Initial State:** At the outset of the experiment, the working electrode is in its initial state, which can be either fully charged or at an equilibrium potential.
- **Galvanostatic Charging:** During the galvanostatic charging phase, a constant current is applied to the working electrode. This applied current induces the accumulation of charge on the electrode's surface, resulting in the charging of the electric double layer (EDL) formed at the electrode-electrolyte interface. As the charge accumulates, the voltage across the working electrode gradually increases.
- **Monitoring Voltage:** During galvanostatic charging, the voltage across the working electrode is monitored over time. This voltage increase is influenced by the specific capacitance of the electrode material and the electrolyte's resistance.
- **Galvanostatic Discharging:** Once the desired charge level is reached or a specific charging time is completed, the constant current is switched off. The supercapacitor is then discharged at a constant current (the same magnitude as the charging current) in the galvanostatic discharging phase. As the discharge progresses, the voltage across the working electrode decreases.
- **Monitoring Voltage Drop:** During galvanostatic discharging, the voltage across the working electrode is monitored over time. The voltage drop occurs as the

stored charge is released from the electrode surface. The rate of voltage drop is also affected by the electrode material's specific capacitance and the internal resistance of the supercapacitor.

4.9.2 Result Interpretation

The galvanostatic charge-discharge experiment provides valuable insights into the supercapacitor's energy storage and discharge capabilities.

- **Charge and Discharge Profiles:** The voltage-time plots obtained during the charging and discharging phases depict the supercapacitor's energy storage and release behavior. The slope of these curves indicates the device's capacitance.
- **Voltage Drop:** The decrease in voltage during discharge reveals the internal resistance of the supercapacitor. A larger voltage drop signifies higher internal resistance, which negatively impacts the supercapacitor's overall performance.
- **Energy and Power Density:** The area beneath the discharge curve represents the energy stored by the supercapacitor. The ratio of the stored energy to the discharge time yields the power density.

By analyzing the charge and discharge profiles, researchers can quantify the energy and power performance of supercapacitor electrode materials and assess their suitability for various applications.

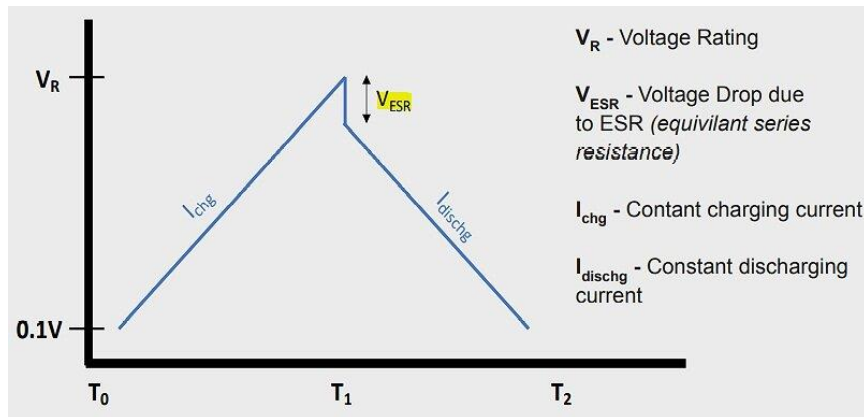


Figure 4.8: Schematic illustration of a GCD plot

4.10 -Electrochemical Impedance Spectroscopy (EIS)

Electrochemical Impedance Spectroscopy (EIS) is an advanced and highly sensitive analytical technique utilized to investigate the electrochemical properties of supercapacitors and other electrochemical systems, particularly within a three-electrode configuration. This method is extensively applied in the assessment of material impedance, offering profound insights into the material's composition, reaction mechanisms, intermediates, and electrochemical interface reactions. EIS is instrumental in various research domains, including sensing technologies, corrosion studies, fuel cell analysis, and capacitor performance assessment. Through EIS, researchers can gain critical understanding of the internal processes, charge transfer kinetics, and resistive characteristics of supercapacitor electrode materials, making it an invaluable tool in the field of electrochemical research.

4.10.1 Working Principle

Electrochemical Impedance Spectroscopy (EIS) measurements are conducted across a range of frequencies, producing a curve composed of two distinct sections: the real axis and a semicircular arc. The shape of this curve is heavily influenced by the material properties under investigation. For optimal capacitive materials, the ideal EIS curve would feature a nearly vertical real axis and a smaller semicircle, indicating superior system performance. The analysis of the Nyquist plot, derived from the EIS data, is crucial for determining the resistances within the system. Selecting an appropriate equivalent circuit model is essential for performing z-fitting and accurately assessing the system's impedance. The EIS spectra reveal several characteristic features that provide valuable insights into the behavior of supercapacitors:

- Electrolyte Resistance (R_s): At high frequencies, the impedance is primarily governed by the solution resistance, which encompasses both the resistance of the electrolyte and the current path within the solution.
- Charge Transfer Resistance (R_{ct}): At intermediate frequencies, the impedance plot exhibits a semicircular feature. This semicircle corresponds to the charge transfer

resistance, representing the resistance encountered during charge transfer reactions at the electrode-electrolyte interface.

- Double-Layer Capacitance (Cdl): The radius of the semicircle is inversely related to the double-layer capacitance, which signifies the capacitance of the electric double layer formed at the electrode-electrolyte interface.
- Warburg Element (W): At low frequencies, the impedance plot displays a sloping line indicative of the Warburg element, which is associated with diffusion-limited processes occurring at the electrode-electrolyte interface.

By analyzing the impedance spectra and fitting them to appropriate equivalent circuit models, researchers can extract quantitative information about the supercapacitor's electrochemical processes, including specific capacitance, charge transfer resistance, diffusion coefficients, and more. EIS is especially valuable for understanding how electrode materials, electrolyte properties, and electrode structure impact the performance of supercapacitors.

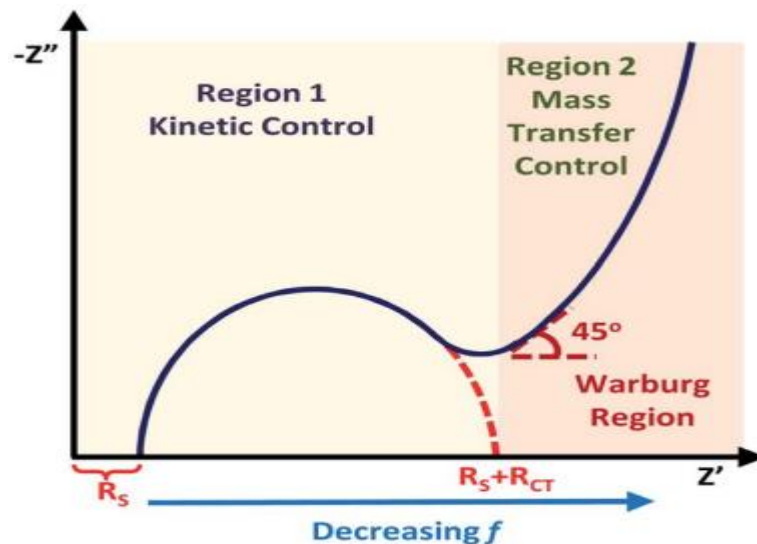


Figure 4.9: Schematic illustration of a Nyquist plot

CHAPTER 5: RESULTS AND DISCUSSION

5.1 Structural, Compositional, and Morphological Analysis

5.1.1 X-Ray Diffraction Analysis (XRD)

The phase purity and crystallinity of the MnO₂/CeO₂/MWCNT ternary composite were meticulously evaluated using X-ray Diffraction (XRD) analysis, as illustrated in Figure 5.1 (a). The resulting diffraction pattern reveals distinct peaks that correspond to MnO₂, CeO₂, and MWCNT, confirming the successful formation of the ternary composite.

The diffraction peaks, observed at 12.7°, 18.1°, 28.9°, 37.5°, 49.8°, and 56.9°, are attributed to the (110), (200), (310), (211), (411), and (431) planes of the α -phase MnO₂ structure, which crystallizes in a tetragonal crystal system, as indexed by JCPDS #44-0141. These peaks are characteristic of the MnO₂ component within the composite, affirming its presence and crystalline integrity.

Further analysis reveals diffraction peaks at 28.5°, 33.0°, 47.4°, and 56.3°, corresponding to the (111), (200), (220), and (311) planes of CeO₂. These peaks, indexed according to JCPDS #34-0394, indicate that the CeO₂ component adopts a face-centered cubic crystal system with an Fm-3m space group. Interestingly, the CeO₂ peaks are noticeably broader than those of MnO₂, suggesting that CeO₂ has a smaller crystallite size compared to MnO₂ within the composite.

The incorporation of multi-walled carbon nanotubes (MWCNTs) into the composite is confirmed by the presence of a distinct diffraction peak at 26.5°, which is characteristic of MWCNTs [153]. This peak further verifies the successful integration of MWCNTs into the ternary structure.

Overall, the XRD pattern effectively demonstrates that the MnO₂, CeO₂, and MWCNT components maintain their original crystal structures within the ternary composite. This is further substantiated by the recorded diffraction pattern of the MnO₂ structure, as depicted in Figure 5.1 (b). The data collectively indicate that the ternary

composite has been synthesized with well-preserved crystalline phases, highlighting the structural integrity and successful combination of the individual materials.

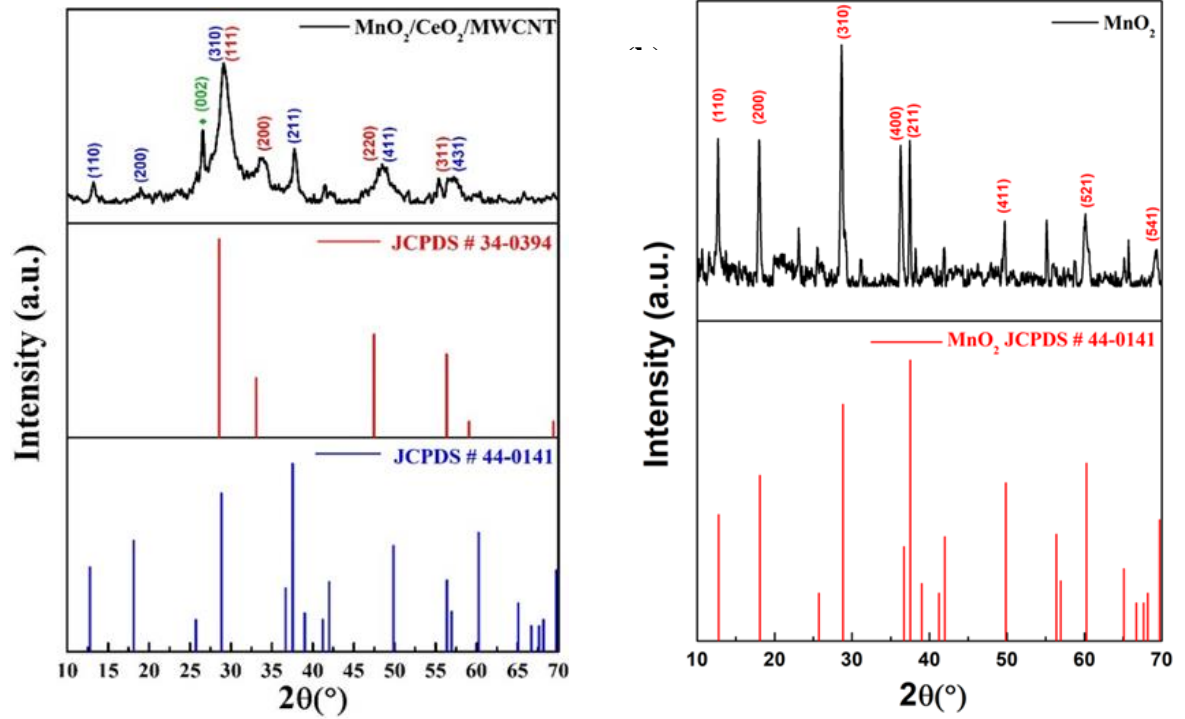


Figure 5.1: XRD pattern of (a) $MnO_2/CeO_2/CNT$ and (b) MnO_2

5.1.2 Raman Analysis

Figure 5.2 presents the Raman spectra of pristine MnO_2 , MWCNT, MnO_2/CeO_2 , and $MnO_2/CeO_2/MWCNT$ structures, captured across the wavelength range of 200 to 1800 cm^{-1} . The spectrum of MnO_2 is dominated by a pronounced peak at 622 cm^{-1} , corresponding to the A_{1g} symmetric vibrational mode within the C_{2h3} spectroscopic space group. This peak is indicative of Mn-O lattice vibrations that occur perpendicular to the MnO_6 octahedral double chain direction, which is characteristic of a well-defined tetragonal structure featuring [2 x 2] channels. This observation underscores the structural integrity of MnO_2 in the material [154].

In the MnO_2/CeO_2 composite spectrum, an additional peak emerges at 448 cm^{-1} , which is a signature of the cubic fluorite structure of CeO_2 , attributed to the F_{2g} vibrational

mode within the Fm3m space group. The broadness of this peak not only suggests a smaller particle size of CeO₂ but also serves as an indicator of the presence of oxygen vacancies within the material, which are crucial for enhancing its electrochemical properties [155].

The Raman spectrum of the MnO₂/CeO₂/MWCNT ternary composite confirms the successful integration of all three components. The characteristic peaks for MnO₂ and CeO₂ are observed at 622 cm⁻¹ and 448 cm⁻¹, respectively. Additionally, the presence of MWCNTs within the composite is confirmed by the detection of the D and G bands at 1344 cm⁻¹ and 1579 cm⁻¹, respectively. The D band is associated with an asymmetric vibrational state known as A_{1g}, representing the breathing mode of sp² carbon atoms in disordered graphite, while the G band corresponds to the E_{2g} vibrational mode, reflecting the in-plane expansion and contraction of sp²-bonded carbon atoms [156].

The ID/IG ratio, a crucial metric for assessing the concentration of defects in carbon-based materials, reveals that the ternary composite exhibits a higher ratio (1.22) compared to pristine MWCNTs (0.96). This increase in the ID/IG ratio indicates a greater number of surface defects within the ternary composite, which is advantageous for enhancing its electrochemical activity, making it particularly well-suited for applications requiring high-performance materials [153].

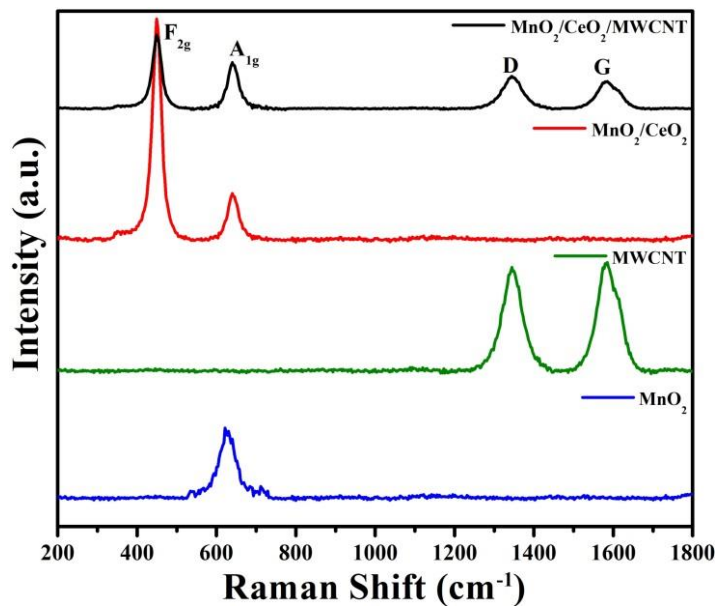


Figure 5.2: Raman plot of MnO₂, MWCNTs, MnO₂/CeO₂, MnO₂/CeO₂/MWCNT

5.1.3 Morphological Analysis

Scanning Electron Microscopy (SEM) is employed to investigate the morphology of the MnO₂/CeO₂/MWCNT ternary nanostructure in detail. Figure 5.3 (a) provides a clear visualization of the nanocomposite, revealing numerous spherical CeO₂ nanoparticles anchored onto the surfaces of MnO₂ nanorods and multi-walled carbon nanotubes (MWCNTs). The image showcases a complex and interconnected network, where the spherical CeO₂ particles are distributed across the MnO₂ nanorods and MWCNTs, creating a robust and integrated composite structure.

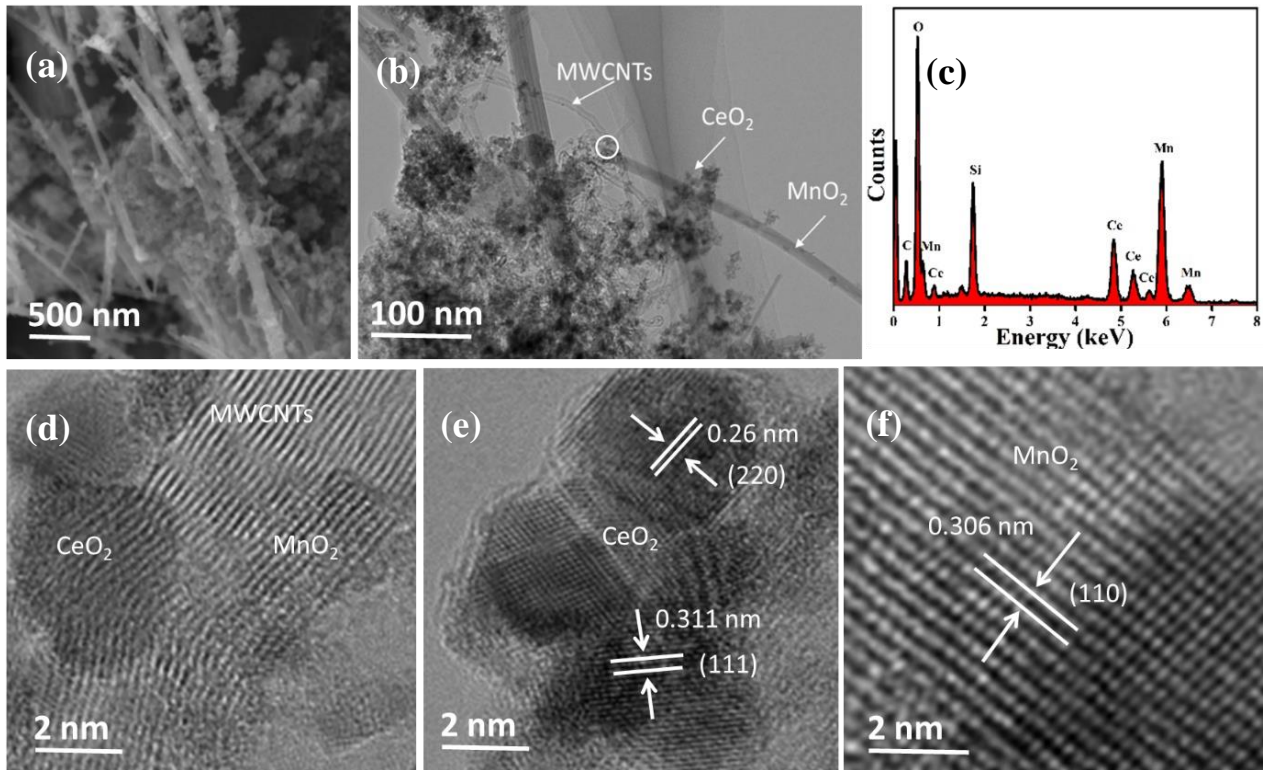


Figure 5.3: (a) SEM (b) TEM image of MnO₂/CeO₂/MWCNT nanocomposite (b) Corresponding EDS, and (d-f) HRTEM images taken from different parts of MnO₂/CeO₂/MWCNT composite.

Figure 5.3 (b) presents the Transmission Electron Microscopy (TEM) micrograph of the MnO₂/CeO₂/MWCNT composite, corroborating the findings observed in the SEM analysis. The TEM image further confirms the successful formation of the ternary

nanocomposite, with marked arrows clearly indicating the presence of all three components: MnO₂ nanorods, CeO₂ nanoparticles, and MWCNTs. Notably, the CeO₂ nanoparticles appear to be non-uniformly anchored on the MnO₂ nanorods and MWCNTs, suggesting a heterogeneous distribution that may influence the composite's overall properties.

Energy Dispersive X-ray Spectroscopy (EDS) analysis, shown in Figure 5.3 (c), provides elemental confirmation of the composite's formation by revealing the presence of Mn, O, Ce, and C elements. This analysis affirms the successful synthesis of the MnO₂/CeO₂/MWCNT composite by identifying the key constituents within the nanostructure.

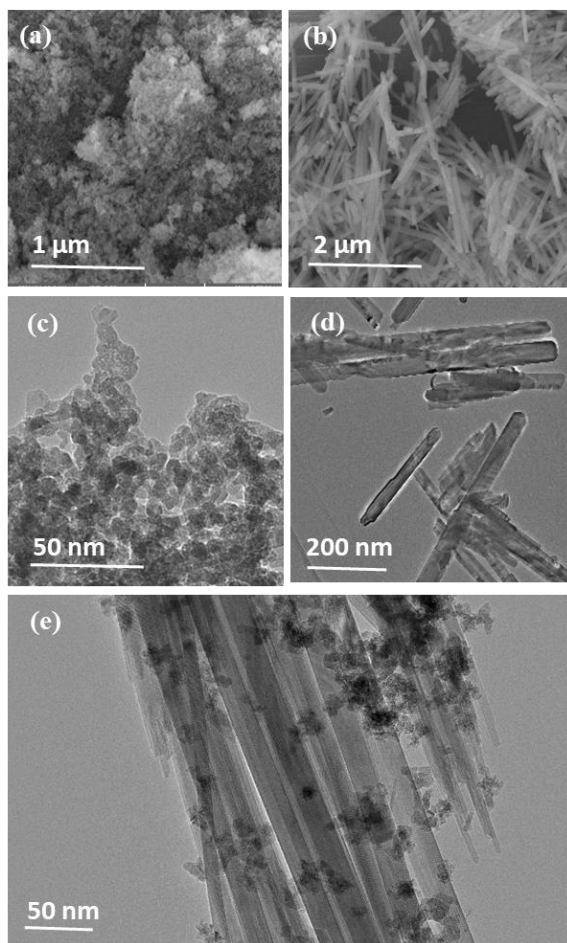


Figure 5.4: (a-b) SEM images of CeO₂ and MnO₂ nanostructures respectively, and (c-e) TEM images of CeO₂, MnO₂ and MnO₂/CeO₂ nanostructures respectively.

Further SEM images, displayed in Figures 5.4 (a) and 5.4 (b), offer a closer look at the individual components, showing CeO₂ nanoparticles with an approximate diameter of 20 nm and MnO₂ nanorods with lengths extending several microns. These images provide additional evidence of the nanoscale dimensions and morphology of the composite components.

High-Resolution Transmission Electron Microscopy (HRTEM) is utilized to delve deeper into the internal structure of the MnO₂/CeO₂/MWCNT ternary composite. Figure 5.3 (d) showcases an HRTEM image focused on a specific area marked with a circle in Figure 5.3 (b), reinforcing the presence of the MnO₂, CeO₂, and MWCNT components. Figures 5.3 (e) and 5.3 (f) further illustrate HRTEM images taken from different regions of the composite. The lattice spacing measured in Figure 5.3 (e) is approximately 0.26 nm and 0.311 nm, corresponding to the (220) and (111) crystallographic planes of the face-centered cubic CeO₂ nanoparticles. Additionally, the planar distance measured for the MnO₂ nanorods is about 0.306 nm, corresponding to the (110) plane of α -MnO₂, as depicted in Figure 5.3 (f).

Moreover, TEM images of the CeO₂ nanoparticles, MnO₂ nanorods, and the MnO₂/CeO₂ composite are also presented in Figures 19(c) to 19(e), offering a comprehensive view of the individual components and their integration into the ternary nanostructure. These images collectively provide a detailed understanding of the morphological and structural characteristics of the MnO₂/CeO₂/MWCNT composite, highlighting the successful synthesis and complex interplay of its constituent materials.

5.1.4 Brunauer, Emmett and Teller Analysis (BET)

Figure 5.5 (a) presents the Brunauer-Emmett-Teller (BET) specific surface area isotherms for MnO₂, MnO₂/CeO₂, and MnO₂/CeO₂/MWCNT structures, measured through nitrogen adsorption-desorption at 77 K. The isotherm for the ternary MnO₂/CeO₂/MWCNT composite displays a characteristic type-IV curve with an H3 hysteresis loop, indicating the mesoporous nature of the material. The presence of this mesoporous structure is critical,

as it facilitates the flow of ions within the material, thereby enhancing its electrochemical performance, particularly in terms of rate capability and power output.

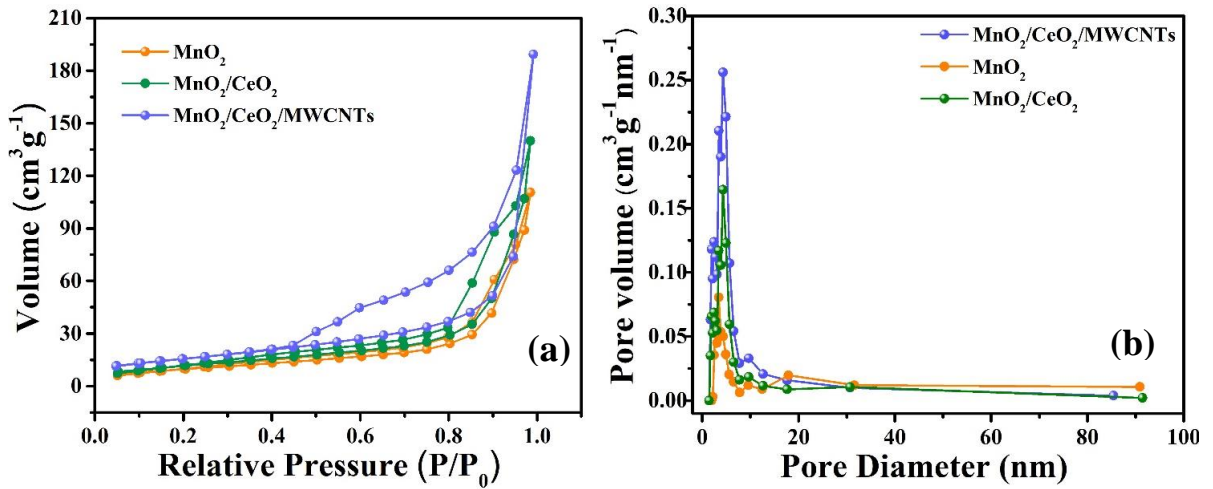


Figure 5.5: (a) Nitrogen adsorption-desorption isotherm, and (b) pore size distribution behavior of MnO₂, MnO₂/CeO₂, and MnO₂/CeO₂/MWCNT composite.

Notably, the surface area of the MnO₂/CeO₂/MWCNT composite shows a significant improvement, reaching 166.7 m²g⁻¹. This is a substantial increase compared to the binary MnO₂/CeO₂ composite, which has a surface area of 130.4 m²g⁻¹, and the pristine MnO₂, with a surface area of 100.2 m²g⁻¹. This enhancement in surface area is a direct consequence of the synergistic interaction between MnO₂, CeO₂, and MWCNTs in the ternary composite, providing an expansive interface for ion exchange and electrochemical reactions. The large surface area, combined with the mesoporous architecture, creates a network of accessible reaction sites, contributing to improved electrochemical activity.

The pore size distribution of these materials was further analyzed using the Barrett-Joyner-Halenda (BJH) method, as depicted in Figure 5.5 (b). The pore size distribution plots reveal the existence of mesopores within the range of 3 to 20 nm across all samples. These mesopores are especially advantageous in electrochemical applications, as they allow for rapid ion transport and diffusion, which is essential for efficient energy storage and conversion processes.

The results underscore that the MnO₂/CeO₂/MWCNT ternary composite, with its high surface area and well-distributed mesopores, provides an extensive network of accessible pathways for ions. This structure promotes faster charge transfer and supports improved electrochemical performance, making it an excellent candidate for high-rate capability and power output applications. The intricate pore network, combined with the increased surface area, ensures that the composite can deliver superior performance in energy storage devices, providing ample active sites for reactions and facilitating efficient ion movement throughout the material.

5.1.5 X-ray Photoelectron Spectroscopy Analysis

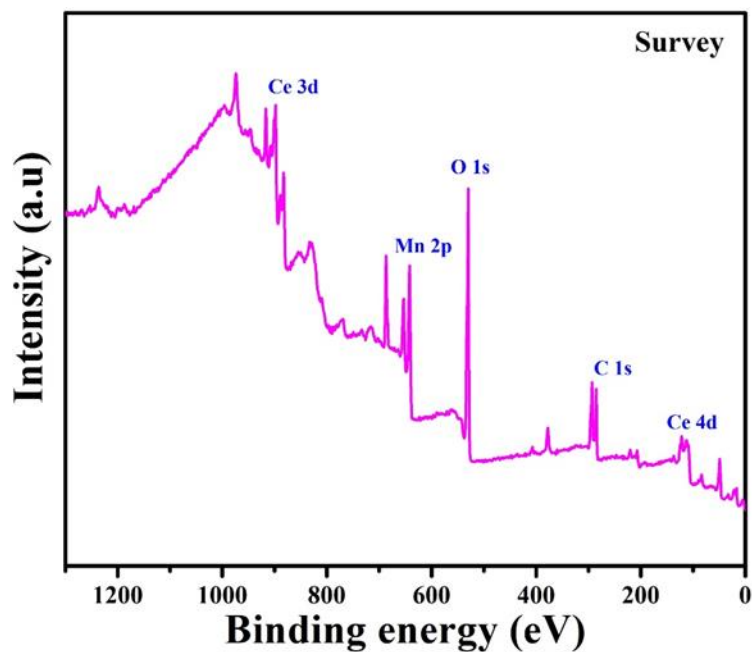


Figure 5.6: XPS Survey spectrum of MnO₂/CeO₂/CNT nanocomposite.

The valence states of the surface atoms and chemical composition of the MnO₂/CeO₂/MWCNT ternary composite were thoroughly investigated using X-ray photoelectron spectroscopy (XPS), a sophisticated technique that provides in-depth insight into the electronic structure and surface chemistry of materials. The broad survey spectrum shown in Figure 5.6 confirms the successful integration of manganese (Mn), oxygen (O), carbon (C), and cerium (Ce) elements in the synthesized composite, affirming its intended

composition. This comprehensive elemental mapping is crucial as it not only validates the formation of the MnO₂/CeO₂/MWCNT composite but also provides preliminary insights into the nature of the interactions between the three components.

Focusing on the high-resolution Mn 2p spectrum presented in Figure 5.7, a well-defined spin-orbit doublet is observed, with distinct peaks at binding energies of 641.8 eV and 653.4 eV. These peaks correspond to the Mn 2p_{3/2} and Mn 2p_{1/2} states, respectively, and the energy splitting between them is approximately 11.6 eV, a value that is consistent with literature reports for manganese oxides [157].

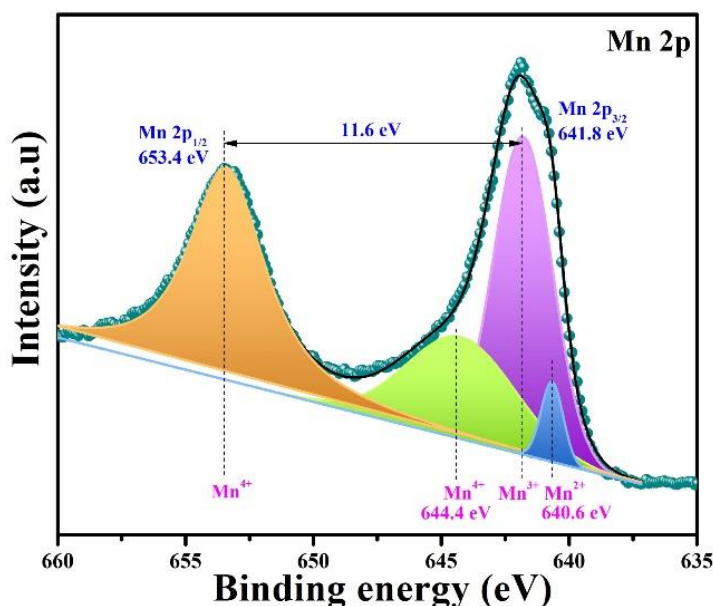


Figure 5.7: High-resolution XPS spectrums of Mn 2p

The precise deconvolution of this spectrum reveals three notable oxidation states of manganese within the composite: Mn²⁺, Mn³⁺, and Mn⁴⁺, appearing at 640.6 eV, 641.8 eV, and 644.4 eV, respectively [158]. The Mn 2p_{1/2} peak at 653.4 eV is solely attributed to Mn⁴⁺, indicating the predominant presence of this higher oxidation state, which is known to facilitate enhanced redox activity [159].

Such multivalent states of Mn are particularly advantageous for redox reactions, as they enable efficient electron exchange between different oxidation states, thereby enhancing the overall electrochemical performance of the composite. The coexistence of

these Mn oxidation states, therefore, plays a pivotal role in promoting electronic charge transfer processes within the composite material, making it highly suitable for applications where electrochemical efficiency is paramount, such as in energy storage devices like supercapacitors and batteries.

Moving on to the oxygen states, the high-resolution O 1s spectrum, illustrated in Figure 5.8, provides critical information regarding the chemical environment of oxygen within the composite. The spectrum is deconvoluted into three major peaks located at binding energies of 529.5 eV, 531.2 eV, and 532.9 eV, each corresponding to distinct types of oxygen species. The peak at 529.5 eV is attributed to lattice oxygen (O_{latt}), which is oxygen that is tightly integrated into the crystal structure of the metal oxides, contributing to the structural integrity of the MnO_2 and CeO_2 phases. The peak at 531.2 eV corresponds to oxygen vacancies (O_v), which are sites where oxygen atoms are missing from the lattice. These vacancies are of particular interest because they are known to enhance the material's catalytic and electrochemical properties by creating active sites for charge transfer and ion diffusion. Finally, the peak at 532.9 eV is assigned to adsorbed hydroxyl groups ($O_{\text{ads-OH}}$) on the surface of the material. These hydroxyl groups may play a role in surface reactions, further influencing the electrochemical behavior of the composite [160].

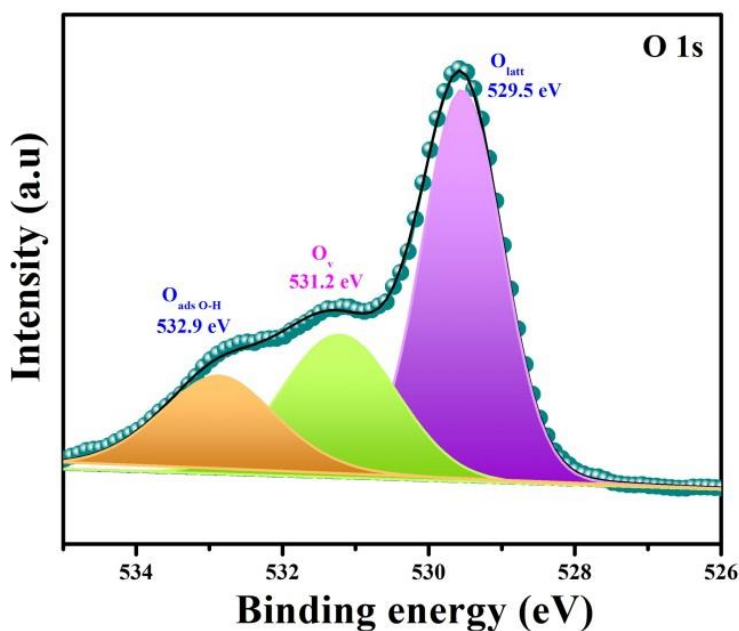


Figure 5.8: High-resolution XPS spectrums of O1s

A noteworthy observation is the significantly higher oxygen vacancy to lattice oxygen ratio (O_v/O_{latt}) of 0.5 for the $MnO_2/CeO_2/MWCNT$ composite compared to a ratio of 0.46 for pristine MnO_2 . This increase in oxygen vacancies is indicative of enhanced defect density within the composite, which is highly desirable for improving the electrochemical performance. Oxygen vacancies serve as active sites for redox reactions, promote ion mobility, and facilitate electron transfer, thus enhancing the efficiency of electrochemical processes such as charge storage and discharge in supercapacitors. The higher O_v/O_{latt} ratio suggests that the ternary composite has a more defect-rich structure compared to the binary and pristine counterparts, making it more effective for energy storage applications.

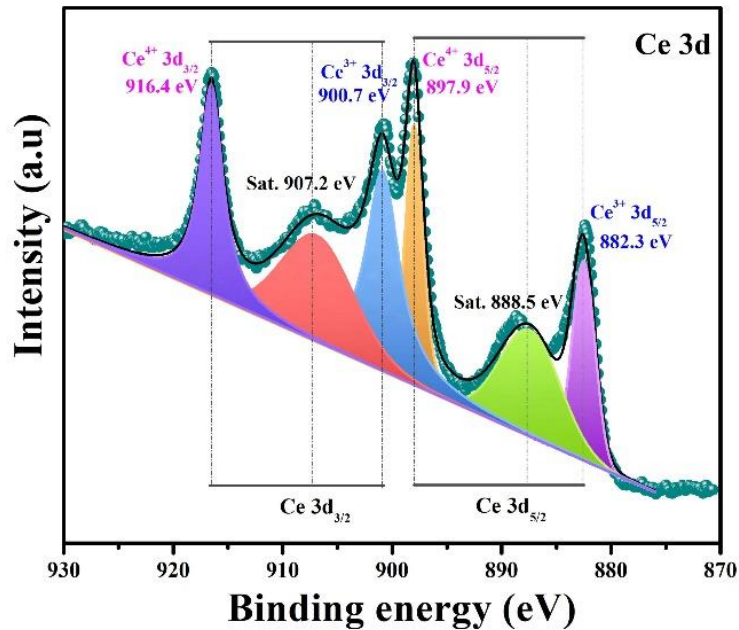


Figure 5.9: High-resolution XPS spectra of Ce 3d

The analysis of the Ce 3d region, as shown in Figure 5.9, offers further insights into the electronic environment of cerium within the composite. The spectrum reveals the coexistence of Ce^{4+} and Ce^{3+} oxidation states, which contribute to the complex electronic structure of the material. The Ce 3d spectrum is characterized by the splitting of d-orbitals into two spin-orbit components, $3d_{3/2}$ and $3d_{5/2}$, due to the strong spin-orbit coupling inherent to cerium [42]. The peaks located at 882.3 eV and 900.7 eV are attributed to Ce^{3+} $3d_{5/2}$ and Ce^{3+} $3d_{3/2}$, respectively, while the peaks at 897.9 eV and 916.4 eV correspond to

$Ce^{4+} 3d_{5/2}$ and $Ce^{4+} 3d_{3/2}$. In addition to these primary peaks, two satellite peaks at 888.5 eV and 907.2 eV, associated with Ce^{3+} , can also be observed in the spectrum [42]. The presence of Ce^{3+} valence states improves the electrical conductivity as well as boosts the electrochemical performance as reported [161]. The presence of Ce^{3+} in the composite plays a crucial role in enhancing the material's electrical conductivity. Ce^{3+} ions are known to facilitate electron transport by increasing the density of free charge carriers, thereby boosting the composite's overall electrochemical performance [162]. Furthermore, the reduction of Ce^{4+} to Ce^{3+} within the composite induces the formation of additional oxygen vacancies, as previously highlighted in the O 1s analysis. These vacancies not only improve conductivity but also create more reactive sites for redox reactions, further enhancing the material's functionality in energy storage devices.

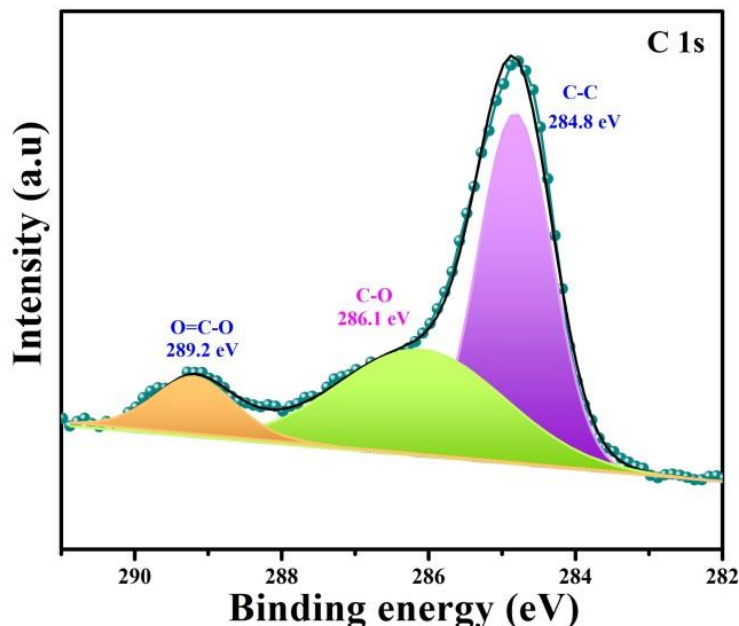


Figure 5.10: High-resolution XPS spectrums of C1s

Finally, the high-resolution C 1s spectrum, depicted in Figure 5.10, provides a detailed analysis of the chemical states of carbon within the $MnO_2/CeO_2/MWCNT$ composite. The deconvolution of the C 1s spectrum reveals three primary peaks located at 284.8 eV, 286.1 eV, and 289.2 eV. The peak at 284.8 eV is attributed to C–C bonds, which represent the sp^2 hybridized carbon atoms in the MWCNTs, contributing to the structural framework of the composite. The peak at 286.1 eV corresponds to C–O bonds, indicating

the presence of oxygenated functional groups on the surface of the MWCNTs, which may arise from surface modifications or interactions with MnO₂ and CeO₂. Lastly, the peak at 289.2 eV is assigned to O=C–O bonds, signifying the presence of carboxyl groups, which can improve the wettability and electrochemical interface between the MWCNTs and the electrolyte. The presence of these functional groups is beneficial as it enhances the interfacial contact between the MWCNTs and the metal oxides, thereby improving charge transfer kinetics and overall electrochemical stability [159].

In conclusion, the XPS analysis provides a comprehensive understanding of the surface chemistry and electronic structure of the MnO₂/CeO₂/MWCNT ternary composite. The presence of multivalent Mn states, oxygen vacancies, Ce³⁺ ions, and functionalized carbon atoms all contribute to the enhanced electrochemical performance of the composite, making it a promising candidate for advanced energy storage applications. The rich surface chemistry and well-defined electronic states uncovered by XPS highlight the potential of this composite for efficient charge storage and fast charge-discharge cycles in supercapacitors and related devices.

5.2 Electrochemical performance of MnO₂/CeO₂/MWCNT electrode

5.2.1 Cyclic Voltammetry (CV)

The electrochemical performance of the MnO₂, MnO₂/CeO₂, and MnO₂/CeO₂/MWCNT electrodes was systematically evaluated by conducting cyclic voltammetry (CV) measurements in a 1 M Na₂SO₄ electrolyte solution. This electrolyte was selected due to its electrochemical stability, which allows for a broader voltage window and accurate assessment of the capacitive behavior of the electrodes. The comparative supercapacitive performance of these electrodes is illustrated in Figure 5.11, which presents the CV curves of all three fabricated electrodes at a scan rate of 20 mV/s. Each of these curves displays a quasi-rectangular shape, a characteristic feature that signifies typical capacitive behavior. This shape suggests that the charge storage mechanism in these electrodes is predominantly electrostatic in nature, consistent with the

ideal behavior of supercapacitors where charges are stored at the electrode-electrolyte interface without significant faradaic reactions [163].

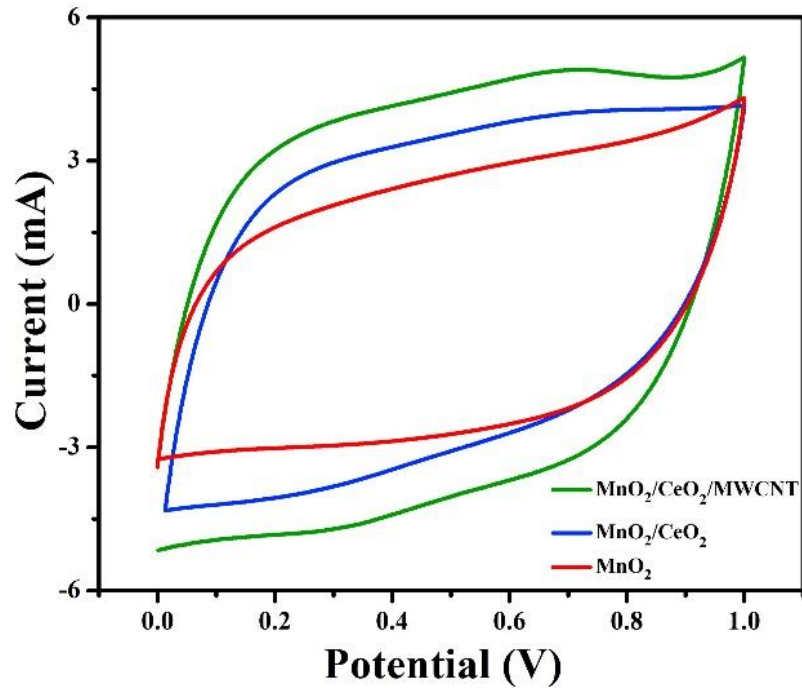


Figure 5.11: CV plots of MnO_2 , MnO_2/CeO_2 , and $MnO_2/CeO_2/MWCNT$ at the scan rate of $20mVs^{-1}$

Of particular importance, the area enclosed by the CV curve of the $MnO_2/CeO_2/MWCNT$ electrode is considerably larger than that of the MnO_2 and MnO_2/CeO_2 electrodes. The area under the CV curve is directly proportional to the charge storage capacity of the electrode material, with a larger area signifying greater charge storage. This observation strongly suggests that the $MnO_2/CeO_2/MWCNT$ ternary composite has superior charge storage capabilities compared to the other two materials. The enhanced performance of this ternary composite can be attributed to several key factors. Firstly, the synergistic combination of MnO_2 , CeO_2 , and MWCNTs leads to an improved electrochemical interface, where MnO_2 contributes to fast redox reactions, CeO_2 provides structural support and enhances electrical conductivity, and MWCNTs offer high surface area and excellent electron transport pathways. The redox activity of MnO_2 is further enhanced by the presence of CeO_2 , which creates more active sites for electron transfer. In addition, the incorporation of MWCNTs into the composite structure

contributes to improved ion accessibility, allowing for faster ion diffusion within the electrode material. These factors collectively result in a significant improvement in the overall charge storage performance of the MnO₂/CeO₂/MWCNT electrode.

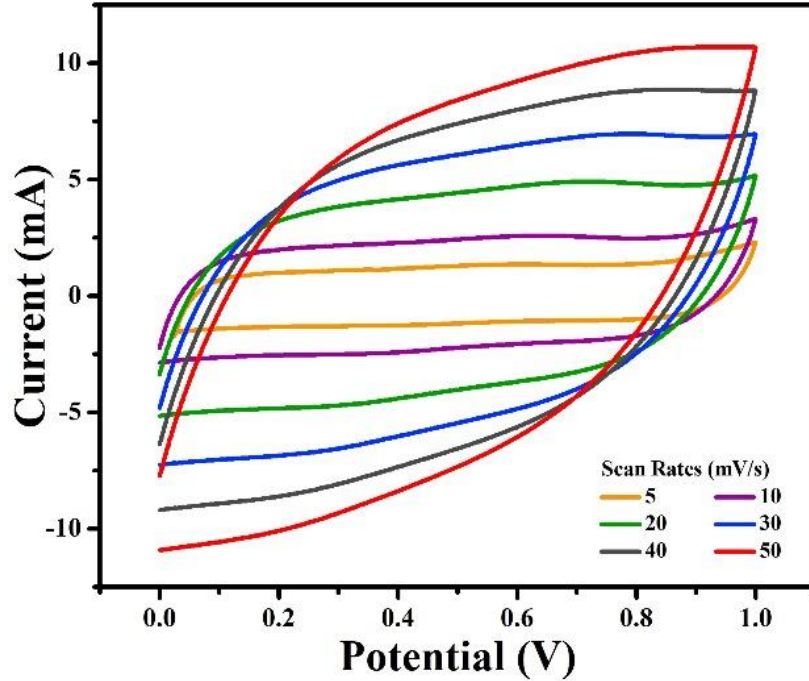


Figure 5.12: CV plots of MnO₂/CeO₂/MWCNT at different scan rates

To further investigate the rate capability and stability of the MnO₂/CeO₂/MWCNT electrode, CV measurements were performed at a range of scan rates from 5 to 50 mV/s, as depicted in Figure 5.12. These measurements were conducted within a voltage window of 0 to 1 V, which is typical for supercapacitor applications to ensure the safe operation of the device while maximizing energy storage. The results demonstrate that the area enclosed by the CV curve increases as the scan rate increases. This increase in the integrated area without significant distortion in the shape of the CV curves indicates that the MnO₂/CeO₂/MWCNT electrode exhibits excellent rate capability. In other words, the electrode can maintain its charge storage performance even at higher scan rates, which is a desirable trait for high-power applications where rapid charge-discharge cycles are required. The ability to sustain a quasi-rectangular CV profile across a wide range of scan rates suggests that the electrode material maintains its capacitive behavior and remains electrochemically stable, with minimal degradation or loss of performance over time.

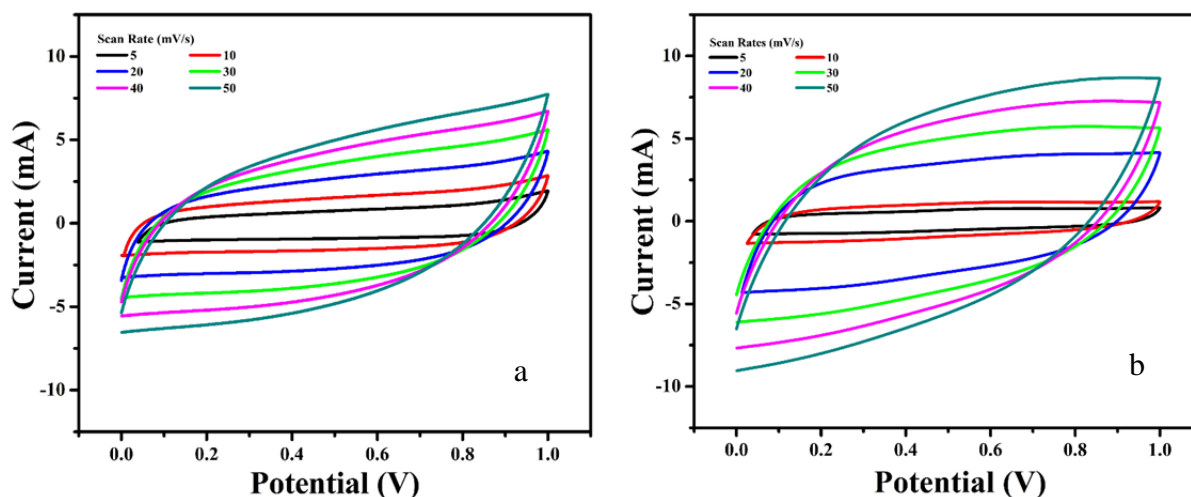


Figure 5.13: CV plots at different scan rates of (a) pristine MnO_2 and (b) $\text{MnO}_2/\text{CeO}_2$ composite.

For comparative purposes, the CV curves of the MnO_2 and $\text{MnO}_2/\text{CeO}_2$ electrodes were also measured at various scan rates, as shown in Figure 5.13. Both electrodes exhibit similar capacitive characteristics, with quasi-rectangular CV curves. However, the integrated area under these curves is noticeably smaller than that of the $\text{MnO}_2/\text{CeO}_2/\text{MWCNT}$ electrode, further emphasizing the superior charge storage capacity of the ternary composite. The smaller integrated area suggests that these electrodes have lower specific capacitance, which can be attributed to the absence of MWCNTs. Without the high surface area and conductive pathways provided by MWCNTs, the MnO_2 and $\text{MnO}_2/\text{CeO}_2$ electrodes are less effective at facilitating rapid ion transport and electron conduction, which are essential for high-performance supercapacitors.

In conclusion, the CV analysis provides compelling evidence that the $\text{MnO}_2/\text{CeO}_2/\text{MWCNT}$ ternary composite electrode offers significantly enhanced electrochemical performance compared to its binary and pristine counterparts. The larger area under the CV curve, coupled with the stable capacitive behavior across various scan rates, indicates that this ternary composite has superior charge storage capabilities, excellent rate capability, and remarkable electrochemical stability. These attributes make the $\text{MnO}_2/\text{CeO}_2/\text{MWCNT}$ composite a highly promising candidate for energy storage devices, particularly in applications requiring high power density and rapid charge-

discharge cycles. The synergy between MnO_2 , CeO_2 , and MWCNTs plays a crucial role in achieving this enhanced performance, highlighting the importance of material design and composite engineering in the development of next-generation supercapacitors.

5.2.2 Galvanostatic Charge Discharge

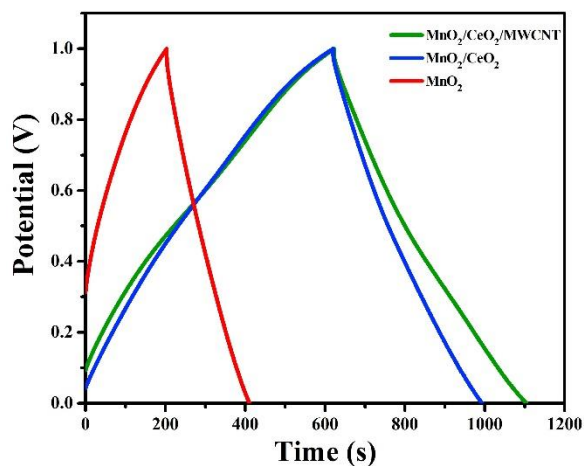


Figure 5.14: GCD curves of MnO_2 , $\text{MnO}_2/\text{CeO}_2$, and $\text{MnO}_2/\text{CeO}_2/\text{MWCNT}$ at the current density of 2.5 Ag^{-1}

The electrochemical properties of MnO_2 , $\text{MnO}_2/\text{CeO}_2$, and $\text{MnO}_2/\text{CeO}_2/\text{MWCNT}$ electrodes were further investigated through galvanostatic charge-discharge (GCD) measurements, as shown in Figure 5.14. The GCD analysis was conducted at a current density of 2.5 A/g over a potential window of 0 to 1 V to evaluate the capacitive behavior and energy storage performance of the electrodes. All three electrodes exhibit a characteristic triangular shape in their GCD curves, which is indicative of ideal capacitive behavior. This shape signifies a uniform charge-discharge process, with minimal faradaic reactions occurring during the cycling, making these electrodes suitable for supercapacitor applications where fast charge-discharge cycles and stable energy storage are critical.

The most notable observation from the GCD analysis is that the $\text{MnO}_2/\text{CeO}_2/\text{MWCNT}$ electrode demonstrates a significantly longer discharge time compared to the MnO_2 and $\text{MnO}_2/\text{CeO}_2$ electrodes. A longer discharge time corresponds to higher energy storage capacity, as it indicates that the electrode can retain and release

more charge over the same potential window. The superior discharge performance of the $\text{MnO}_2/\text{CeO}_2/\text{MWCNT}$ electrode can be attributed to the synergistic effects of the ternary composite structure. The combination of MnO_2 , CeO_2 , and MWCNTs offers enhanced redox activity, improved conductivity, and increased surface area, allowing for more efficient charge storage and transfer. MnO_2 contributes to rapid faradaic reactions, CeO_2 improves structural integrity and electrical conductivity, and MWCNTs provide a high surface area and excellent electron transport pathways, all of which contribute to the electrode's improved electrochemical performance.

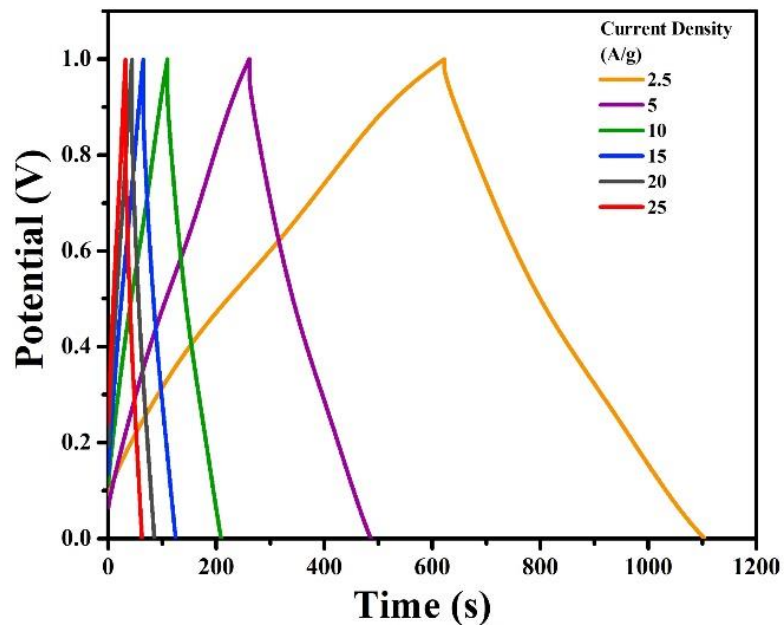


Figure 5.15: GCD curves of the $\text{MnO}_2/\text{CeO}_2/\text{MWCNT}$ electrode at various current densities

Figure 5.15 presents the GCD curves of the $\text{MnO}_2/\text{CeO}_2/\text{MWCNT}$ electrode at various current densities, ranging from 2.5 A/g to 25 A/g. As the current density increases, the discharge time shortens, which is expected as higher current densities lead to faster charge-discharge cycles. Despite this, the electrode retains its characteristic triangular shape across all current densities, demonstrating its stability and ability to maintain capacitive behavior even at high current densities. The specific capacitance of the $\text{MnO}_2/\text{CeO}_2/\text{MWCNT}$ electrode was calculated from the GCD curves using Eq. (1) and the corresponding discharge times. The computed specific capacitance values are 1204, 1126,

1000, 921, 838, and 775 F/g at current densities of 2.5, 5, 10, 15, 20, and 25 A/g, respectively. Notably, the MnO₂/CeO₂/MWCNT electrode exhibits the highest specific capacitance of 1204 F/g at 2.5 A/g and retains a specific capacitance of 775 F/g at 25 A/g, indicating a capacitance retention of approximately 64.37%. This high retention capacity at elevated current densities is a desirable feature for supercapacitors, as it suggests that the electrode can operate efficiently under high-power conditions without significant loss of performance.

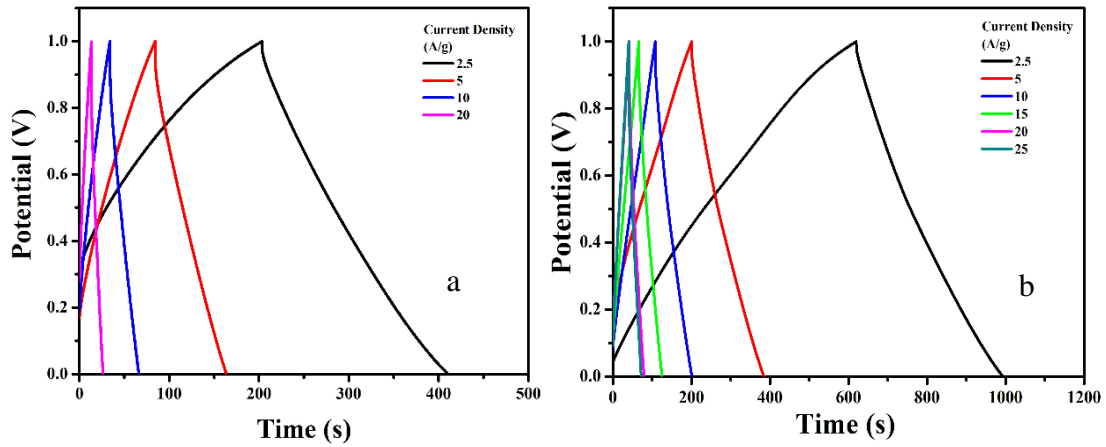


Figure 5.16: GCD plots of (a) pristine MnO₂ and (b) MnO₂/CeO₂ composite.

For comparison, GCD measurements were also conducted on the MnO₂ and MnO₂/CeO₂ electrodes at varying current densities, with the results depicted in Figure 5.16. Similar to the MnO₂/CeO₂/MWCNT electrode, both the MnO₂ and MnO₂/CeO₂ electrodes exhibit triangular GCD curves, reflecting capacitive behavior. However, the discharge times and specific capacitance values of these two electrodes are significantly lower than those of the ternary composite. This observation highlights the enhanced energy storage performance of the MnO₂/CeO₂/MWCNT electrode, which can be attributed to the improved conductivity and redox activity provided by the combination of MnO₂, CeO₂, and MWCNTs. The addition of MWCNTs significantly boosts the specific surface area and provides an efficient pathway for electron transport, allowing for faster ion diffusion and higher charge storage capacity.

The specific capacitance of the electrodes were also ascertained using the Eq. (5) [164].

$$C_s = \frac{I_d \times T_d}{\Delta V \times m} \quad (5)$$

Where m is the electrode's active mass, I_d is the current (mA), V is the voltage window, T_d is the discharge period (s), and C_s is the specific capacitance ($F\ g^{-1}$). The calculated specific capacitance values provide a clear comparison of the energy storage performance of the three electrodes.

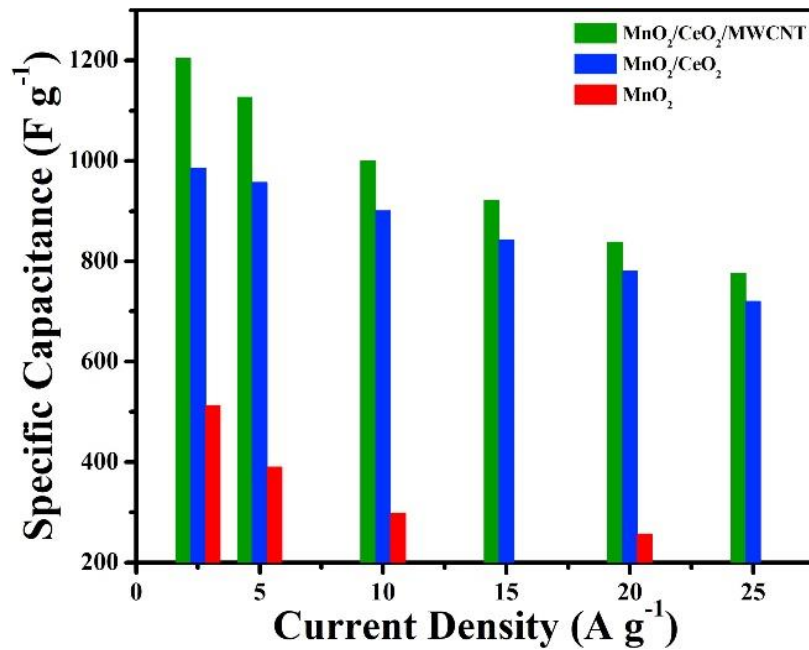


Figure 5.17: *Specific capacitance vs current density for $MnO_2/CeO_2/MWCNT$, MnO_2/CeO_2 , and MnO_2*

Figure 5.17 presents a comparison of the specific capacitance values for MnO_2 , MnO_2/CeO_2 , and $MnO_2/CeO_2/MWCNT$ electrodes at different current densities (ranging from 2.5 A/g to 25 A/g). As shown, the $MnO_2/CeO_2/MWCNT$ electrode outperforms the MnO_2 and MnO_2/CeO_2 electrodes across all current densities, achieving a remarkable specific capacitance of 1204 F/g at 2.5 A/g. In contrast, the MnO_2 and MnO_2/CeO_2 electrodes exhibit lower specific capacitance values, highlighting the advantage of incorporating MWCNTs into the composite structure.

The enhanced specific capacitance of the $\text{MnO}_2/\text{CeO}_2/\text{MWCNT}$ electrode is primarily due to the increased number of surface-active sites provided by the MWCNTs, which promote redox activity and facilitate faster charge transfer. The high surface area of the MWCNTs enables more electrolyte ions to access the active sites of the electrode material, resulting in higher capacitance. Additionally, the presence of CeO_2 in the composite provides structural stability and improves the conductivity of the electrode, further contributing to the improved electrochemical performance. The combination of these factors leads to a highly efficient energy storage material with superior charge storage capacity, making the $\text{MnO}_2/\text{CeO}_2/\text{MWCNT}$ electrode an excellent candidate for high-performance supercapacitors.

In conclusion, the GCD analysis provides valuable insights into the charge storage capabilities of the MnO_2 , $\text{MnO}_2/\text{CeO}_2$, and $\text{MnO}_2/\text{CeO}_2/\text{MWCNT}$ electrodes. The $\text{MnO}_2/\text{CeO}_2/\text{MWCNT}$ electrode demonstrates significantly longer discharge times, higher specific capacitance, and better capacitance retention at high current densities compared to the MnO_2 and $\text{MnO}_2/\text{CeO}_2$ electrodes. These findings underscore the potential of the $\text{MnO}_2/\text{CeO}_2/\text{MWCNT}$ ternary composite as a highly effective electrode material for supercapacitor applications, particularly in scenarios requiring high power density and long cycle life.

5.2.3 Electrochemical Impedance Spectroscopy (EIS)

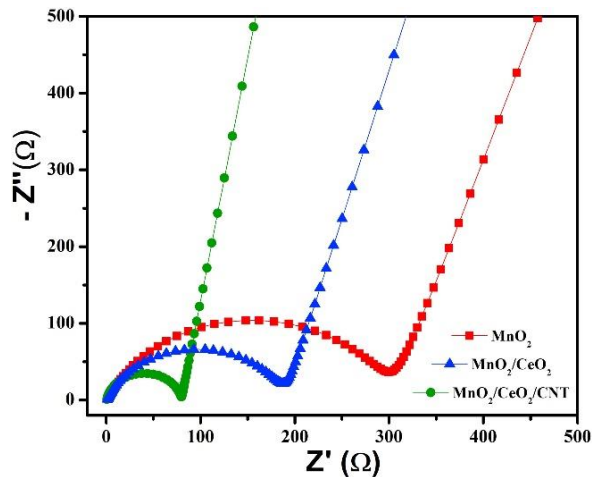


Figure 5.18: Nyquist diagram for $\text{MnO}_2/\text{CeO}_2/\text{MWCNT}$, $\text{MnO}_2/\text{CeO}_2$, and MnO_2

To further understand the kinetics of electron transfer and ion diffusion within the electrode materials, electrochemical impedance spectroscopy (EIS) was conducted, and the results are presented in Figure 5.18. The Nyquist plot illustrates the real and imaginary components of the impedance for the pristine MnO₂, MnO₂/CeO₂, and MnO₂/CeO₂/MWCNT electrodes, offering insights into their charge transfer and ion diffusion properties. The Nyquist plot comprises two distinct regions: a high-frequency region where semi-circular arcs are observed, and a low-frequency region with a linear slope. The diameter of the semi-circle in the high-frequency region is directly related to the charge transfer resistance (R_{ct}) at the electrode-electrolyte interface. The R_{ct} value is a crucial parameter that reflects the ease with which electrons move across the electrode interface during electrochemical reactions.

As shown in the plot, the semi-arc of the pristine MnO₂ electrode is significantly larger compared to the other two composite electrodes. Specifically, the MnO₂/CeO₂/MWCNT composite electrode exhibits the smallest semi-arc diameter, indicating the lowest R_{ct} value and suggesting the most efficient charge transfer at the interface. The measured R_{ct} values for MnO₂, MnO₂/CeO₂, and MnO₂/CeO₂/MWCNT are 301.7, 188.9, and 79.03 Ω, respectively. This remarkable reduction in charge transfer resistance for the MnO₂/CeO₂/MWCNT composite can be attributed to the synergistic effect of the materials within the composite, particularly the presence of highly conductive multi-walled carbon nanotubes (MWCNTs) and oxygen vacancies induced by the Ce³⁺ ions. The MWCNTs provide efficient pathways for electron transport, while the oxygen vacancies, resulting from the incorporation of CeO₂, enhance redox activity and ion diffusion within the electrode. These characteristics significantly improve the conductivity of the MnO₂/CeO₂/MWCNT electrode in the electrochemical system.

Additionally, the Warburg resistance, observed as the angle between the real axis and the linear line in the low-frequency region of the Nyquist plot, is an indicator of ion diffusion and electrode reversibility. A lower Warburg resistance corresponds to faster ion diffusion and better reversibility, which are desirable for high-performance energy storage devices [153]. The MnO₂/CeO₂/MWCNT electrode displays a nearly vertical line approaching 90° from the horizontal axis, which signifies prominent capacitive behavior

and superior ion diffusion. This enhanced ion diffusion can be attributed to the abundant electroactive sites and the oxygen vacancies introduced by the Ce^{3+} ions in the composite, facilitating faster ion movement and charge storage.

The solution resistance (R_s) values, which represent the resistance of the electrolyte and the electrode material to ion movement, were also measured for the electrodes. The R_s values for MnO_2 , MnO_2/CeO_2 , and $MnO_2/CeO_2/MWCNT$ were found to be 1.88, 1.05, and 0.77Ω , respectively. The low R_s value of the $MnO_2/CeO_2/MWCNT$ electrode reflects its superior ionic conductivity, further enhancing its overall electrochemical performance. The decreased R_s and R_{ct} values demonstrate that the $MnO_2/CeO_2/MWCNT$ composite offers enhanced electronic and ionic conductivity, as well as strong reversibility, making it a promising candidate for energy storage applications. The improved ion diffusion and charge transport are primarily due to the oxygen vacancies, which provide more active sites for ion interaction and facilitate rapid electron movement throughout the electrode.

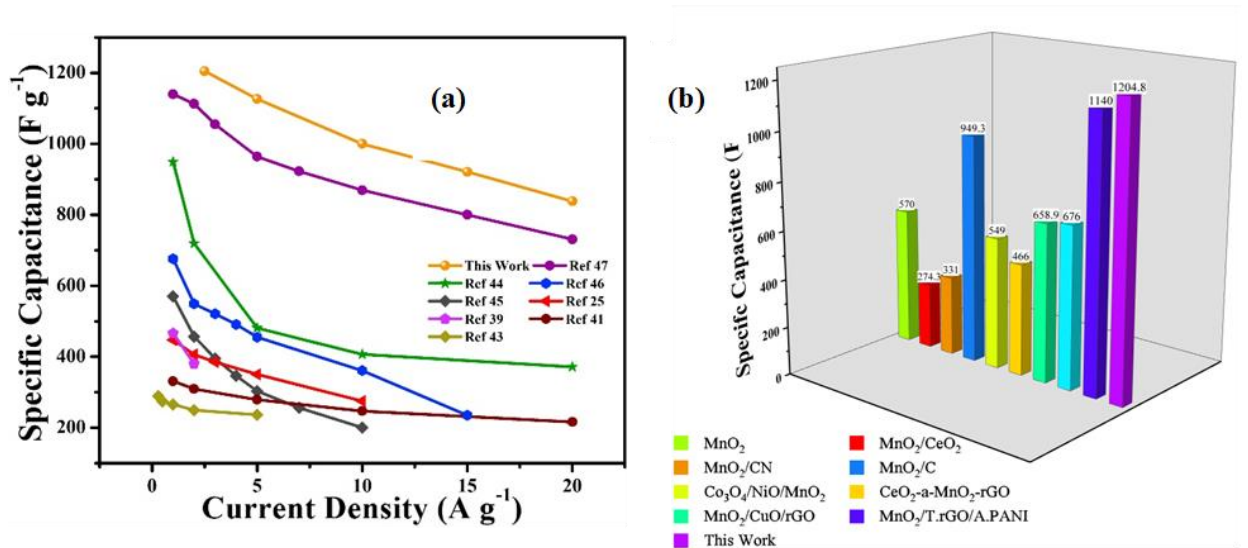


Figure 5.19: (a) Comparison of specific capacitance obtained at different current densities of the present and the previously reported work (b) Comparative analysis of maximum specific capacitance achieved by $MnO_2/CeO_2/MWCNT$ and the previously reported MnO_2 -based binary and ternary composites.

In Figure 5.19 (a-b), the electrochemical performance of the $MnO_2/CeO_2/MWCNT$ electrode is compared with previously reported MnO_2 -based binary and ternary

nanocomposites. The results highlight the significant improvement in performance achieved by the MnO₂/CeO₂/MWCNT composite. Due to the synergistic effects of all three components—MnO₂, CeO₂, and MWCNT—the composite demonstrates exceptional performance, outperforming both the MnO₂/CeO₂ binary composite and pristine MnO₂. This synergy arises from the increased density of electroactive sites on the MnO₂ surface, which improves ion accessibility and enhances electron transfer throughout the composite.

The presence of Ce³⁺ ions and surface oxygen vacancies in the CeO₂ component further increases the reactivity of the electrode surface and boosts its electrical conductivity, accelerating the interaction between the electrode and the electrolyte during the charge-discharge process.

Moreover, the MWCNTs play a critical role in maintaining the structural integrity of the electrode during prolonged cycling, providing resistance against volumetric deformation and offering efficient channels for electron transport. The MWCNTs also help to shorten the ion transport path, allowing for faster charge storage and release, which is crucial for high-performance supercapacitors.

Table 5.1: Electrochemical performance of MnO₂/CeO₂/MWCNT electrode compared with other electrode materials reported in the literature.

Electrode	Specific Capacitance (F g⁻¹)	Current Density (A g⁻¹) or scan Rate (mVs⁻¹)	Capacity Retention (%)	Cycle Number	Refs.
α -Fe ₂ O ₃ /MnO ₂ /rGO	447	1	92	5000	[39]
MnO ₂ /CuO/rGO	658.9	1	83.7	5000	[146]
CF/ MnO ₂ /PANI	373	1	73	1000	[38]

CeO ₂ - α -MnO ₂ -rGO	466	1	100	10,000	[42]
Co ₃ O ₄ /NiO/MnO ₂	549	0.5	76	600	[149]
MnO ₂ / CNT	331	1	91.3	5000	[165]
MnO ₂ -NiO	375	0.5	56.87	1000	[166]
MnO ₂ /CeO ₂	274.3	0.5	93.9	1000	[167]
MnO ₂ /C	949.3	1	93	100	[168]
α MnO ₂	570	1	80	10,000	[169]
MnO ₂ @SnO ₂ /T-NC	676	1	93	6,000	[150]
MnO ₂ /T.rGO/A.PANI	1140	1	64	5,000	[151]
MnO ₂ /CeO ₂ /MWCNT	1204	2.5	94	10,000	This work

Table 5.1 provides a comprehensive comparison between the fabricated MnO₂/CeO₂/MWCNT electrodes and previously reported MnO₂-based binary and ternary electrodes, highlighting the key performance characteristics and potential advancements of the current composite.

The improved charge transfer kinetics, lower resistance values, and enhanced ion diffusion capabilities of the MnO₂/CeO₂/MWCNT composite underscore its potential as a superior electrode material for next-generation supercapacitors and other energy storage devices.

5.3 Electrochemical performance of MnO₂/CeO₂/MWCNT // AC Asymmetric Coin Cell

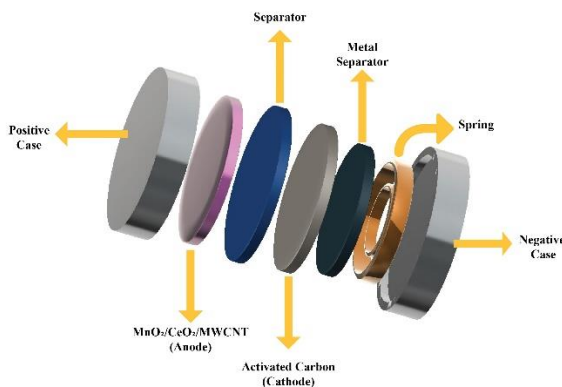


Figure 5.20: Coin cell assembly for asymmetric supercapacitor.

The practical feasibility of the MnO₂/CeO₂/MWCNT electrode was assessed by assembling an aqueous asymmetric supercapacitor coin cell, as illustrated in Figure 5.20. In this device, 1.0 M Na₂SO₄ was used as the electrolyte, activated carbon (AC) served as the negative electrode, and MnO₂/CeO₂/MWCNT functioned as the positive electrode. The performance of the device was evaluated using a two-electrode configuration. Figure 5.21 (a) depicts the cyclic voltammetry (CV) response of the device at various scan rates ranging from 10 to 50 mV s⁻¹ within a wide potential window of -0.2 to 1.4 V. The nearly rectangular shape of the CV curves indicates efficient charge transfer and typical capacitive behavior. Importantly, the shape of the CV curves remains stable across both low and high scan rates, demonstrating excellent reversibility and rate capability, which are essential for practical energy storage devices.

To further evaluate the operational competence of the supercapacitor, CV measurements were conducted by varying the potential window, as shown in Figure 5.21 (b). The findings reveal that the device can operate at an extended potential difference of up to 1.6 V, further confirming its robust performance under different operating conditions. Figure 5.22 (a) presents the galvanostatic charge-discharge (GCD) curves of the device,

recorded at several potential windows ranging from -0.2 to 1.4 V at a constant current density of 1 A g⁻¹. These results confirm the device's stable operation across different potential ranges.

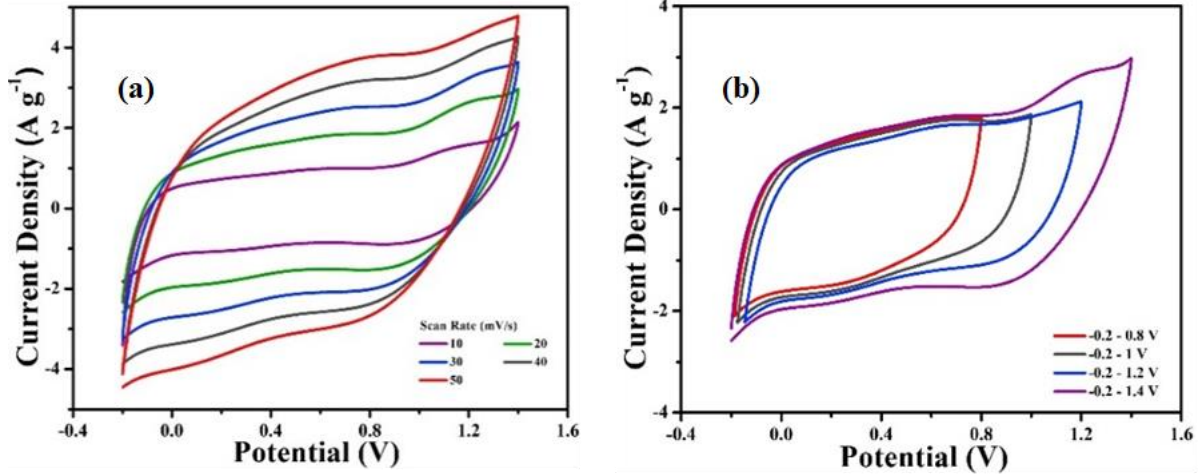


Figure 5.21: (a-b) CV curves of MnO₂/CeO₂/MWCNT//AC asymmetric supercapacitor at different scan rates and potential windows respectively.

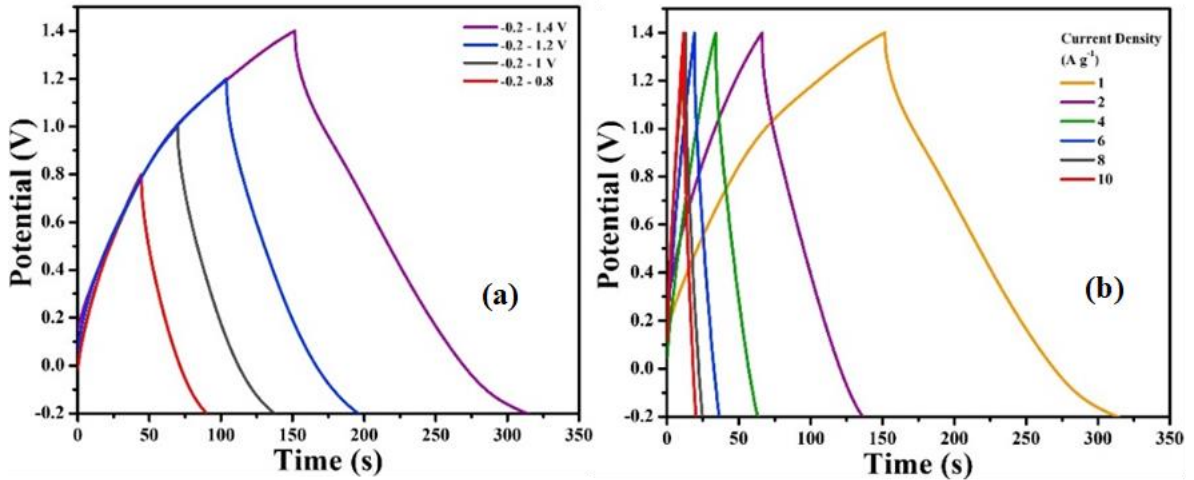


Figure 5.22: GCD curves of asymmetric supercapacitor at different current densities and potential windows respectively.

Moreover, the GCD curves recorded at different current densities, as shown in Figure 5.22 (b), exhibit an asymmetrical triangular shape, indicating the high reversibility of the device during the charge-discharge cycles. This suggests that the

MnO₂/CeO₂/MWCNT // AC coin cell has excellent electrochemical stability, a key factor in maintaining performance over time. The specific capacitance of the device was also calculated from the GCD curves, with the results presented in Figure 5.23. The device achieves a maximum specific capacitance of 101.25 F g⁻¹ at a current density of 1 A g⁻¹ and retains 64 F g⁻¹ at a higher current density of 10 A g⁻¹, reflecting a retention capacity of 63.49%. These results underscore the significant rate capability of the device, which is crucial for real-world applications where high power and stable performance are required.

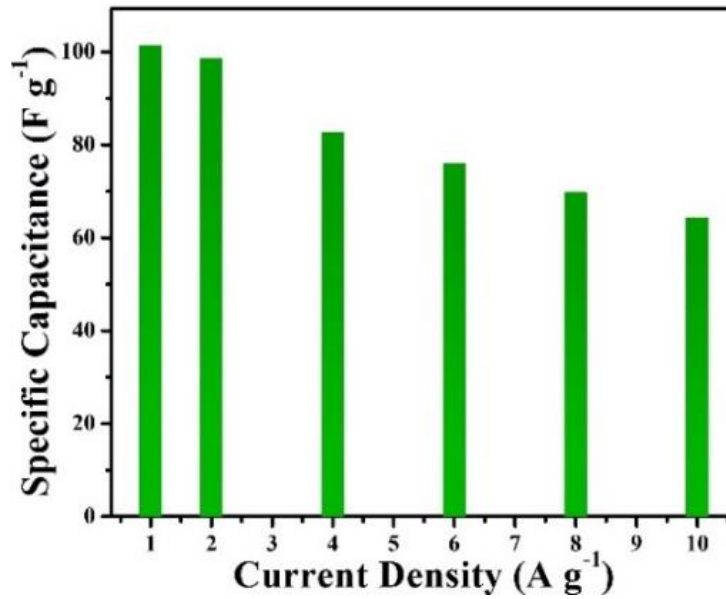


Figure 5.23: *Specific capacitance vs. current density plot.*

In addition to specific capacitance, the energy density (E) and power density (P) of the fabricated coin cell were calculated using the following equations:

$$E = \frac{C_s \times \Delta V^2}{7.2} \quad (6)$$

$$P = \frac{3600E}{T} \quad (7)$$

The Ragone plot, is shown in Figure 5.24, illustrates the energy and power density of the device, revealing that it achieves a maximum energy density of 36 Wh kg⁻¹ at a power density of 800 W kg⁻¹. This balance between energy and power density is a critical parameter for supercapacitor performance, as it reflects the device's ability to store and

deliver energy efficiently. The practical applicability of the supercapacitor was further demonstrated by powering a commercially available LED, as shown in the inset of Fig. 39. This real-time operation highlights the practical utility of the MnO₂/CeO₂/MWCNT // AC coin cell for energy storage applications.

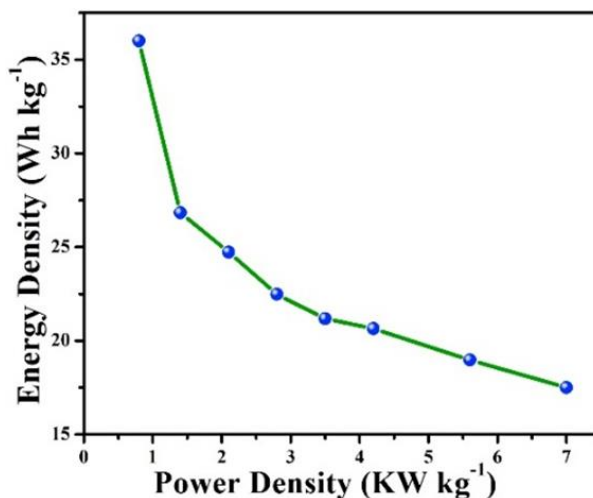


Figure 5.24: Ragone plot of asymmetric supercapacitor.

To better understand the device kinetics, a Nyquist plot was generated, as shown in Figure 5.25. This plot offers insights into the device's electrochemical impedance, revealing a low internal resistance, which is essential for fast electron and ion transport during charge-discharge processes. The low impedance further supports the high performance and efficiency of the device.

Figure. 5.26 displays the cyclic stability of the device, which was tested over 10,000 cycles at a current density of 10 A g⁻¹. Remarkably, after 10,000 cycles, the device maintained 94% of its initial capacitance, highlighting the outstanding cyclic performance and longevity of the MnO₂/CeO₂/MWCNT // AC coin cell. The inset shows the device's cyclic stability over the first 12 cycles at a current density of 2.5 A g⁻¹, indicating consistent performance even during the early stages of cycling.

-The performance of the fabricated MnO₂/CeO₂/MWCNT // AC coin cell device exceeds that of previously reported MnO₂-based devices, demonstrating significant advancements in specific capacitance, energy density, and cycle life. The synergistic effect

of MnO₂, CeO₂, and MWCNT plays a crucial role in enhancing the overall electrochemical performance, making this composite electrode a promising candidate for next-generation supercapacitors and other high-performance energy storage systems [39, 150, 151].

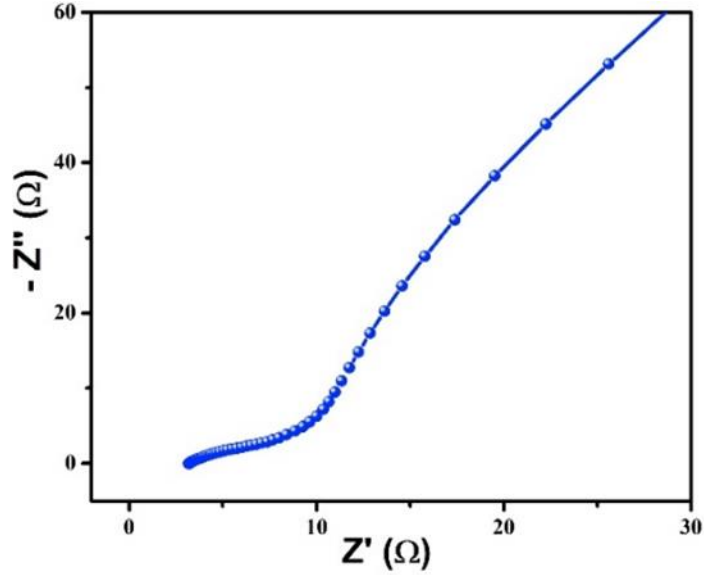


Figure 5.25: Nyquist diagram of the asymmetric supercapacitor.

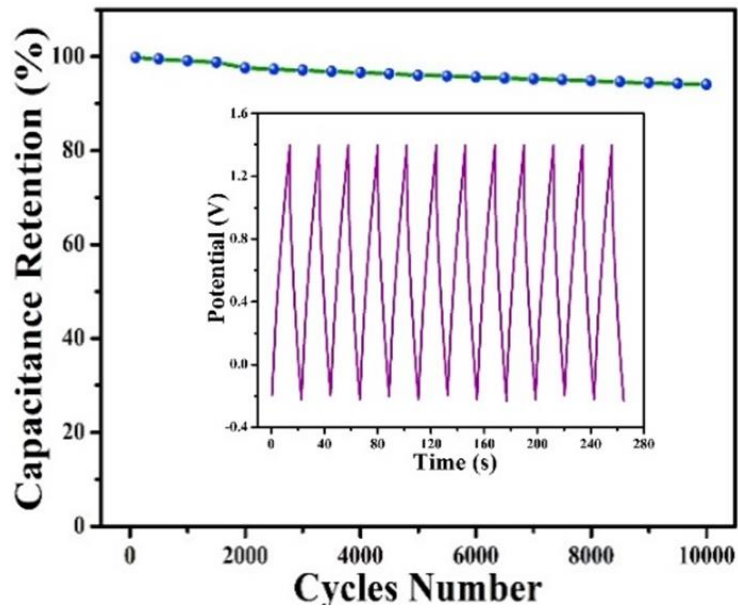


Figure 5.26: Cycling performance of asymmetric supercapacitor.

CHAPTER 6: CONCLUSIONS AND FUTURE RECOMMENDATION

6.1 Conclusion

In conclusion, the MnO₂/CeO₂/MWCNT ternary composite was successfully synthesized using a simple and cost-effective hydrothermal method. This composite, which benefits from surface defects, a high surface area, and improved kinetic properties, presents itself as a strong candidate for supercapacitor applications. When compared to pristine and binary electrodes, it demonstrates a notably enhanced specific capacitance of 1204 F g⁻¹ at a current density of 2.5 A g⁻¹. Additionally, the fabricated MnO₂/CeO₂/MWCNT//AC device achieved a substantial energy density of 36 Wh kg⁻¹ at a power density of 800 W kg⁻¹, underscoring its potential for practical use. Moreover, the device displayed excellent cyclic stability, retaining 94% of its specific capacitance even after 10,000 cycles at 10 A g⁻¹. These findings emphasize the effectiveness of the synergistic strategy in enhancing the redox activity and electrochemical performance of the composite for supercapacitor applications.

6.2 Future Recommendations

This approach holds promise for the development of novel nanomaterials with superior electrochemical properties, which could be key for advancing future energy storage technologies.

REFERENCES

- [1] S. Singh *et al.*, "Hydrogen: A sustainable fuel for future of the transport sector," *Renewable and sustainable energy reviews*, vol. 51, pp. 623-633, 2015.
- [2] M. Ciccarelli and F. Marotta, "Demand or supply? An empirical exploration of the effects of climate change on the macroeconomy," *Energy Economics*, vol. 129, p. 107163, 2024.
- [3] W. Zappa, M. Junginger, and M. Van Den Broek, "Is a 100% renewable European power system feasible by 2050?," *Applied energy*, vol. 233, pp. 1027-1050, 2019.
- [4] G. Navarro, J. Torres, M. Blanco, J. Nájera, M. Santos-Herran, and M. Lafoz, "Present and future of supercapacitor technology applied to powertrains, renewable generation and grid connection applications," *Energies*, vol. 14, no. 11, p. 3060, 2021.
- [5] A. Mauger, C. Julien, A. Paoletta, M. Armand, and K. Zaghib, "Recent progress on organic electrodes materials for rechargeable batteries and supercapacitors," *Materials*, vol. 12, no. 11, p. 1770, 2019.
- [6] P. E. Lokhande, U. S. Chavan, and A. Pandey, "Materials and fabrication methods for electrochemical supercapacitors: overview," *Electrochemical Energy Reviews*, vol. 3, pp. 155-186, 2020.
- [7] G. Bullard, H. Sierra-Alcazar, H. Lee, and J. Morris, "Operating principles of the ultracapacitor," *IEEE Transactions on magnetics*, vol. 25, no. 1, pp. 102-106, 1989.
- [8] M. Sarno, "Nanotechnology in energy storage: The supercapacitors," in *Studies in surface science and catalysis*, vol. 179: Elsevier, 2020, pp. 431-458.
- [9] C.-q. Yi, J.-p. Zou, H.-z. Yang, and L. Xian, "Recent advances in pseudocapacitor electrode materials: transition metal oxides and nitrides," *Transactions of Nonferrous Metals Society of China*, vol. 28, no. 10, pp. 1980-2001, 2018.
- [10] H. Shen *et al.*, "Investigation of strategies for improving the energy density of symmetric electrical double-layer capacitors," *Journal of Energy Storage*, vol. 79, p. 110127, 2024.
- [11] A. Muzaffar, M. B. Ahamed, K. Deshmukh, and J. Thirumalai, "A review on recent advances in hybrid supercapacitors: Design, fabrication and applications," *Renewable and sustainable energy reviews*, vol. 101, pp. 123-145, 2019.
- [12] Z. Yu, L. Tetard, L. Zhai, and J. Thomas, "Supercapacitor electrode materials: nanostructures from 0 to 3 dimensions," *Energy & Environmental Science*, vol. 8, no. 3, pp. 702-730, 2015.

- [13] X. Wu, R. Liu, J. Zhao, and Z. Fan, "Advanced carbon materials with different spatial dimensions for supercapacitors," *Nano Materials Science*, vol. 3, no. 3, pp. 241-267, 2021.
- [14] Y. Ma *et al.*, "Recent advances in transition metal oxides with different dimensions as electrodes for high-performance supercapacitors," *Advanced Composites and Hybrid Materials*, pp. 1-19, 2021.
- [15] A. Kumar, H. K. Rathore, D. Sarkar, and A. Shukla, "Nanoarchitected transition metal oxides and their composites for supercapacitors," *Electrochemical Science Advances*, vol. 2, no. 6, p. e2100187, 2022.
- [16] K. S. Kumar, N. Choudhary, Y. Jung, and J. Thomas, "Recent advances in two-dimensional nanomaterials for supercapacitor electrode applications," *ACS Energy Letters*, vol. 3, no. 2, pp. 482-495, 2018.
- [17] S. W. Bokhari *et al.*, "Advances in graphene-based supercapacitor electrodes," *Energy Reports*, vol. 6, pp. 2768-2784, 2020.
- [18] M. Guan, Q. Wang, X. Zhang, J. Bao, X. Gong, and Y. Liu, "Two-dimensional transition metal oxide and hydroxide-based hierarchical architectures for advanced supercapacitor materials," *Frontiers in Chemistry*, vol. 8, p. 390, 2020.
- [19] D. Monga, S. Sharma, N. P. Shetti, S. Basu, K. R. Reddy, and T. M. Aminabhavi, "Advances in transition metal dichalcogenide-based two-dimensional nanomaterials," *Materials Today Chemistry*, vol. 19, p. 100399, 2021.
- [20] S. Panda, K. Deshmukh, S. K. Pasha, J. Theerthagiri, S. Manickam, and M. Y. Choi, "MXene based emerging materials for supercapacitor applications: Recent advances, challenges, and future perspectives," *Coordination Chemistry Reviews*, vol. 462, p. 214518, 2022.
- [21] Y. Da, J. Liu, L. Zhou, X. Zhu, X. Chen, and L. Fu, "Engineering 2D architectures toward high-performance micro-supercapacitors," *Advanced Materials*, vol. 31, no. 1, p. 1802793, 2019.
- [22] H. Zhao and Y. Lei, "3D nanostructures for the next generation of high-performance nanodevices for electrochemical energy conversion and storage," *Advanced Energy Materials*, vol. 10, no. 28, p. 2001460, 2020.
- [23] C. Verma, E. Berdimurodov, D. K. Verma, K. Berdimuradov, A. Alfantazi, and C. Hussain, "3D nanomaterials: The future of industrial, biological, and environmental applications," *Inorganic Chemistry Communications*, p. 111163, 2023.
- [24] S. Kumar, G. Saeed, L. Zhu, K. N. Hui, N. H. Kim, and J. H. Lee, "0D to 3D carbon-based networks combined with pseudocapacitive electrode material for high energy density supercapacitor: A review," *Chemical Engineering Journal*, vol. 403, p. 126352, 2021.

- [25] L. Zhang, X. Hu, Z. Wang, F. Sun, and D. G. Dorrell, "A review of supercapacitor modeling, estimation, and applications: A control/management perspective," *Renewable and Sustainable Energy Reviews*, vol. 81, pp. 1868-1878, 2018.
- [26] G. Zhang, X. Xiao, B. Li, P. Gu, H. Xue, and H. Pang, "Transition metal oxides with one-dimensional/one-dimensional-analogue nanostructures for advanced supercapacitors," *Journal of Materials Chemistry A*, vol. 5, no. 18, pp. 8155-8186, 2017.
- [27] U. Banik, M. T. U. Malik, S. S. M. Rahat, and A. K. Mallik, "Performance enhancement of ruthenium-based supercapacitors: A review," *Energy Storage*, vol. 5, no. 3, p. e380, 2023.
- [28] W. Guo *et al.*, "Strategies and insights towards the intrinsic capacitive properties of MnO₂ for supercapacitors: challenges and perspectives," *Nano Energy*, vol. 57, pp. 459-472, 2019.
- [29] U. K. Chime *et al.*, "Recent progress in nickel oxide-based electrodes for high-performance supercapacitors," *Current Opinion in Electrochemistry*, vol. 21, pp. 175-181, 2020.
- [30] H. Qin, S. Liang, L. Chen, Y. Li, Z. Luo, and S. Chen, "Recent advances in vanadium-based nanomaterials and their composites for supercapacitors," *Sustainable Energy & Fuels*, vol. 4, no. 10, pp. 4902-4933, 2020.
- [31] J. Xu, A. Yan, X. Wang, B. Wang, and J. Cheng, "A review of cobalt monoxide and its composites for supercapacitors," *Ceramics International*, vol. 47, no. 16, pp. 22229-22239, 2021.
- [32] M. Mustaqeem *et al.*, "Rational design of Cu based composite electrode materials for high-performance supercapacitors—A review," *Journal of Energy Storage*, vol. 51, p. 104330, 2022.
- [33] T. Bhat, S. Jadhav, S. Bknalkar, S. Patil, and P. Patil, "MnO₂ core-shell type materials for high-performance supercapacitors: a short review," *Inorganic Chemistry Communications*, vol. 141, p. 109493, 2022.
- [34] T. Yue, B. Shen, and P. Gao, "Carbon material/MnO₂ as conductive skeleton for supercapacitor electrode material: A review," *Renewable and Sustainable Energy Reviews*, vol. 158, p. 112131, 2022.
- [35] C. Wu, Y. Zhu, M. Ding, C. Jia, and K. Zhang, "Fabrication of plate-like MnO₂ with excellent cycle stability for supercapacitor electrodes," *Electrochimica Acta*, vol. 291, pp. 249-255, 2018.
- [36] M. A. A. M. Abdah, N. H. N. Azman, S. Kulandaivalu, and Y. Sulaiman, "Review of the use of transition-metal-oxide and conducting polymer-based fibres for high-performance supercapacitors," *Materials & Design*, vol. 186, p. 108199, 2020.

- [37] G. Wang, Q. Tang, H. Bao, X. Li, and G. Wang, "Synthesis of hierarchical sulfonated graphene/MnO₂/polyaniline ternary composite and its improved electrochemical performance," *Journal of power sources*, vol. 241, pp. 231-238, 2013.
- [38] Y. Shetty, S. R. Holla, D. Sangeetha, and M. Selvakumar, "Ternary Composite Electrode Carbon Fiber/mno₂/polyaniline for Supercapacitor Applications Based on Naturally Available Broom and Bamboo Sticks," 2022.
- [39] M. Geerthana, S. Prabhu, and R. Ramesh, "Hierarchical α -Fe₂O₃/MnO₂/rGO ternary composites as an electrode material for high performance supercapacitors application," *Journal of Energy Storage*, vol. 47, p. 103529, 2022.
- [40] Y. Liu, D. He, J. Duan, Y. Wang, and S. Li, "Synthesis of MnO₂/graphene/carbon nanotube nanostructured ternary composite for supercapacitor electrodes with high rate capability," *Materials Chemistry and Physics*, vol. 147, no. 1-2, pp. 141-146, 2014.
- [41] A. H. P. de Oliveira, M. L. F. Nascimento, and H. P. de Oliveira, "Carbon nanotube@ MnO₂@ polypyrrole composites: chemical synthesis, characterization and application in supercapacitors," *Materials Research*, vol. 19, pp. 1080-1087, 2016.
- [42] A. Xie *et al.*, "Mesoporous CeO₂- α -MnO₂-reduced graphene oxide composite with ultra-high stability as a novel electrode material for supercapacitor," *Surfaces and Interfaces*, vol. 25, p. 101177, 2021.
- [43] M. Kazamel and P. P. Warren, "History of electromyography and nerve conduction studies: A tribute to the founding fathers," *Journal of Clinical Neuroscience*, vol. 43, pp. 54-60, 2017.
- [44] D. Fitzgerald, "Improvements in electrical condensers or accumulators," *British patent*, no. 3466, p. 1876, 1876.
- [45] J. Both, "The modern era of aluminum electrolytic capacitors," *IEEE Electrical Insulation Magazine*, vol. 31, no. 4, pp. 24-34, 2015.
- [46] A. Noori, M. F. El-Kady, M. S. Rahmanifar, R. B. Kaner, and M. F. Mousavi, "Towards establishing standard performance metrics for batteries, supercapacitors and beyond," *Chemical Society Reviews*, vol. 48, no. 5, pp. 1272-1341, 2019.
- [47] G. Z. Chen, "Understanding supercapacitors based on nano-hybrid materials with interfacial conjugation," *Progress in Natural Science: Materials International*, vol. 23, no. 3, pp. 245-255, 2013.
- [48] B. Luo, X. Wang, H. Wang, Z. Cai, and L. Li, "P (VDF-HFP)/PMMA flexible composite films with enhanced energy storage density and efficiency," *Composites Science and Technology*, vol. 151, pp. 94-103, 2017.

- [49] T. D. Huan *et al.*, "Advanced polymeric dielectrics for high energy density applications," *Progress in Materials Science*, vol. 83, pp. 236-269, 2016.
- [50] B. Luo *et al.*, "Chemical composition and temperature dependence of the energy storage properties of Ba_{1-x}Sr_xTiO₃ ferroelectrics," *Journal of the American Ceramic Society*, vol. 101, no. 7, pp. 2976-2986, 2018.
- [51] B. Luo *et al.*, "Giant permittivity and low dielectric loss of Fe doped BaTiO₃ ceramics: Experimental and first-principles calculations," *Journal of the European Ceramic Society*, vol. 38, no. 4, pp. 1562-1568, 2018.
- [52] H. Zhang *et al.*, "A review on the development of lead-free ferroelectric energy-storage ceramics and multilayer capacitors," *Journal of Materials Chemistry C*, vol. 8, no. 47, pp. 16648-16667, 2020.
- [53] H. Pan *et al.*, "Ultrahigh energy storage in superparaelectric relaxor ferroelectrics," *Science*, vol. 374, no. 6563, pp. 100-104, 2021.
- [54] B. Fan, M. Zhou, C. Zhang, D. He, and J. Bai, "Polymer-based materials for achieving high energy density film capacitors," *Progress in Polymer Science*, vol. 97, p. 101143, 2019.
- [55] K. Hong, T. H. Lee, J. M. Suh, S.-H. Yoon, and H. W. Jang, "Perspectives and challenges in multilayer ceramic capacitors for next generation electronics," *Journal of Materials Chemistry C*, vol. 7, no. 32, pp. 9782-9802, 2019.
- [56] Y.-X. Liu, S.-F. Wang, Y.-F. Hsu, and W.-Y. Yeh, "Solid oxide fuel cells incorporating doped lanthanum gallate films deposited by radio-frequency magnetron sputtering at various Ar/O₂ ratios and annealing conditions," *Surface and Coatings Technology*, vol. 344, pp. 507-513, 2018.
- [57] K. Sharma, A. Arora, and S. K. Tripathi, "Review of supercapacitors: Materials and devices," *Journal of Energy Storage*, vol. 21, pp. 801-825, 2019.
- [58] Y. Shao *et al.*, "Design and mechanisms of asymmetric supercapacitors," *Chemical reviews*, vol. 118, no. 18, pp. 9233-9280, 2018.
- [59] M. Ho, P. S. Khiew, D. Isa, T. Tan, W. S. Chiu, and C. H. Chia, "A review of metal oxide composite electrode materials for electrochemical capacitors," *Nano*, vol. 9, no. 06, p. 1430002, 2014.
- [60] B. E. Conway, "Transition from "supercapacitor" to "battery" behavior in electrochemical energy storage," *Journal of the Electrochemical Society*, vol. 138, no. 6, p. 1539, 1991.
- [61] S. Trasatti and G. Buzzanca, "Ruthenium dioxide: A new interesting electrode material. Solid state structure and electrochemical behaviour," *Journal of*

electroanalytical chemistry and interfacial electrochemistry, vol. 29, no. 2, pp. A1-A5, 1971.

- [62] K. K. Kar, *Handbook of nanocomposite supercapacitor materials II*. Springer, 2020.
- [63] M. Conte, "Supercapacitors technical requirements for new applications," *Fuel cells*, vol. 10, no. 5, pp. 806-818, 2010.
- [64] M. Khot and A. Kiani, "A review on the advances in electrochemical capacitive charge storage in transition metal oxide electrodes for pseudocapacitors," *International Journal of Energy Research*, vol. 46, no. 15, pp. 21757-21796, 2022.
- [65] Z. S. Iro, C. Subramani, and S. Dash, "A brief review on electrode materials for supercapacitor," *International Journal of Electrochemical Science*, vol. 11, no. 12, pp. 10628-10643, 2016.
- [66] S. Kour, S. Tanwar, and A. Sharma, "A review on challenges to remedies of MnO₂ based transition-metal oxide, hydroxide, and layered double hydroxide composites for supercapacitor applications," *Materials Today Communications*, vol. 32, p. 104033, 2022.
- [67] N. R. Chodankar *et al.*, "True meaning of pseudocapacitors and their performance metrics: asymmetric versus hybrid supercapacitors," *Small*, vol. 16, no. 37, p. 2002806, 2020.
- [68] M. Divya, S. Natarajan, Y. S. Lee, and V. Aravindan, "Biomass-derived carbon: a value-added journey towards constructing high-energy supercapacitors in an asymmetric fashion," *ChemSusChem*, vol. 12, no. 19, pp. 4353-4382, 2019.
- [69] P. Kour and K. Yadav, "Electrochemical performance of mixed-phase 1T/2H MoS₂ synthesized by conventional hydrothermal v/s microwave-assisted hydrothermal method for supercapacitor applications," *Journal of Alloys and Compounds*, vol. 922, p. 166194, 2022.
- [70] N. Singh, S. Tanwar, A. Sharma, and B. Yadav, "Advanced cyclic stability and highly efficient different shaped carbonaceous nanostructured electrodes for solid-state energy storage devices," *International Journal of Hydrogen Energy*, vol. 47, no. 66, pp. 28254-28271, 2022.
- [71] S. Sadavar *et al.*, "Anion storage for hybrid supercapacitor," *Materials Today Energy*, p. 101388, 2023.
- [72] B. K. Kim, S. Sy, A. Yu, and J. Zhang, "Electrochemical supercapacitors for energy storage and conversion," *Handbook of clean energy systems*, pp. 1-25, 2015.
- [73] R. Kumar *et al.*, "Heteroatom doped graphene engineering for energy storage and conversion," *Materials Today*, vol. 39, pp. 47-65, 2020.

- [74] G. Wang, L. Zhang, and J. Zhang, "A review of electrode materials for electrochemical supercapacitors," *Chemical Society Reviews*, vol. 41, no. 2, pp. 797-828, 2012.
- [75] P. Chamoli, M. K. Das, and K. K. Kar, "Urea-assisted low temperature green synthesis of graphene nanosheets for transparent conducting film," *Journal of Physics and Chemistry of Solids*, vol. 113, pp. 17-25, 2018.
- [76] A. Mendhe and H. Panda, "A review on electrolytes for supercapacitor device," *Discover Materials*, vol. 3, no. 1, p. 29, 2023.
- [77] F. Béguin, V. Presser, A. Balducci, and E. Frackowiak, "Carbons and electrolytes for advanced supercapacitors," *Advanced materials*, vol. 26, no. 14, pp. 2219-2251, 2014.
- [78] B. Pal, S. Yang, S. Ramesh, V. Thangadurai, and R. Jose, "Electrolyte selection for supercapacitive devices: a critical review," *Nanoscale Advances*, vol. 1, no. 10, pp. 3807-3835, 2019.
- [79] L. Zhang *et al.*, "Three-dimensional structures of graphene/polyaniline hybrid films constructed by steamed water for high-performance supercapacitors," *Journal of Power Sources*, vol. 342, pp. 1-8, 2017.
- [80] K. D. Verma, P. Sinha, S. Banerjee, K. K. Kar, and M. K. Ghorai, "Characteristics of separator materials for supercapacitors," *Handbook of Nanocomposite Supercapacitor Materials I: Characteristics*, pp. 315-326, 2020.
- [81] E. Raymundo-Piñero, M. Cadek, and F. Béguin, "Tuning carbon materials for supercapacitors by direct pyrolysis of seaweeds," *Advanced Functional Materials*, vol. 19, no. 7, pp. 1032-1039, 2009.
- [82] T. Liu, F. Zhang, Y. Song, and Y. Li, "Revitalizing carbon supercapacitor electrodes with hierarchical porous structures," *Journal of Materials Chemistry A*, vol. 5, no. 34, pp. 17705-17733, 2017.
- [83] M. D. Stoller *et al.*, "Interfacial capacitance of single layer graphene," *Energy & Environmental Science*, vol. 4, no. 11, pp. 4685-4689, 2011.
- [84] P. Simon and Y. Gogotsi, "Materials for electrochemical capacitors," *Nature materials*, vol. 7, no. 11, pp. 845-854, 2008.
- [85] N. Syarif, A. Tribidasari, and W. Wibowo, "Direct synthesis carbon/Metal oxide composites for electrochemical capacitors electrode," *Int. Trans. J. Eng. Manag. Appl. Sci. Technol*, vol. 3, pp. 21-34, 2012.
- [86] C. Bessagnet, E. Dantras, C. Lacabanne, M. Chevalier, and G. Michon, "Piezoelectric and mechanical behavior of NaNbO₃/PEKK lead-free nanocomposites," *Journal of Non-Crystalline Solids*, vol. 459, pp. 83-87, 2017.

- [87] A. G. Pandolfo and A. F. Hollenkamp, "Carbon properties and their role in supercapacitors," *Journal of power sources*, vol. 157, no. 1, pp. 11-27, 2006.
- [88] E. Raymundo-Piñero, K. Kierzek, J. Machnikowski, and F. Béguin, "Relationship between the nanoporous texture of activated carbons and their capacitance properties in different electrolytes," *Carbon*, vol. 44, no. 12, pp. 2498-2507, 2006.
- [89] K. Lota, A. Sierczynska, I. Acznik, and G. Lota, "Effect of aqueous electrolytes on electrochemical capacitor capacitance," *Chemik*, vol. 67, no. 11, pp. 1138-1145, 2013.
- [90] Q. Cheng, J. Tang, J. Ma, H. Zhang, N. Shinya, and L.-C. Qin, "Graphene and carbon nanotube composite electrodes for supercapacitors with ultra-high energy density," *Physical Chemistry Chemical Physics*, vol. 13, no. 39, pp. 17615-17624, 2011.
- [91] P. Chen, H.-B. Zhang, G.-D. Lin, Q. Hong, and K. Tsai, "Growth of carbon nanotubes by catalytic decomposition of CH₄ or CO on a Ni · MgO catalyst," *Carbon*, vol. 35, no. 10-11, pp. 1495-1501, 1997.
- [92] L. Phor, A. Kumar, and S. Chahal, "Electrode materials for supercapacitors: a comprehensive review of advancements and performance," *Journal of Energy Storage*, vol. 84, p. 110698, 2024.
- [93] C. Du and N. Pan, "High power density supercapacitor electrodes of carbon nanotube films by electrophoretic deposition," *Nanotechnology*, vol. 17, no. 21, p. 5314, 2006.
- [94] E. Pop, V. Varshney, and A. K. Roy, "Thermal properties of graphene: Fundamentals and applications," *MRS bulletin*, vol. 37, no. 12, pp. 1273-1281, 2012.
- [95] V. Nithya, "A review on holey graphene electrode for supercapacitor," *Journal of Energy Storage*, vol. 44, p. 103380, 2021.
- [96] Y. Wang *et al.*, "Supercapacitor devices based on graphene materials," *The Journal of Physical Chemistry C*, vol. 113, no. 30, pp. 13103-13107, 2009.
- [97] L. L. Zhang *et al.*, "Highly conductive and porous activated reduced graphene oxide films for high-power supercapacitors," *Nano letters*, vol. 12, no. 4, pp. 1806-1812, 2012.
- [98] M. D. Stoller, S. Park, Y. Zhu, J. An, and R. S. Ruoff, "Graphene-based ultracapacitors," *Nano letters*, vol. 8, no. 10, pp. 3498-3502, 2008.
- [99] S. Kannappan *et al.*, "Graphene based supercapacitors with improved specific capacitance and fast charging time at high current density," *arXiv preprint arXiv:1311.1548*, 2013.

- [100] T. N. J. I. Edison, R. Atchudan, and Y. R. Lee, "Facile synthesis of carbon encapsulated RuO₂ nanorods for supercapacitor and electrocatalytic hydrogen evolution reaction," *International Journal of Hydrogen Energy*, vol. 44, no. 4, pp. 2323-2329, 2019.
- [101] I.-H. Kim and K.-B. Kim, "Ruthenium oxide thin film electrodes for supercapacitors," *Electrochemical and Solid-State Letters*, vol. 4, no. 5, p. A62, 2001.
- [102] B.-O. Park, C. Lokhande, H.-S. Park, K.-D. Jung, and O.-S. Joo, "Performance of supercapacitor with electrodeposited ruthenium oxide film electrodes—effect of film thickness," *Journal of power sources*, vol. 134, no. 1, pp. 148-152, 2004.
- [103] Y.-z. Zheng, H.-y. Ding, and M.-l. Zhang, "Preparation and electrochemical properties of nickel oxide as a supercapacitor electrode material," *Materials Research Bulletin*, vol. 44, no. 2, pp. 403-407, 2009.
- [104] U. Patil, R. Salunkhe, K. Gurav, and C. Lokhande, "Chemically deposited nanocrystalline NiO thin films for supercapacitor application," *Applied Surface Science*, vol. 255, no. 5, pp. 2603-2607, 2008.
- [105] F. Yu, L. Zhu, T. You, F. Wang, and Z. Wen, "Preparation of chestnut-like porous NiO nanospheres as electrodes for supercapacitors," *RSC advances*, vol. 5, no. 116, pp. 96165-96169, 2015.
- [106] A. Paravannoor *et al.*, "Chemical and structural stability of porous thin film NiO nanowire based electrodes for supercapacitors," *Chemical engineering journal*, vol. 220, pp. 360-366, 2013.
- [107] M. N. Sakib, S. Ahmed, S. S. M. Rahat, and S. B. Shuchi, "A review of recent advances in manganese-based supercapacitors," *Journal of Energy Storage*, vol. 44, p. 103322, 2021.
- [108] O. Ghodbane, J.-L. Pascal, and F. Favier, "Microstructural effects on charge-storage properties in MnO₂-based electrochemical supercapacitors," *ACS applied materials & interfaces*, vol. 1, no. 5, pp. 1130-1139, 2009.
- [109] C. Sun, Y. Zhang, S. Song, and D. Xue, "Tunnel-dependent supercapacitance of MnO₂: effects of crystal structure," *Journal of Applied Crystallography*, vol. 46, no. 4, pp. 1128-1135, 2013.
- [110] Q. Meng, K. Cai, Y. Chen, and L. Chen, "Research progress on conducting polymer based supercapacitor electrode materials," *Nano Energy*, vol. 36, pp. 268-285, 2017.
- [111] A. Eftekhari, L. Li, and Y. Yang, "Polyaniline supercapacitors," *Journal of Power Sources*, vol. 347, pp. 86-107, 2017.

- [112] S. Sivakkumar, W. J. Kim, J.-A. Choi, D. R. MacFarlane, M. Forsyth, and D.-W. Kim, "Electrochemical performance of polyaniline nanofibres and polyaniline/multi-walled carbon nanotube composite as an electrode material for aqueous redox supercapacitors," *Journal of power sources*, vol. 171, no. 2, pp. 1062-1068, 2007.
- [113] H. Li, J. Wang, Q. Chu, Z. Wang, F. Zhang, and S. Wang, "Theoretical and experimental specific capacitance of polyaniline in sulfuric acid," *Journal of Power Sources*, vol. 190, no. 2, pp. 578-586, 2009.
- [114] Q. Yang, Z. Hou, and T. Huang, "Self-assembled polypyrrole film by interfacial polymerization for supercapacitor applications," *Journal of Applied Polymer Science*, vol. 132, no. 11, 2015.
- [115] M. Rajesh, C. J. Raj, B. C. Kim, B.-B. Cho, J. M. Ko, and K. H. Yu, "Supercapacitive studies on electropolymerized natural organic phosphate doped polypyrrole thin films," *Electrochimica Acta*, vol. 220, pp. 373-383, 2016.
- [116] G. A. Snook, P. Kao, and A. S. Best, "Conducting-polymer-based supercapacitor devices and electrodes," *Journal of power sources*, vol. 196, no. 1, pp. 1-12, 2011.
- [117] A. Laforgue, P. Simon, C. Sarrazin, and J.-F. Fauvarque, "Polythiophene-based supercapacitors," *Journal of power sources*, vol. 80, no. 1-2, pp. 142-148, 1999.
- [118] B. H. Patil, A. D. Jagadale, and C. D. Lokhande, "Synthesis of polythiophene thin films by simple successive ionic layer adsorption and reaction (SILAR) method for supercapacitor application," *Synthetic Metals*, vol. 162, no. 15-16, pp. 1400-1405, 2012.
- [119] M. Fu *et al.*, "Microwave assisted growth of MnO₂ on biomass carbon for advanced supercapacitor electrode materials," *Journal of Materials Science*, vol. 56, pp. 6987-6996, 2021.
- [120] Y. Zhou *et al.*, "High-performance hierarchical MnO₂/CNT electrode for multifunctional supercapacitors," *Carbon*, vol. 184, pp. 504-513, 2021.
- [121] W. Feng *et al.*, "Template synthesis of a heterostructured MnO₂@ SnO₂ hollow sphere composite for high asymmetric supercapacitor performance," *ACS Applied Energy Materials*, vol. 3, no. 8, pp. 7284-7293, 2020.
- [122] O. Ghodbane, M. Louro, L. Coustan, A. Patru, and F. Favier, "Microstructural and morphological effects on charge storage properties in MnO₂-carbon nanofibers based supercapacitors," *Journal of the Electrochemical Society*, vol. 160, no. 11, p. A2315, 2013.
- [123] Y. Huo, H. Zhang, J. Jiang, and Y. Yang, "A three-dimensional nanostructured PANI/MnO_x porous microspheres and its capacitive performance," *Journal of Materials Science*, vol. 47, pp. 7026-7034, 2012.

- [124] S. Jadhav *et al.*, "Manganese dioxide/reduced graphene oxide composite an electrode material for high-performance solid state supercapacitor," *Electrochimica Acta*, vol. 299, pp. 34-44, 2019.
- [125] Q. Li, Z.-L. Wang, G.-R. Li, R. Guo, L.-X. Ding, and Y.-X. Tong, "Design and synthesis of MnO₂/Mn/MnO₂ sandwich-structured nanotube arrays with high supercapacitive performance for electrochemical energy storage," *Nano letters*, vol. 12, no. 7, pp. 3803-3807, 2012.
- [126] S. Dong *et al.*, "One dimensional MnO₂/titanium nitride nanotube coaxial arrays for high performance electrochemical capacitive energy storage," *Energy & Environmental Science*, vol. 4, no. 9, pp. 3502-3508, 2011.
- [127] J. Liu *et al.*, "Co₃O₄ nanowire@ MnO₂ ultrathin nanosheet core/shell arrays: a new class of high-performance pseudocapacitive materials," *Advanced Materials*, vol. 18, no. 23, pp. 2076-2081, 2011.
- [128] H. Jiang, C. Li, T. Sun, and J. Ma, "High-performance supercapacitor material based on Ni(OH)₂ nanowire-MnO₂ nanoflakes core-shell nanostructures," *Chemical Communications*, vol. 48, no. 20, pp. 2606-2608, 2012.
- [129] D. Sarkar, G. G. Khan, A. K. Singh, and K. Mandal, "High-performance pseudocapacitor electrodes based on α -Fe₂O₃/MnO₂ core-shell nanowire heterostructure arrays," *The Journal of Physical Chemistry C*, vol. 117, no. 30, pp. 15523-15531, 2013.
- [130] A.-L. Yan, W.-D. Wang, W.-Q. Chen, X.-C. Wang, F. Liu, and J.-P. Cheng, "The synthesis of NiCo₂O₄-MnO₂ core-shell nanowires by electrodeposition and its supercapacitive properties," *Nanomaterials*, vol. 9, no. 10, p. 1398, 2019.
- [131] G. Liu, L. Ma, and Q. Liu, "The preparation of Co₃O₄@ MnO₂ hierarchical nano-sheets for high-output potential supercapacitors," *Electrochimica Acta*, vol. 364, p. 137265, 2020.
- [132] J. Jia, X. Lian, M. Wu, F. Zheng, Y. Gao, and H. Niu, "Self-assembly of α -MnO₂/Mn₃O₄ hierarchical structure on carbon cloth for asymmetric supercapacitors," *Journal of Materials Science*, vol. 56, pp. 3246-3255, 2021.
- [133] R. Peng *et al.*, "Construction of 0D CeO₂/2D MnO₂ heterostructure with high electrochemical performance," *Electrochimica Acta*, vol. 319, pp. 95-100, 2019.
- [134] Z. Fan, J. Chen, B. Zhang, F. Sun, B. Liu, and Y. Kuang, "Electrochemically induced deposition method to prepare γ -MnO₂/multi-walled carbon nanotube composites as electrode material in supercapacitors," *Materials Research Bulletin*, vol. 43, no. 8, pp. 2085-2091, 2008/08/04/ 2008.

- [135] R. K. Sharma, A. C. Rastogi, and S. B. Desu, "Manganese oxide embedded polypyrrole nanocomposites for electrochemical supercapacitor," *Electrochimica Acta*, vol. 53, no. 26, pp. 7690-7695, 2008/11/01/ 2008.
- [136] Z. Li, J. Wang, X. Liu, S. Liu, J. Ou, and S. Yang, "Electrostatic layer-by-layer self-assembly multilayer films based on graphene and manganese dioxide sheets as novel electrode materials for supercapacitors," *Journal of Materials Chemistry*, vol. 21, no. 10, pp. 3397-3403, 2011.
- [137] Z. Su *et al.*, "Co-electro-deposition of the MnO₂-PEDOT: PSS nanostructured composite for high areal mass, flexible asymmetric supercapacitor devices," *Journal of Materials Chemistry A*, vol. 1, no. 40, pp. 12432-12440, 2013.
- [138] Z. Zhou, N. Cai, and Y. Zhou, "Capacitive characteristics of manganese oxides and polyaniline composite thin film deposited on porous carbon," *Materials Chemistry and Physics*, vol. 94, no. 2, pp. 371-375, 2005/12/15/ 2005.
- [139] M. Zhi, A. Manivannan, F. Meng, and N. Wu, "Highly conductive electrospun carbon nanofiber/MnO₂ coaxial nano-cables for high energy and power density supercapacitors," *Journal of Power Sources*, vol. 208, pp. 345-353, 2012/06/15/ 2012.
- [140] S. Ghasemi, S. R. Hosseini, and O. Boore-talari, "Sonochemical assisted synthesis MnO₂/RGO nanohybrid as effective electrode material for supercapacitor," *Ultrasonics Sonochemistry*, vol. 40, pp. 675-685, 2018/01/01/ 2018.
- [141] J. Shao *et al.*, "Mechanism analysis of the capacitance contributions and ultralong cycling-stability of the isomorphous MnO₂@ MnO₂ core/shell nanostructures for supercapacitors," *Journal of Materials Chemistry A*, vol. 3, no. 11, pp. 6168-6176, 2015.
- [142] Y. Wang, W. Huo, X. Yuan, and Y. Zhang, "Composite of manganese dioxide and two-dimensional materials applied to supercapacitors," *Acta Phys. Chim. Sin.*, vol. 36, no. 2, 2020.
- [143] Q. J. Le *et al.*, "Biotemplate derived three dimensional nitrogen doped graphene@ MnO₂ as bifunctional material for supercapacitor and oxygen reduction reaction catalyst," *Journal of colloid and interface science*, vol. 544, pp. 155-163, 2019.
- [144] A. Ehsani, A. A. Heidari, and H. M. Shiri, "Electrochemical pseudocapacitors based on ternary nanocomposite of conductive polymer/graphene/metal oxide: an introduction and review to it in recent studies," *The Chemical Record*, vol. 19, no. 5, pp. 908-926, 2019.
- [145] J. M. Gonçalves, M. I. da Silva, H. E. Toma, L. Angnes, P. R. Martins, and K. Araki, "Trimetallic oxides/hydroxides as hybrid supercapacitor electrode materials: a review," *Journal of Materials Chemistry A*, vol. 8, no. 21, pp. 10534-10570, 2020.

- [146] P. J. S. Jennifer *et al.*, "Investigation of MnO₂/CuO/rGO ternary nanocomposite as electrode material for high-performance supercapacitor," *Inorganic Chemistry Communications*, vol. 146, p. 110218, 2022.
- [147] N. Arshad *et al.*, "Nanoengineering of NiO/MnO₂/GO ternary composite for use in high-energy storage asymmetric supercapacitor and oxygen evolution reaction (OER)," *Nanomaterials*, vol. 13, no. 1, p. 99, 2022.
- [148] G. Zhang, Q. Li, E. Allahyarov, Y. Li, and L. Zhu, "Challenges and opportunities of polymer nanodielectrics for capacitive energy storage," *ACS Applied Materials & Interfaces*, vol. 13, no. 32, pp. 37939-37960, 2021.
- [149] L. Su, Y. Wang, Y. Sha, and M. Hao, "Ternary active site Co₃O₄/NiO/MnO₂ electrode with enhanced capacitive performances," *Journal of Alloys and Compounds*, vol. 656, pp. 585-589, 2016.
- [150] S. Vargheese, R. S. Kumar, R. T. R. Kumar, J.-J. Shim, and Y. Haldorai, "Binary metal oxide (MnO₂/SnO₂) nanostructures supported triazine framework-derived nitrogen-doped carbon composite for symmetric supercapacitor," *Journal of Energy Storage*, vol. 68, p. 107671, 2023.
- [151] B. Chameh, K. Adib, H. M. Aydisheh, and F. Gravand, "Ultrasound assist synthesis of rod-like MnO₂/thermal reduced GO/annealed PANI ternary composite and used as a cathode for asymmetrical 2032-coin cell supercapacitors," *Journal of Energy Storage*, vol. 84, p. 110939, 2024.
- [152] M. Asif *et al.*, "Improved performance of a MnO₂@ PANI nanocomposite synthesized on 3D graphene as a binder free electrode for supercapacitors," *RSC advances*, vol. 6, no. 52, pp. 46100-46107, 2016.
- [153] X.-M. Cao *et al.*, "Facile synthesis of bead-chain structured MWCNTs@ CeO₂ with oxygen vacancies-rich for promoting electrochemical energy storage," *Chemical Engineering Journal*, vol. 479, p. 147663, 2024.
- [154] G. Marciniuk *et al.*, "Enhancing hydrothermal formation of α -MnO₂ nanoneedles over nanographite structures obtained by electrochemical exfoliation," *Bulletin of Materials Science*, vol. 44, pp. 1-11, 2021.
- [155] G. Jayakumar, A. Albert Irudayaraj, and A. Dhayal Raj, "A comprehensive investigation on the properties of nanostructured cerium oxide," *Optical and Quantum Electronics*, vol. 51, no. 9, p. 312, 2019.
- [156] M. T. T. Moghadam, M. Seifi, F. Jamali, S. Azizi, and M. B. Askari, "ZnWO₄-CNT as a superior electrode material for ultra-high capacitance supercapacitor," *Surfaces and Interfaces*, vol. 32, p. 102134, 2022.

- [157] G. Xie *et al.*, "The evolution of α -MnO₂ from hollow cubes to hollow spheres and their electrochemical performance for supercapacitors," *Journal of Materials Science*, vol. 52, pp. 10915-10926, 2017.
- [158] J. Wang, D. Zhang, F. Nie, R. Zhang, X. Fang, and Y. Wang, "The role of MnO₂ crystal morphological scale and crystal structure in selective catalytic degradation of azo dye," *Environmental Science and Pollution Research*, vol. 30, no. 6, pp. 15377-15391, 2023.
- [159] K. Zhu, W. Yan, S. Liu, X. Wu, S. Cui, and X. Shen, "One-step hydrothermal synthesis of MnO_x-CeO₂/reduced graphene oxide composite aerogels for low temperature selective catalytic reduction of NO_x," *Applied Surface Science*, vol. 508, p. 145024, 2020.
- [160] H. Su *et al.*, "Comparative Study of α - and β -MnO₂ on Methyl Mercaptan Decomposition: The Role of Oxygen Vacancies," *Nanomaterials*, vol. 13, no. 4, p. 775, 2023.
- [161] D. Joung, V. Singh, S. Park, A. Schulte, S. Seal, and S. I. Khondaker, "Anchoring ceria nanoparticles on reduced graphene oxide and their electronic transport properties," *The Journal of Physical Chemistry C*, vol. 115, no. 50, pp. 24494-24500, 2011.
- [162] M. Kumar *et al.*, "Role of Ce³⁺ valence state and surface oxygen vacancies on enhanced electrochemical performance of single step solvothermally synthesized CeO₂ nanoparticles," *Electrochimica Acta*, vol. 284, pp. 709-720, 2018.
- [163] X.-S. Li *et al.*, "MnO₂@ Corncob carbon composite electrode and all-solid-state supercapacitor with improved electrochemical performance," *Materials*, vol. 12, no. 15, p. 2379, 2019.
- [164] S. S. Rabbani *et al.*, "Nickel foam supported hierarchical NiCo₂S₄@ NiFe LDH heterostructures as highly efficient electrode for long cycling stability supercapacitor," *Electrochimica Acta*, vol. 446, p. 142098, 2023.
- [165] J.-W. Wang, Y. Chen, and B.-Z. Chen, "Synthesis and control of high-performance MnO₂/carbon nanotubes nanocomposites for supercapacitors," *Journal of Alloys and Compounds*, vol. 688, pp. 184-197, 2016.
- [166] A. Sayah *et al.*, "Electrodeposition mode effects on the electrochemical performance of MnO₂-NiO eco-friendly material for supercapacitor electrode application," *Journal of Materials Science: Materials in Electronics*, vol. 35, no. 1, p. 62, 2024.
- [167] H. Zhang *et al.*, "Hierarchical porous MnO₂/CeO₂ with high performance for supercapacitor electrodes," *Chemical Engineering Journal*, vol. 286, pp. 139-149, 2016.

- [168] J. Jablonskiene *et al.*, "Synthesis of carbon-supported mno₂ nanocomposites for supercapacitors application," *Crystals*, vol. 11, no. 7, p. 784, 2021.
- [169] M. Jayachandran, A. Rose, T. Maiyalagan, N. Poongodi, and T. Vijayakumar, "Effect of various aqueous electrolytes on the electrochemical performance of α -MnO₂ nanorods as electrode materials for supercapacitor application," *Electrochimica acta*, vol. 366, p. 137412, 2021.